NEW FRACTURE TOUGHNESS TESTS FOR ROCK AND CONCRETE WITH PARTICULAR REFERENCE TO ROCK STRUCTURE DESIGN

by

Terence J. Bear B.Sc.,M.Sc.,F.G.S.

A thesis submitted for the degree of
Doctor of Philosophy, C.N.A.A., London.

August 1976

Department of Civil Engineering and Building,
The Polytechnic of Wales,
Treforest,
Mid-Glamorgan.

This thesis is dedicated to my wife,

Patricia.

CONTENTS

ACKNOWLEDGEMENTS

The work presented in this thesis was supervised by Dr. B.I.G. Barr and Mr. G.O. Rowlands, to whom the author wishes to express his thanks for their help and guidance.

The author also wishes to thank the technical staff in the Department of Civil Engineering and Building at the Polytechnic of Wales for their invaluable assistance during the course of this work.

The Science Research Council provided funds for most of the project, which the author gratefully acknowledges.

Thanks are also due to Ms. B. Miles for her prompt and efficient typing of this thesis.

CERTIFICATION OF RESEARCH

This is to certify that, except when specific reference is made, the work described in this Dissertation is the result of the investigation of the candidate.

T. J. Bear

.....

Candidate

Benjamin Bear

.....

Director of Studies

This is to certify that neither this Dissertation, nor any part of it, has been presented, or is being concurrently submitted, in candidature for any degree at any other university.

T. J. Bear

Candidate

Summary

This thesis applies the concepts of Fracture Mechanics to some of the problems of Rock Mechanics.

A review of the literature shows that Fracture Mechanics is applicable to ceramic materials, such as rocks and concrete, but no test has been available which can quickly and easily measure the fracture toughness of these materials.

Three new fracture toughness tests are proposed which are relatively easy to apply to in situ materials. The stress intensity factor for each test specimen is derived.

The tests are developed, to varying degrees, using concrete as a test material. The relative merits of the three tests are discussed, and their advantages emphasised. The tests are shown to give reproducible results for two rock types.

Fracture failure criteria are derived for three simple rock structures, and use the results obtained from the new fracture toughness tests. The criteria are compared with conventional tensile strength ones.

The final chapter draws conclusions from the project, and makes suggestions for a future program of work.

CHAPTER 1

Introduction

Rock has been used as a construction material, both above and below ground, since prehistoric times. Until the eighteenth century, a qualitative description of rocks was all that was available. However, because of the complexities of modern structures, a detailed knowledge of the engineering properties of rocks is now vital.

To design a rock structure it is usual to ensure that the stress in any part of the structure is less than the strength of the rock. The stresses may be either tensile or compressive, and it is necessary to know the rock strength in tension and compression. Also, the rock may be in a uniaxial, biaxial or triaxial state of stress, and so several different parameters may be required to accurately describe the response of rock to a given stress distribution.

The tensile strength of rock is very much less than the compressive strength, and for this reason, most structures are designed to avoid large tensile stresses. In some situations tensile stresses are unavoidable, as for example, in a tunnel of rectangular cross-section. In such cases, the tensile strength of rock has to be known.

Many tests have been proposed to measure the tensile strength of rock (Jaeger & Cook 1969). However, most of the tests have one factor in common; they produce a large scatter in results. Also, the various tests often give different strength measurements (Hardy & Jayaraman 1970). The direct tensile test of rock is particularly difficult to perform and often gives very variable results.

To predict the stresses in rock structures, it is usually necessary to assume that the rock is a continuum, and that simple elasticity theory applies (Obert & Duvall 1967). Also, it is assumed that once the stress in a structure exceeds the rock strength, then the structure will fail. These assumptions can be limiting in real situations.

Most failure criteria are based on empirical results and offer no explanation as to the actual mechanism of failure. Griffith (1921) proposed that the strength of a brittle material is determined by the presence of micro-cracks in the material. These micro-cracks (or sometimes called 'Griffith cracks') act as stress concentrators, and failure is caused by their extension. Even under triaxial compressive stress conditions tensile stresses develop at the crack tips, and eventually may cause failure. Griffith suggested that a material will fail when the stress at a crack tip reaches a critical value. This hypothesis can be used to derive a failure criterion in terms of gross stresses in a body.

The Griffith failure criterion has a limitation when considering rock failure, especially under compressive stresses. To explain the limitations, a distinction has to be made between fracture initiation and propagation (Bieniawski 1967a). Fracture initiation is the process by which cracks in a material start to extend. Fracture propagation is the process by which cracks are extending subsequent to fracture initiation. The Griffith failure criterion states that a material will fail when fracture initiation takes place. For compressive stresses this is usually not true. In tension, fracture initiation and propagation usually occur simultaneously, as illustrated

by the sudden failure of specimens tested in tension. Therefore, fracture failure criteria are more easily applied to tensile situations, and this thesis will be mainly concerned with tensile failure.

The behaviour of materials containing cracks can be investigated using Fracture Mechanics. The response of a material to crack initiation and propagation, and therefore to failure, can be described by a material property, K_{1c}. Fracture Mechanics has been well established for metals and plastics but not for ceramics. One reason for this lack of development is that a suitable test for K_{1c} measurement for ceramics has not been available, and the property is difficult to measure by the existing techniques which are used for metals and plastics.

Once the material property, K_{1c}, has been measured, there are two approaches to the application of Fracture Mechanics to design. K_{1c} can be used to derive the tensile strength, and to use this value in conventional design criteria. Another method is to replace conventional strength criteria by equivalent fracture criteria and use K_{1c} directly.

This thesis aims to apply Fracture Mechanics to rock structures design, and is basically divided into two parts. In the first part, new fracture tests are developed to enable K_{1c} to be easily and quickly measured for rock. In the second part, design criteria are derived to enable K_{1c} to be directly applied to practical situations. The use of Fracture Mechanics is of particular advantage where conventional tensile strength design criteria are now used. The fracture tests are designed to enable K_{1c} to be measured more easily than the tensile strength tests.

Rock is an unsuitable material for testing technique development because it is, in general, an inhomogeneous material. It is difficult to separate variations in test technique with variations in rock properties. Therefore, a fine-grained concrete has been used as a test material to simulate rock. A concrete mix can be prepared in large quantities with reproducible properties and is ideal for test development.

The fracture tests and design criteria described in this thesis are equally suitable for both concrete and rock. It is expected that the application of Fracture Mechanics to ceramics will be useful to the construction and mining industries.

CHAPTER 2

This chapter reviews the literature regarding the Fracture Mechanics of concrete and rocks. The various methods for measuring the fracture toughness of these materials, and their limitations, are discussed in detail.

2.1 Griffith's Theory of Brittle Fracture

The science of Fracture Mechanics started with the publication of the paper 'The Phenomena of Rupture and Flow of Solids' by Griffith (1921). Griffith proposed that the failure of a brittle material is caused by the extension of cracks in the material. It is well known that the tensile strength of a material is very much less than that predicted from consideration of inter-atomic forces. At the ends of cracks in a material stress concentrations arise which can locally increase stresses to a value greater than that necessary to cause rupture of interatomic bonds. Griffith showed that the tensile strength of annealed glass, containing few cracks, approached the theoretical value.

Griffith considered the energy balance involved in propagating a crack in an elastic material. The total energy, U, in a body is given by:-

$$U = S - P + U_s \qquad (2.1)$$

where S is the strain energy stored in the body, P is the work done by external loads acting on the body, U_s is the surface energy necessary to create new crack surfaces.

For the crack in the body to be in equilibrium:-

$$\frac{dU}{dt} = 0 \qquad (2.2)$$

where t is the crack length.

For an elastic body under a constant applied stress,

$$P = 2S \qquad (2.3)$$

and (2.2) becomes, for equilibrium:-

$$\frac{d}{dt}(-S+U_s) = 0 \qquad (2.4)$$

Griffith illustrated his concept by considering a crack, of length 2t, in a plate of unit thickness, under a tensile stress, σ. The strain energy change by the introduction of the crack is given by:-

$$S = \frac{\sigma^2 \pi t^2}{E} \qquad (2.5)$$

for plane stress, where E is Young's Modulus.

The energy absorbed, U_s, by the crack is simply $4t\alpha$, where α is the surface tension of the material. Therefore, for equilibrium:-

$$\frac{d}{dt}\left(\frac{-\sigma^2 \pi t^2}{E} + 4t\alpha\right) = 0 \qquad (2.6)$$

or,

$$\sigma = \sqrt{\frac{2\alpha E}{\pi t}} \qquad (2.7)$$

This is the condition that a crack will grow. For crack propagation, the stress must exceed this value, and the failure condition, for plane stress becomes:-

$$\sigma > \sqrt{\frac{2\alpha E}{\pi t}} \qquad (2.8)$$

For conditions of plane strain, E is replaced by $E/(1-\nu^2)$. For rocks, a typical value for Poisson's ratio, ν, is 0.25. The difference between E and $E/(1-\nu^2)$ is only 6%. For simplicity, this thesis will assume plane stress conditions.

At failure, $\sigma = T_o$, the tensile strength of the material, and:-

$$T_o\sqrt{t} = \sqrt{\frac{2\alpha E}{\pi}} \qquad (2.9)$$

All the quantities on the right of the equation are constants for a material. and so Griffith's theory predicts that $T_o\sqrt{t}$ is a material constant.

Griffith's failure criterion has been modified by Irwin (1948) and Orowan (1950) to allow for non-elastic energy associated with crack extension. They proposed that the parameter α should include all energy terms associated with crack extension, such as plastic deformation energy. In ceramics, there is little or no ductility to allow plastic deformation to occur, but there is extra work done during cracking. For example, friction occurs between crack faces, but it is assumed that the failure criterion (2.8) still applies to ceramics if α includes all additional energy terms.

2.2 The Stress Intensity Factor

Griffith realised that the strength of a material is controlled by processes occurring at crack tips so that a stress analysis of these areas should yield a failure criterion in terms of elastic stresses.

Irwin (1957) used a method of stress analysis formulated by Westergaard (1939) to derive the stress field at a crack tip. He derived the stresses in terms of a parameter $\mathcal{G}$, called the strain energy release rate. Irwin (1960) later introduced an equivalent parameter K, called the stress intensity factor. Irwin showed that the stresses at a crack tip can be completely specified by K, which is a function of specimen geometry and loading arrangement. Figure 2.1

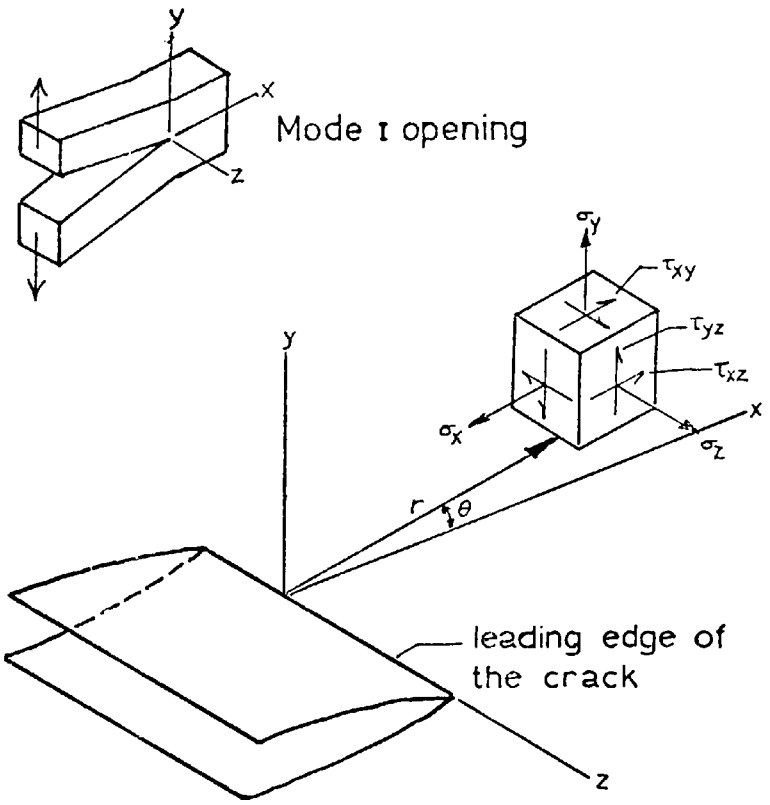

$$\sigma_x = \frac{K_I}{(2\pi r)^{1/2}} \cos\frac{\theta}{2}\left[1-\sin\frac{\theta}{2}\sin\frac{3\theta}{2}\right]$$

$$\sigma_y = \frac{K_I}{(2\pi r)^{1/2}} \cos\frac{\theta}{2}\left[1+\sin\frac{\theta}{2}\sin\frac{3\theta}{2}\right]$$

$$\tau_{xy} = \frac{K_I}{(2\pi r)^{1/2}} \sin\frac{\theta}{2}\cos\frac{\theta}{2}\cos\frac{3\theta}{2}$$

$$\sigma_z = \nu(\sigma_x + \sigma_y), \quad \tau_{xz} = \tau_{yz} = 0$$

Fig 2.1 Coordinates and stress components in the crack tip stress field for plane strain conditions.

shows the crack tip coordinate system and gives the stress equations for a crack opening under normal forces (mode 1). For this loading geometry, the stress intensity factor is designated K_1.

Usually, cracks will open under more general conditions with shear and tearing stresses present (modes II and III). However, this thesis will be concerned only with situations in which cracks open under tensile stresses and mode I conditions predominate, and the stress intensity factor used in experiments and theory is K_1.

Griffith's theory suggests that fracture initiation occurs at crack tips, and if two geometrically identical specimens of the same material have the same stress field then the failure load will be equal. Failure will occur when K_1 reaches a critical value, denoted K_{1c} and Irwin proposed that K_{1c} is a material constant. The failure criterion then becomes:-

$$K_1 > K_{1c} \text{ for failure.}$$

2.3 Quasi-static Crack Propagation

Griffith considered energy equilibria for particular crack geometries, but a crack initiation criterion can be derived from consideration of more general energy changes in a body (Irwin & Kies 1954), (Gurney & Hunt 1967).

Consider a cracked body with an external force, F, acting on it. The force causes a displacement, y. The work theorem of statics states that the work done by all forces, internal or external, during a quasi-static displacement process is zero. An equation can be written for quasi-static crack propagation:-

$$Fdy - d(\text{strain energy}) - \mathcal{G}_{1c}dA = 0 \qquad (2.10)$$

where $\mathcal{G}_{1c}$ is the strain energy release rate at the point of crack initiation. It is also the work necessary, per unit crack area, to propagate the crack. The area A of the crack is taken as being only one side of the crack. For a linearly elastic system the strain energy = yF/2. The equation (2.10) can be rearranged to give:-

$$\mathcal{G}_{1c} = \frac{d}{dA}\left(\tfrac{1}{2}Fy\right) \qquad (2.11)$$

The failure criteria becomes:-

$$\mathcal{G}_{1c} < \frac{d}{dA}\left(\tfrac{1}{2}yF\right) \qquad (2.12)$$

The material property $\mathcal{G}_{1c}$ can easily be measured from a load-deflection graph for a specimen cracked under quasi-static conditions as yF/2 divided by the increase in crack area. The constant $\mathcal{G}_{1c}$ corresponds to 2α in Irwin and Orowans modification of Griffith's theory.

The material properties, $\mathcal{G}_{1c}$ and K_{1c}, are related by the expression:-

$$K_{1c}^{\ 2} = E\mathcal{G}_{1c} \qquad (2.13)$$

for plane stress.

2.4 The application of Griffith's Theory of Brittle Fracture to Concrete and Rock

To apply Fracture Mechanics to ceramics such as rock and concrete, it has to be demonstrated that failure in these materials is caused by crack propagation. Evans (1946) investigated the mechanism of strain

in concrete. Previous experimenters had shown that the stress-strain curve for concrete was similar to that for metals (fig. 2.2), and had supposed that the mechanism of strain was the same as that for metal. Evans tested concrete specimens in tension and flexure and found that very small cracks open up in the specimens at loads very much less than the failure load. A high powered microscope was necessary to observe the cracks, but it was clear that it was the cracks causing the abnormally high strains at large loads.

Several researchers have discovered that rocks emit microseisms when subjected to stress (Cook 1965, Brown & Singh 1966). The microseisms have been attributed to the formation of small cracks in the rock, Cook found that the intensity of the microseismic activity increased as the load on a specimen increased, especially near to failure. Brown and Singh measured both the frequency of occurence and energy of microseisms. There was a distinct correlation between the microseismic energy release and the tensile strength of the rock under test. This observation is in agreement with the Griffith theory of brittle fracture. Each microseism is caused by the formation of a new crack, and is a measure of the energy required to produce the crack. Therefore, the total microseismic energy is a measure of the energy required to produce enough cracks to rupture the rock.

As a direct test of the validity of the application of the Griffith theory to rock fracture, Brace (1961) investigated the relationship between rock strength and grain size. He measured the average grain diameter of two similar limestones and their compressive strengths. He found that the ratio of the compressive strengths was similar to the ratio of the square roots of the grain sizes. Brace also measured values of α, E and compressive strengths to predict the

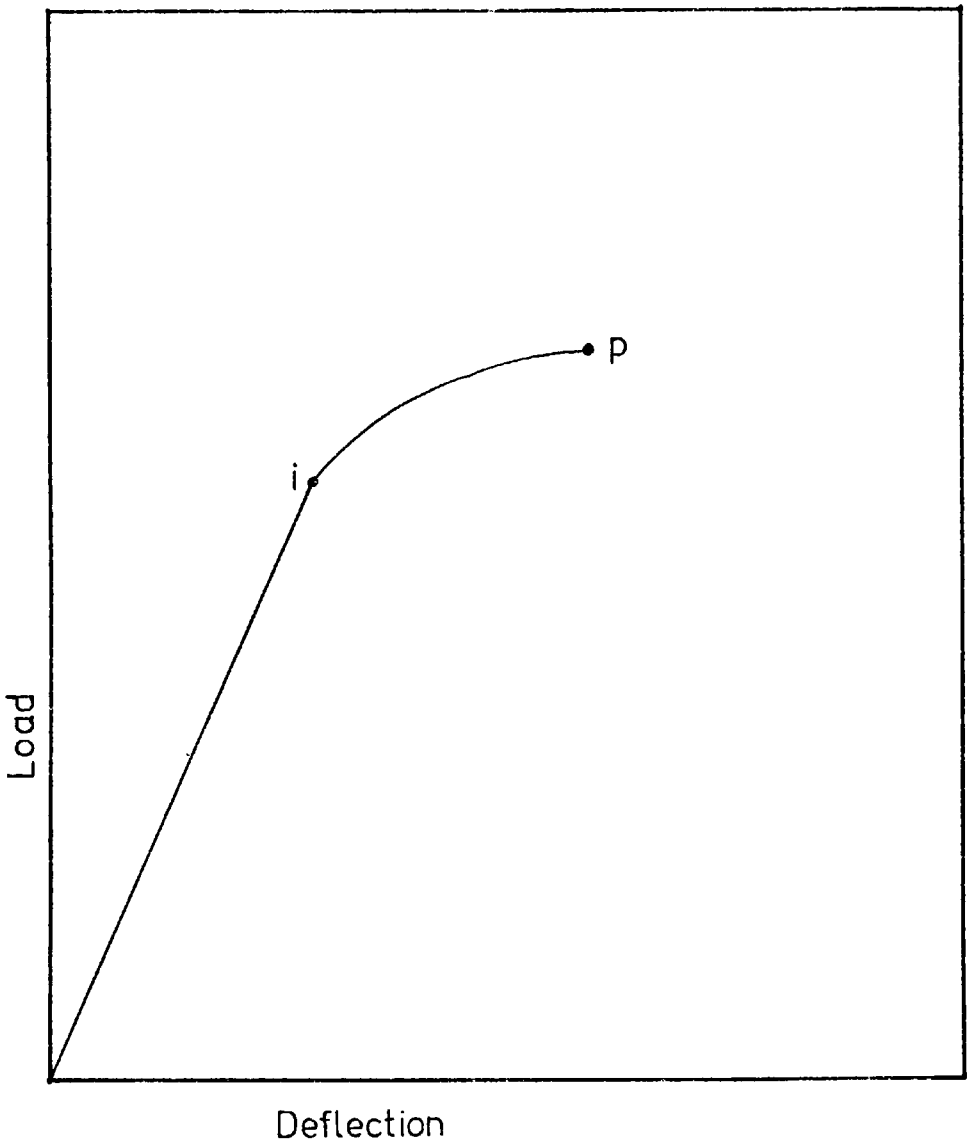

Fig 2.2 A typical load-deflection graph for concrete.

size of Griffith cracks for a rock. He found that the size of these cracks corresponded to the average size of the rock grains. Brace suggested that the Griffith cracks, or fracture initiators, were either in the rock grains or at the grain boundaries.

2.5 Measurement of the Fracture Properties of Rocks and Concrete

One of the first experiments to measure the surface energy, α, for a mineral, was conducted by Obreimoff (1930). He measured the surface energy of mica, which is a mineral with a good cleavage. His method is interesting because it illustrates how a fracture criterion can be derived from simple considerations of energy changes involved in the cracking process.

The experimental arrangement is shown in figure 2.3. A glass wedge, of thickness h, is inserted beneath a thin flake of mica, of thickness c and unit breadth, and made to drive a crack along the cleavage plane. The force exerted by the wedge does not move perpendicular to the base of the specimen, and so it does no work. Using the notation of (2.1) P = 0. From simple beam theory, the strain energy stored in the flake is:-

$$W = \frac{Ec^3h^2}{8L^2} \qquad (2.14)$$

The energy absorbed by the cracking process, U_s is simply $2\alpha L$.

Substituting P, W and U_s in equation (2.1), the total energy of the system, U, is given as:-

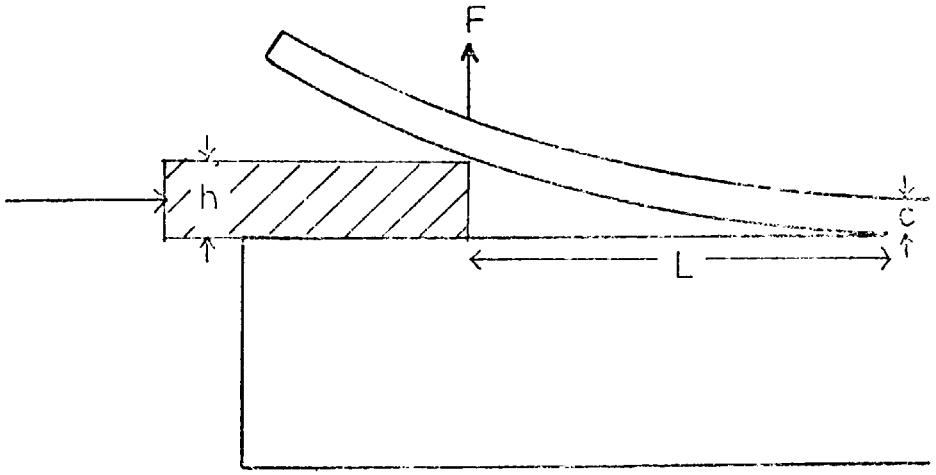

Fig 2.3 Schematic diagram of Obreimoff's experiment on mica.

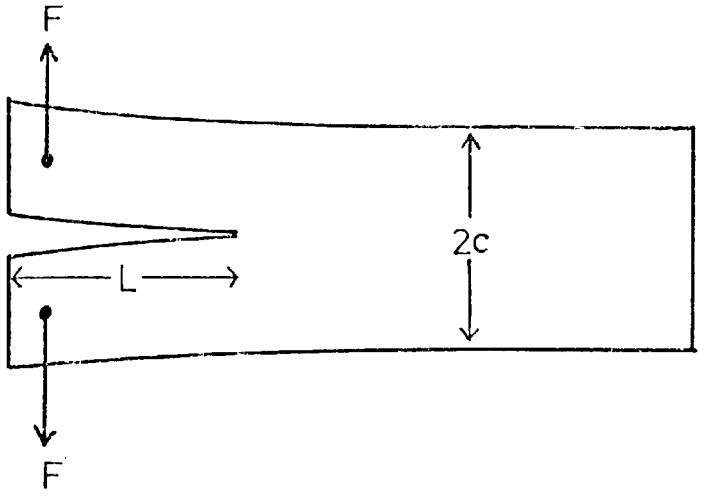

Fig 2.4 Schematic diagram of Gilman's experiment on single crystals.

$$U = \frac{Ec^3h^2}{8L^2} + 2\alpha L \qquad (2.15)$$

For equilibrium, dU/dL = 0, and the final result is:-

$$\alpha = \frac{3Ec^3h^2}{16L^4} \qquad (2.16)$$

As the wedge is pushed forward, the specimen cleaves until equilibrium is reached. Obreimoff measured L,E,c and h, and obtained a measure of the surface energy, α. He found that α was a function of the test environment, and changed dramatically with different air pressures.

A similar method was used by Gilman (1960) to measure surface energies of single crystals of several ceramics and elements. He used specimens as shown in figure 2.4, which have since been called double cantilever beam specimens (DCB). By pulling the two arms of a DCB in opposite directions, a crack is made to propagate along it.

Gilman considered a specimen as being equivalent to two cantilevers with fixed ends. Because the system is under constant force conditions, P = 2W. The strain energy in one cantilever of unit thickness is given by:-

$$W = \frac{2F^2L^3}{Ec^3} \qquad (2.17)$$

where the parameters are defined in figure 2.4.

The total energy of the system is:-

$$U = \frac{-4F^2L^3}{Ec^3} + 2\alpha L \qquad (2.18)$$

For equilibrium, $dU/dL = 0$ and:-

$$\alpha = \frac{6F^2L^2}{Ec^3} \qquad (2.19)$$

By measuring F, L and c, and assuming a value for E, Gilman was able to calculate α for several materials.

He also considered the contribution of kinetic and shear strain energies to the overall energy balance, but concluded that they were too small to greatly influence the final result. The calculated values of α were in general agreement with results calculated from atomic theory.

There is an important distinction between the experiments of Obreimoff and Gilman. In the former experiments, as the crack propagates (i.e. as L increases), the mechanical energy of the system (-P + W) decreases. There is less energy available for crack propagation, and so the system is stable. By contrast, in DCB specimens, as L increases, the mechanical energy also increases, making more energy available for the creation of new crack surfaces. Thus the DCB arrangement is unstable once crack initiation has occurred. In fracture toughness tests on ceramics, it is usually the latter mode of behaviour which predominates.

Kaplan (1961) measured $\mathcal{G}_{1c}$ for concrete by two different methods. $\mathcal{G}_{1c}$ can be derived from considerations of stresses at a crack tip (Irwin 1957) or from energy changes in a body as a whole (Irwin & Kies 195

Kaplan derived an expression for $\mathcal{G}_1$ for a crack opening in the base of a concrete beam under three or four-point loading (figure 2.5). By measurement of the failure load and the length of the crack at failure, he was able to derive a value for $\mathcal{G}_{1c}$ for concrete. The expression for $\mathcal{G}_{1c}$, derived from equation (2.10) is:-

$$\mathcal{G}_{1c} = \frac{F^2}{2} \frac{d}{dA}\left(\frac{y}{F}\right) \qquad (2.20)$$

Kaplan used this expression to give an alternative estimate of $\mathcal{G}_{1c}$.

Kaplan found that $\mathcal{G}_{1c}$ was independent of crack length in a beam but varied with loading arrangement and beam size. Also the two methods for measuring $\mathcal{G}_{1c}$ differed by about 21%. He also illustrated how $\mathcal{G}_{1c}$ can be used to give practical design criteria for concrete.

Brace and Walsh (1962) measured for single mineral crystals of quartz and orthoclase by considering energy changes at a crack tip. However, their method is limited to small speciments of homogeneous materials.

Nakayama (1965) carried out experiments to measure the effective surface energy α_{eff} of glass and firebrick using notched beams under three-point loading. The difference between the true and apparent (or effective) surface energies is that, for the latter, the crack surface area is taken as the nominal area of the specimen cross-section as opposed to the actual area. For an inhomogeneous material, the meanderings of the crack path make the nominal crack area less than the true area. Nakayama measured the area under the load-deflection graphs for the beam speciments and divided by the nominal crack area.

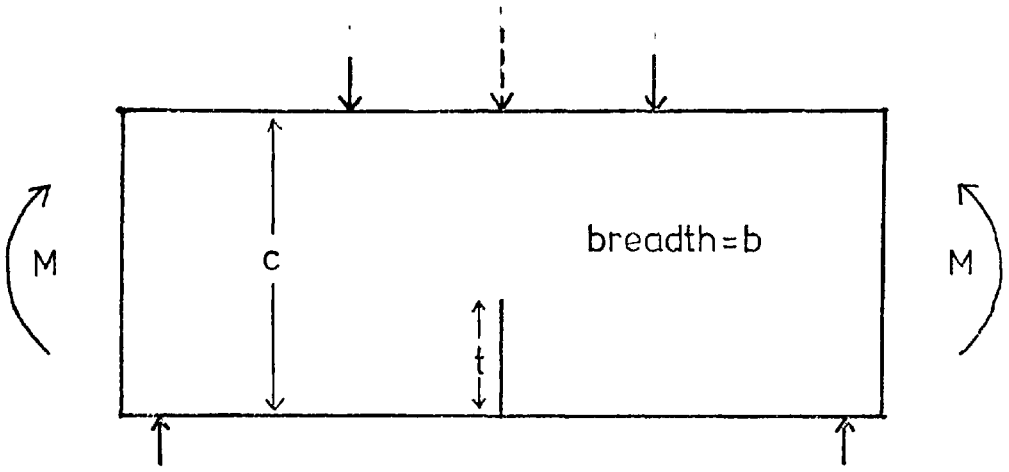

Fig 2.5 A notched beam under three or four-point loading.

He found it was necessary to cut a notch part-way through the beam to ensure that the fracture process was stable. His values for α_{eff} for brick were larger than expected, and this was thought to be due to the meandering path of the crack, and the underestimation of the true crack area.

Lott and Kesler (1966) published a paper in which they considered the mechanism of crack propagation in concrete. Previous researchers had shown (Glucklich 1963) that microcracking occurs at crack tips in concrete, and the energy requirements of the microcracks is greater than that of the main crack. Lott and Kesler suggested that the zone of microcracking increases with crack size because the stress at the crack tip also increases. Therefore, the energy required for crack propagation increases with increasing size until it reaches a critical level and rapid crack propagation occurs.

Lott and Kesler suggested that there are two critical stress intensity factors. K_{Ici} is the critical stress intensity factor at the onset of stable crack propagation (point i in figure 2.2), and is not necessarily a material property. K'_{Icp} is the 'pseudo' stress intensity factor at the onset of rapid crack propagation (point p in figure 2.2) and is a material property. It is usually this factor which is measured in fracture toughness tests. Furthermore, K'_{Icp} is divided into two parts:-

$$K'_{Icp} = K_{Icp} + f(ARR) \qquad (2.21)$$

where K_{Icp} is the critical stress intensity factor, assuming a homogeneous material, and f(ARR) is a function describing the effect of aggregate and matrix on the crack propagation. By experiment, Lott and Kesler

showed that K'_{1cp} increased as the amount of coarse aggregate was increased, but was constant for varying water/cement ratios.

Perkins and Krech (1966) measured the effective surface energy, α_{eff}, for rock using the same method as that of Gilman (1961). They found that the measured values of α_{eff} were largely independent of crack propagation speeds, but increased under high confining pressures.

Moavenzadeh and Kuguel (1969) carried out experiments on concrete to determine K_{1c} and $\mathcal{G}_{1c}$. They used notched beams, similar to the method of Kaplan (Figure 2.4) and measured K_{1c} from the relationship:-

$$K_{1c} = \frac{6M}{bc^2} \left(\frac{2c}{\pi}.h\left(\frac{t}{c}\right)\right)^{\frac{1}{2}} \qquad (2.22)$$

where h(t/c) is a polynomial function of t/c.

To determine $\mathcal{G}_{1c}$ from the equation (2.20) the researchers measured the actual crack area (as opposed to the nominal area) using quantitative microscopy. They found that the actual crack area can be as much as 20 times the nominal area. Using equation (2.13), they were able to compare the two methods of determining $\mathcal{G}_{1c}$ - from expended energy and the stress intensity approach.

Moavenzadeh and Kuguel found that the values for $\mathcal{G}_{1c}$ calculated from the two methods differed by about 37%. The researchers suggested that the discrepancy might be due to slow crack growth prior to failure, as demonstrated by Evans (1946). They also emphasised the distinction between α, and α_{eff}. For a mortar, the difference between the nominal and actual crack area is smaller than the same difference for a concrete. They suggest that $\alpha_{eff} = 2.5\alpha$ for mortar,

and $\alpha_{eff} = 7.5\alpha$ for concrete. Thus the effect of increasing aggregate size is to increase the fracture resistance of a concrete.

As indicated in chapter 1, Bieniawski (1967a) made a distinction between fracture initiation and fracture propagation. Using the distinction, it is apparent that microseismic events occur in rock specimens during fracture initiation, and failure follows crack propagation. Bieniawski further defined two types of crack propagation, stable, and unstable and suggested that the criterion for rock failure should be when the process goes from stable to unstable. This criterion can be expressed in terms of the critical strain energy release rate, previously introduced by Irwin (1957) and is given by equation (2.20).

Bieniawski (1967b) conducted experiments to show the distinction between stable and unstable crack propagation in rocks. He used an ultra-high speed camera to photograph a crack in a rock beam as it broke under a bending stress. He was able to identify three modes of crack propagation, stable, unstable and crack coalescence. During crack propagation the crack velocity rose from 500 m/sec to 1900 m/sec for unstable propagation. Bieniawski also measured $\mathcal{G}_{1c}$ and concluded that it was a material property which specified when crack propagation in a rock changed from stable to unstable, and could be used to give a valid criterion for failure.

Glucklich and Cohen (1968) published a paper which illustrates some of the difficulties involved in the measurement of K_{1c} or $\mathcal{G}_{1c}$. They conducted experiments on gypsum specimens and found that the tensile, compressive and flexural strengths varied dramatically with specimen size and stiffness. For example, if a spring were placed

in series with a specimen in a compressive or tensile test, the measured strength was reduced by 30%. Also, if the loading span of a beam were halved, then the flexural strength was increased by 18%.

These results show that any test designed to measure K_{1c} necessarily cannot give an 'absolute' result. Any derived value of K_{1c} will be a function of specimen size, shape and the response of the testing machine, and these factors have to be taken into account when comparing fracture toughness results.

Naus and Lott (1969) measured K_{1c} for many different types of concrete and cements. They used the notched beam specimens as did most previous researchers. The compositions of the cements and concrete were varied and the effects on K_{1c} were shown. The regularity of the variation of K_{1c} with different compositions lend support to the hypothesis that K_{1c} is a material constant for cements and concrete.

Peng (1970) measured K_{1c} for rocks using notched beam specimens and found that it was closely related to the ultimate strength of the rocks.

The difference between the true and effective fracture energies, α and α_{eff}, was also emphasised by Friedman, Handin and Alani (1972). They pointed out that published values for α_{eff} for rocks were orders of magnitude larger than values measured for constituent crystals.

Friedman et al measured α_{eff}, also using a notched beam technique, and conducted an X-ray analysis of the area of rock immediately surrounding the fracture path.

They found that strain relaxation in the rock grains had occurred during crack propagation, and had therefore absorbed some energy. If

this energy is subtracted from the total work done during crack propagation, the resultant value for α_{eff} approaches the value obtained from single crystals.

Brown (1972) measured K_{1c} (and $\mathcal{G}_{1c}$) for concrete and mortars using notched beams and double cantilever beam (DCB) specimens. He used expression (2.20) as used by Kaplan. A theoretical expression for d/dA(v/F) was derived from work by Brown and Srawley (1969). Brown loaded and unloaded the notched beams to obtain the slope of the load-deflection curve. A ratio was calculated between the slope at a particular crack length and the slope when no notch was present. This ratio was then compared with the theoretical relation. In this way, Brown was able to accurately determine the crack length and so reduce errors due to slow crack growth prior to failure.

The DCB specimens were cast in moulds (figure 2.6). The specimens were designed so that the crack would propagate at a constant load, and would thus be stable.

The values of K_{1c} derived from the notched beam experiments were largely independent of notch depth. However, K_{1c} measured from the DCB method increased as the crack went through the beam, and reached a limiting value. The average values of K_{1c} from the two types of experiment differed by about 25%, the DCB method giving the higher result.

Most researchers have used the notched beam under bending to investigate the fracture properties of ceramics (figure 2.4). The load-deflection graphs for three-point loading of such a specimen have been analysed by Hardy, Hudson and Fairhurst (1973). They used

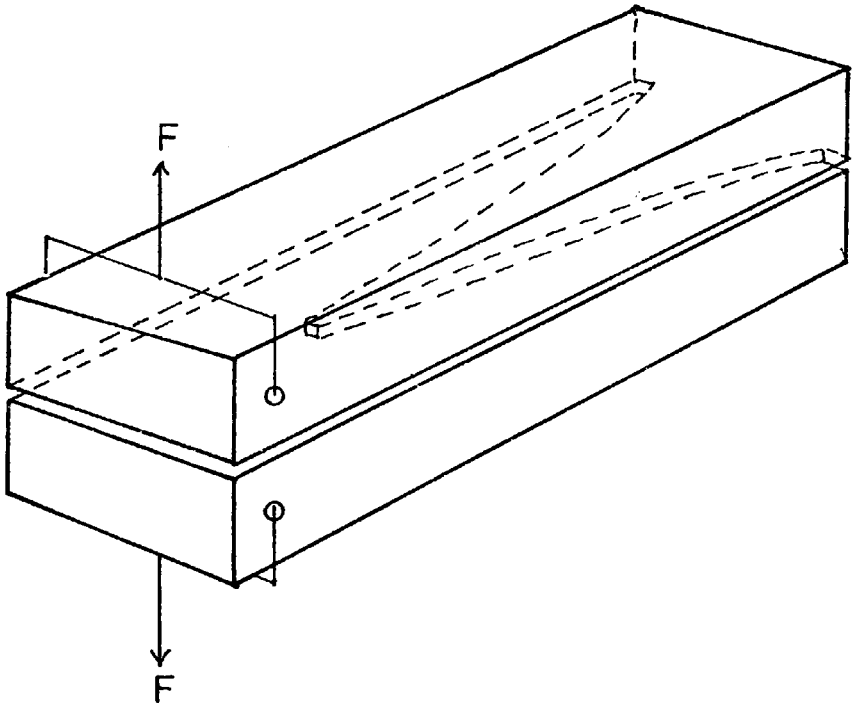

Fig 2.6 Tapered double-cantilever beam (DCB) specimen as used by Brown (1972).

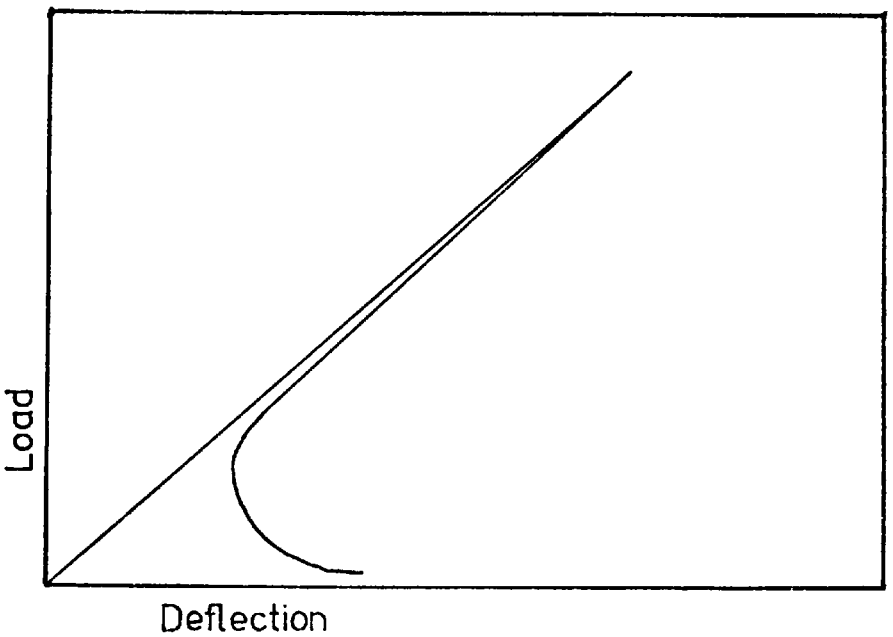

Fig 2.7 Theoretical load-deflection graph for a notched beam specimen.

a finite element program and Perspex models to predict the load-deflection graphs for rock. An example of such a graph is shown in figure 2.7.

The graph shows that, for stable crack propagation, the specimen has to be rapidly unloaded as soon as crack propagation occurs. This can only be achieved using automatic strain control on a servo-controlled testing machine, where the strain is measured across the crack (Hudson, Crouch & Fairhurst 1972). If strain control is not used, catastrophic failure of the beam occurs.

Hardy et al also showed that the work of fracture of rock is not elastic, i.e. if a crack is propagated through a small distance and the load is then removed, the strain across the crack does not return to zero. Therefore, work is being done in addition to the work associated with creating new crack surfaces. . The non-elastic work changes the shape of the load-deflection graph, and also alters the stability conditions. In extreme cases, where the material shows a predominance of non-elastic work during crack propagation, the notched beam may become completely stable for most notch depths, as illustrated by Brown (1972).

Hardy et al suggested a procedure for separating the elastic and non-elastic energy terms. This can only be done if the compliance (y/F) is known for any crack length. In the absence of such knowledge, only the total fracture energy can be determined, and it is this energy which was measured by Nakayama (1965) and others.

The Griffith theory of brittle fracture was extended by Krech (1974) to inhomogeneous materials, such as rock. Krech postulated that

cracks within a volume of a specimen will extend within that volume where sufficient energy is available to extend the cracks. This is the same energy as measured by Nakayama and others. It is calculated as the area under a load-deflection graph divided by the nominal fracture area. Krech also suggested that the fracture topography would be similar for similar strain energy regimes for the same material. This latter suggestion has been borne out by many previous researchers, as shown by the constancy of the measured parameter, α_{eff}.

Krech used a servo-controlled testing machine, operating in strain control, to obtain complete load-deflection curves for several rock specimens under tension. He found that the fracture energy was essentially independent of the gauge length used to control the failure, but stability was more easily achieved for small gauge lengths. His conclusion was that fracture energy is a reproducible material constant.

Similar results were published by Krech and Chamberlain (1974). Also using a servo-controlled testing machine, they were able to determine the complete load-deflection curves for rock specimens in tension, compression, torsion and shear. The results show that the fracture energy is different for each mode of failure.

The papers described above have shown Griffith's theory of brittle fracture to be applicable to rocks and concrete. They show that the material fracture properties K_{1c}, $\mathcal{G}_{1c}$, α and α_{eff} are reproducible measurements in the laboratory tests.

All of the fracture tests described require an oblong-shaped specimen, either for a notched beam under bending or a double

cantilever. These methods are only suitable for concrete, where the specimens can be moulded into shape. For rocks, it is very difficult to shape oblong specimens, and the methods are certainly not suitable for testing a large number of samples. What is needed is a test which uses easily shaped specimens which can be mass-produced, and this thesis aims to develop such a test.

With the exception of a paper by Kaplan (1961), none of the authors have shown how fracture toughness testing can be used to give design guidance to engineers. This thesis will derive relationships which can directly apply fracture test results to practical design problems.

CHAPTER 3

The stress intensity factor, K_1, is derived for three proposed fracture toughness tests - a circumferentially notched round bar under bending or eccentric loading, and a slotted disc under diametral loading.

3.1 The stress intensity factor for a Circumferentially Notched Round Bar under Bending (CNRBB).

The stress intensity factor, K_1, for a CNRBB specimen can be calculated from a knowledge of the stress field in the specimen (fig. 3.1). The maximum tensile stress will occur at the notch root on the tensile side of the specimen. Therefore, cracking is likely to initiate at this point, and so it is only necessary to study the stress field in this small area.

It can be shown (Irwin 1960) that K_1 is related to the maximum stress at the root of a crack or notch by the relationship:-

$$K_1 = \lim_{\rho \to 0} \frac{1}{2} \sigma_m (\pi\rho)^{\frac{1}{2}} \qquad (3.1)$$

where σ_m = the maximum stress at the notch root,

ρ = the radius of curvature of the notch root.

The stresses at notch roots have been extensively studied by Neuber (1937) who derived an expression for σ_m for a CNRBB specimen. He expressed σ_m as the nominal stress (i.e. the stress which would occur without the notch) multiplied by a stress concentration factor (SCF). If the nominal stress is denoted by σ, and the SCF by S, then:-

$$K_1 = \lim_{\rho \to 0} \frac{1}{2} S\sigma (\pi\rho)^{\frac{1}{2}} \qquad (3.2)$$

Neuber considered two cases; that of a deep notch, and that of a shallow one. He assumed that the SCF for a shallow notch in a CNRBB specimen approximated to a shallow notch in a thin plate. Also, to facilitate computations, he considered the shallow notch as having an

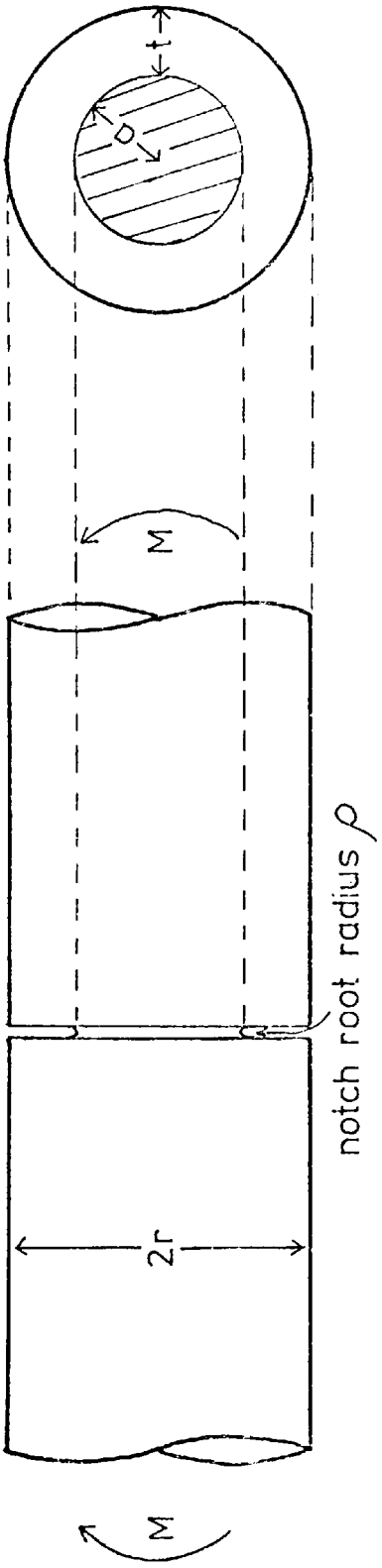

Fig 3.1

Circumferentially notched round bar under bending (CNRBB) specimen.

elliptical profile, and the deep one a hyperbolic profile. Denoting the SCF for a shallow notch as S_1, Neuber obtained the simple relationship:-

$$S_1 = 1 + 2\sqrt{\frac{t}{\rho}} \qquad (3.3)$$

where t and ρ are defined in figure 3.2.

For a deep notch Neuber obtained the relationship for the SCF, S_2:-

$$S_2 = \frac{3}{4}\cdot\frac{1}{N}\left(\sqrt{\frac{a}{\rho}+1}\right)\left(\frac{3a}{\rho} - \left(1 - \frac{2}{m}\right)\sqrt{\frac{a}{\rho}+1} + 4 + \frac{1}{m}\right) \qquad (3.4)$$

where:-

$$N = 3\left(\frac{a}{\rho}+1\right) + \left(1 + \frac{4}{m}\right)\sqrt{\frac{a}{\rho}+1} + \frac{1+\frac{1}{m}}{1+\sqrt{\frac{a}{\rho}+1}}$$

and 1/m = Poisson's ratio, and a and ρ are defined in figure 3.2.

The two expressions (3.3) and (3.4) can be combined to give the SCF for an arbitrarily deep notch:-

$$S = 1 + \frac{(S_1 - 1)(S_2 - 1)}{\sqrt{(S_1 - 1)^2 + (S_2 - 1)^2}} \qquad (3.5)$$

This expression is for a notch which gradually changes profile from elliptical to hyperbolic as the notch depth increases. In practice, an expression is needed for a notch of constant profile, whatever its depth.

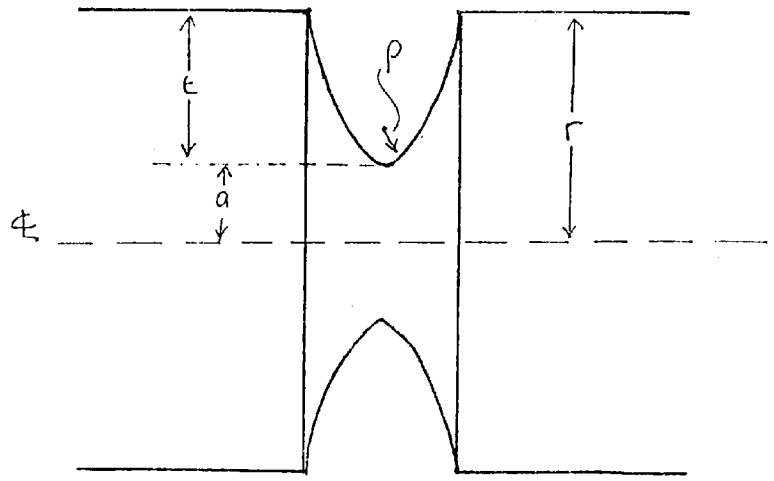

Fig 3.2 Detail of a notch in a CNRBB specimen defining notch parameters.

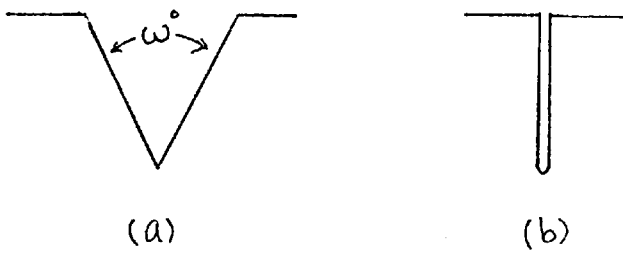

Fig 3.3 The two alternative straight-sided notch profiles.

There are two notch profiles which are suitable for practical specimens; either with straight sides and an included angle (figure 3.3a) or with parallel sides (figure 3.3b). The first option would be suitable because a cutting tool could be shaped to give a sharp point at the notch root, so that equation (3.1) would be valid.

Neuber devised a procedure whereby equations (3.3) and (3.4) could be amended to include the effect of straight sides to the notches. He introduced a parameter called a notch factor. This factor can be calculated for both straight and curved notches, and so the relationship between the profiles can be obtained. For a deep notch, the notch factor for a curved notch N_c of hyperbolic profile is:-

$$N_c = \frac{\sqrt{\frac{a}{\rho}}}{\mathrm{Tan}^{-1}\sqrt{\frac{a}{\rho}}} \qquad (3.6)$$

For a deep notch with straight sides, including a flank angle ω, the notch factor N_s is given by:-

$$N_s = \left(\frac{(2n)!}{(n!)^2}\right)^{\frac{1}{2n+1}} \left(\frac{1+\sqrt{\frac{2n+2}{2n+3}}}{2\pi n} \cdot \frac{a}{\rho}\right)^{\frac{2n}{2n+1}} \qquad (3.7)$$

where $n = \frac{1}{2}\left(1 - \frac{\omega}{2\pi}\right)$

Neuber suggested that for a given flank angle, the ratio a/ρ could be adjusted so that equation (3.4) is still valid. If a/ρ and ω are substituted in equation (3.7) to give a value for N_s, the a/ρ in equation (3.6) can be calculated so that $N_c = N_s$. This new value for a/ρ can be inserted in equation (3.4) to give S_2.

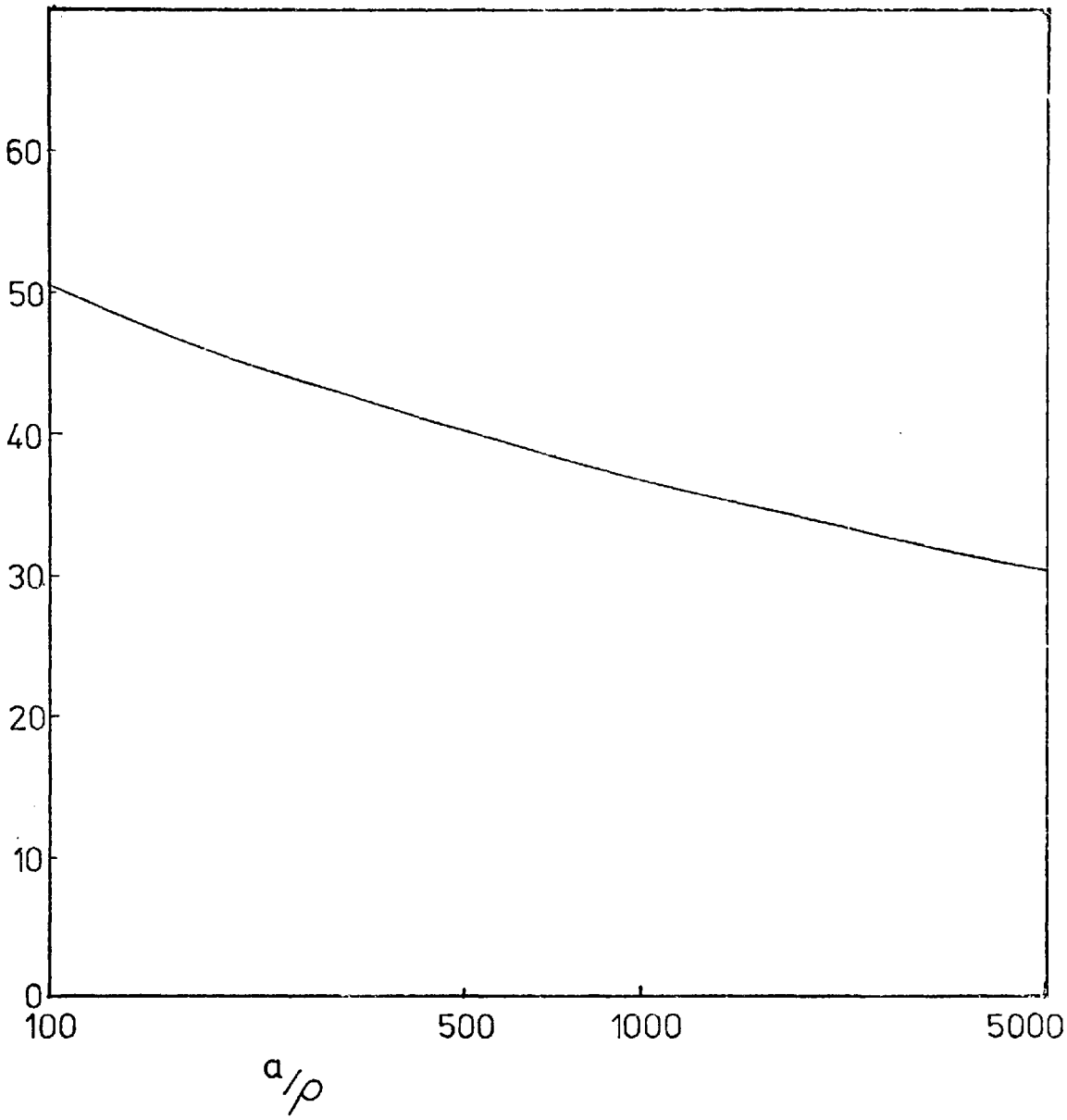

Fig 3.4 Graph of ω vs a/ρ for which the notch factor for a straight-sided notch equals that for a hyperbolic one.

In practical specimens the ratio a/ρ is not known exactly and so the alternative is to try to choose a flank angle ω so that $N_c = N_s$ for any value of a/ρ. Figure 3.4 is a graph of ω vs a/ρ for which $N_c = N_s$. It can be seen that ω is not constant for any a/ρ. Therefore it is not possible to use a straight-sided notch, with an included angle because the value of S_2 for such a configuration is not calculable.

The other practical alternative is to use a parallel-sided notch. Neuber showed that the maximum stress at the root of such a notch is the same as that for a deep, hyperbolic one. The stress intensity factor for a shallow, parallel-sided notch in a rectangular plate has been derived by Bowie (1964). He obtained the relationship:-

$$K_1 = 1.12\sqrt{\pi t}\ \sigma \qquad (3.8)$$

Unfortunately, in the literature, confusion often arises because some authors use the expression $\sqrt{\pi}$ in the equations for K_1 and others omit it. Bowie omitted $\sqrt{\pi}$, so in his paper, the value for K_1 is different from equation (3.8).

Equation (3.8) can be compared with equation (3.1). If equation (3.3) is amended to:-

$$S_1 = 1 + 2.24\sqrt{\frac{t}{\rho}} \qquad (3.9)$$

then substitution of S_1 into equation (3.2) gives Bowie's result. Thus S is known for parallel-sided notches for both the deep and shallow cases.

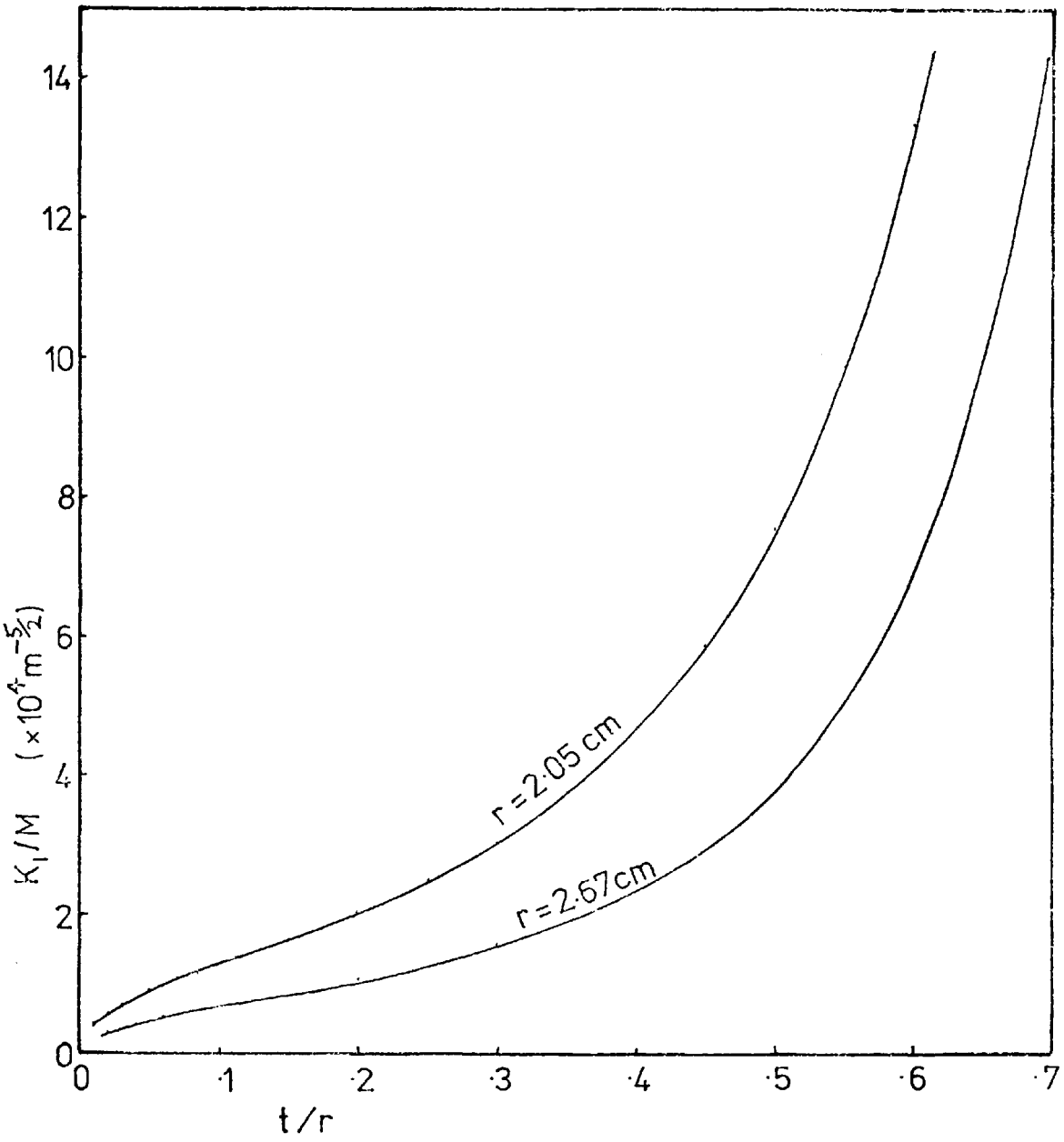

Fig 3.5 Graphical representation of equation (3.12)

Substitution of the expressions for S_1 and S_2 into equation (3.5), and then substituting the result into equation (3.2) gives (see appendix 3a):-

$$K_1 = \frac{\sigma}{2}\pi^{\frac{1}{2}} \frac{3}{4}\sqrt{\frac{4a}{4 + .448\frac{a}{t}}} \qquad (3.10)$$

The nominal maximum stress in the bar in the absence of a notch is given by:-

$$\sigma = \frac{4M}{\pi a^3} \qquad (3.11)$$

where M = bending moment.

Finally, substitution of this equation gives the expression for K_1 for a parallel-sided notch of arbitrary depth:1

$$K_1 = 3M\sqrt{\frac{1}{\pi a^5(4 + .448\frac{a}{t})}} \qquad (3.12)$$

This result has been derived by Harris (1967), but he used notches shaped as in figure 3.3a. Consequently, his result is not strictly true for the specimen he considered.

The function K_1/M is plotted in figure 3.5 for specimen diameters of 4.05 and 5.35 cm. These sizes have been used extensively in experiment described in Chapter 4. The parameters t and r are defined in the same figure. The graph shows that the function varies rapidly for values of t/r less than 0.1 or greater than 0.5. Consequently, to minimise errors in the measurement of K_1/M due to errors in the measurement of t or a, it is advisable to keep t/r between these two values.

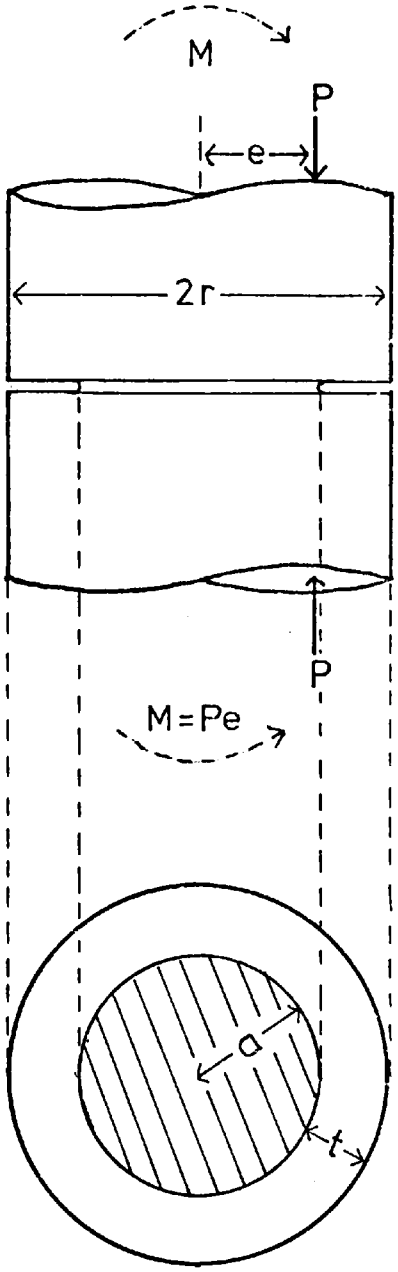

Fig 3.6 Circumferentially notched round bar under eccentric loading (CNRBEL) specimen

3.2 The stress intensity factor for a Circumferentially Notched Round Bar under Eccentric Loading (CNRBEL).

When a cylindrical specimen of an elastic material is subjected to an eccentric compressive load along its axis, the resultant forces on the specimen can be resolved into two components (fig. 3.6). The components are a compressive load, acting along the axis of the cylinder, and a bending moment. If the eccentricity of the load is sufficient, a tensile stress will develop in the specimen, and thus provide conditions for the opening of a crack in a mode 1 situation. A similar arrangement was used by Liebowitz (1969) who used notched columns of aluminium under eccentric loading to measure K_{1c}.

The stress intensity factor for a CNRBEL specimen is composed of two parts:-

$$K_1 = K_{1B} - K_{1T} \qquad (3.13)$$

where K_{1B} is the stress intensity factor for the bending stress field, and K_{1T} is the same for the compressive field. The second term is negative because it represents forces causing crack closure. The term K_{1B} has already been derived in section 3.1, and remains unchanged. The analysis concerning the notch shape still applies, and so any formulae derived for CNRBEL specimens will assume parallel-sided notches.

The stress intensity factor K_{1T} can be derived from Neuber's (1937) expressions for stress concentration factors in the same manner as for K_{1B} (see appendix 3b). The final result for K_{1T} is:-

$$K_{1T} = \sigma_n \sqrt{\frac{ta}{4t + 0.8a}} \qquad (3.14)$$

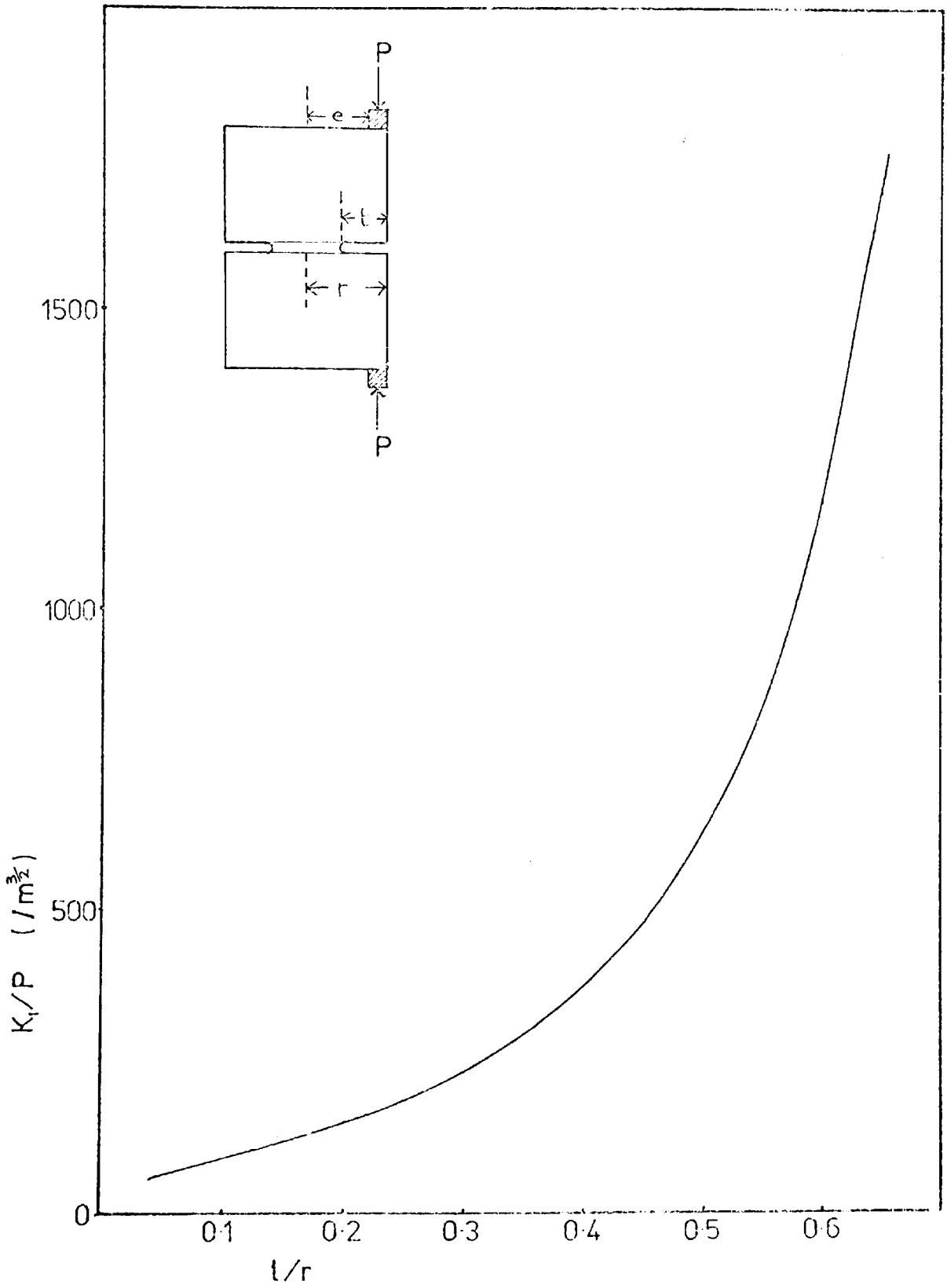

Fig 3.7 Graphical representation of equation (3.16) and definition of specimen parameters

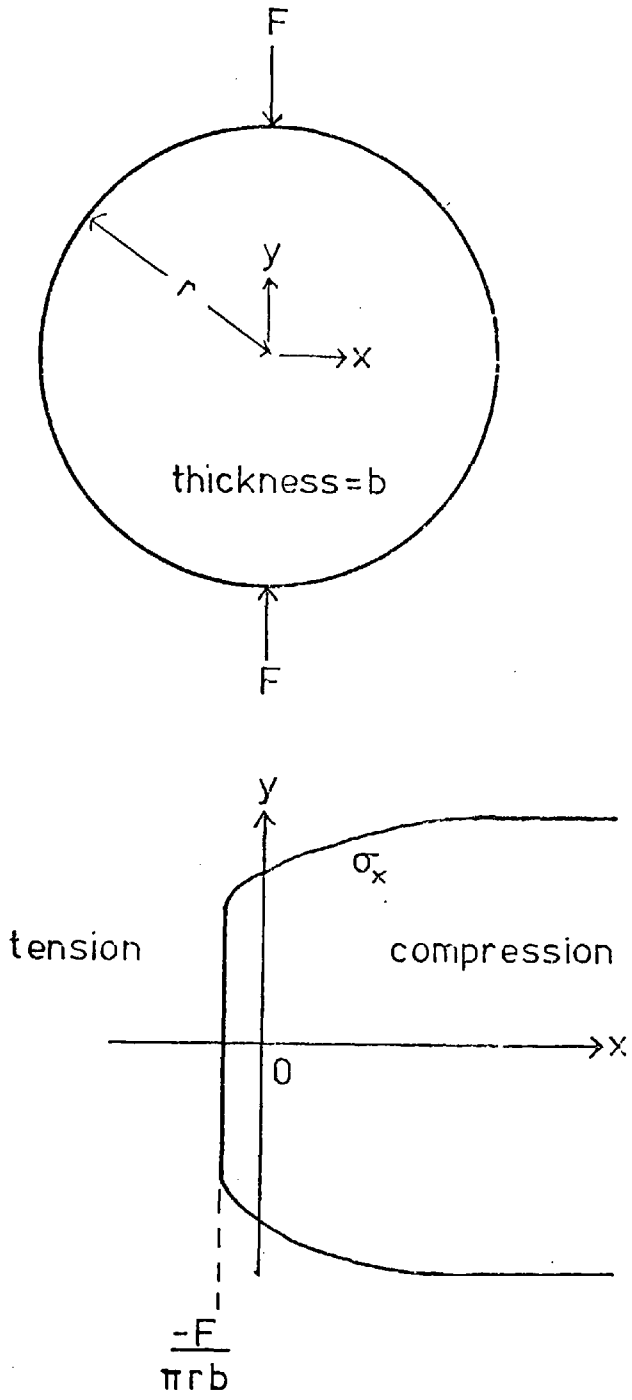

Fig 3.8 The diametral compression of a disc and the distribution of stress, σ_x, along the diameter $x = 0$.

where t and a are defined in figure 3.6 and $_n$ is the nominal compressive stress. The total expression for K_1 becomes:-

$$K_1 = 3M\sqrt{\frac{1}{\pi a^5(4+.448\frac{a}{t})}} - \sigma_N\sqrt{\frac{\pi t a}{4t+0.8a}} \qquad (3.15)$$

The bending moment due to the eccentricity of the load is given by M = Pe (fig. 3.6) and the nominal compressive stress, at the section of the circumferential notch is $\sigma_N = P/\pi a^2$. The final result for K_1 is:-

$$K_1 = P\left\{3e\sqrt{\frac{1}{\pi a^5(4+.448\frac{a}{t})}} - \sqrt{\frac{1}{\pi a^3(4+.8\frac{a}{t})}}\right\} \qquad (3.16)$$

The expression K_1/P is plotted in figure 3.7 for a specimen diameter of 5.35 cm., and e = 0.6 cm. These dimensions were used for experiments described in Chapter 4.

3.3 The stress intensity factor for a Slotted Disc under Diametral Loading

A loading arrangement which is used extensively for indirect tensile testing of rocks and concrete is the diametral compression of cylinders or discs, as in figure 3.8 (Jaeger & Cook 1969). As a compressive load, F, is applied, a tensile stress develops perpendicular to the direction of loading. The tensile stress σ_T is given (to a first approximation) by

$$\sigma_T = \frac{F}{\pi r b}$$

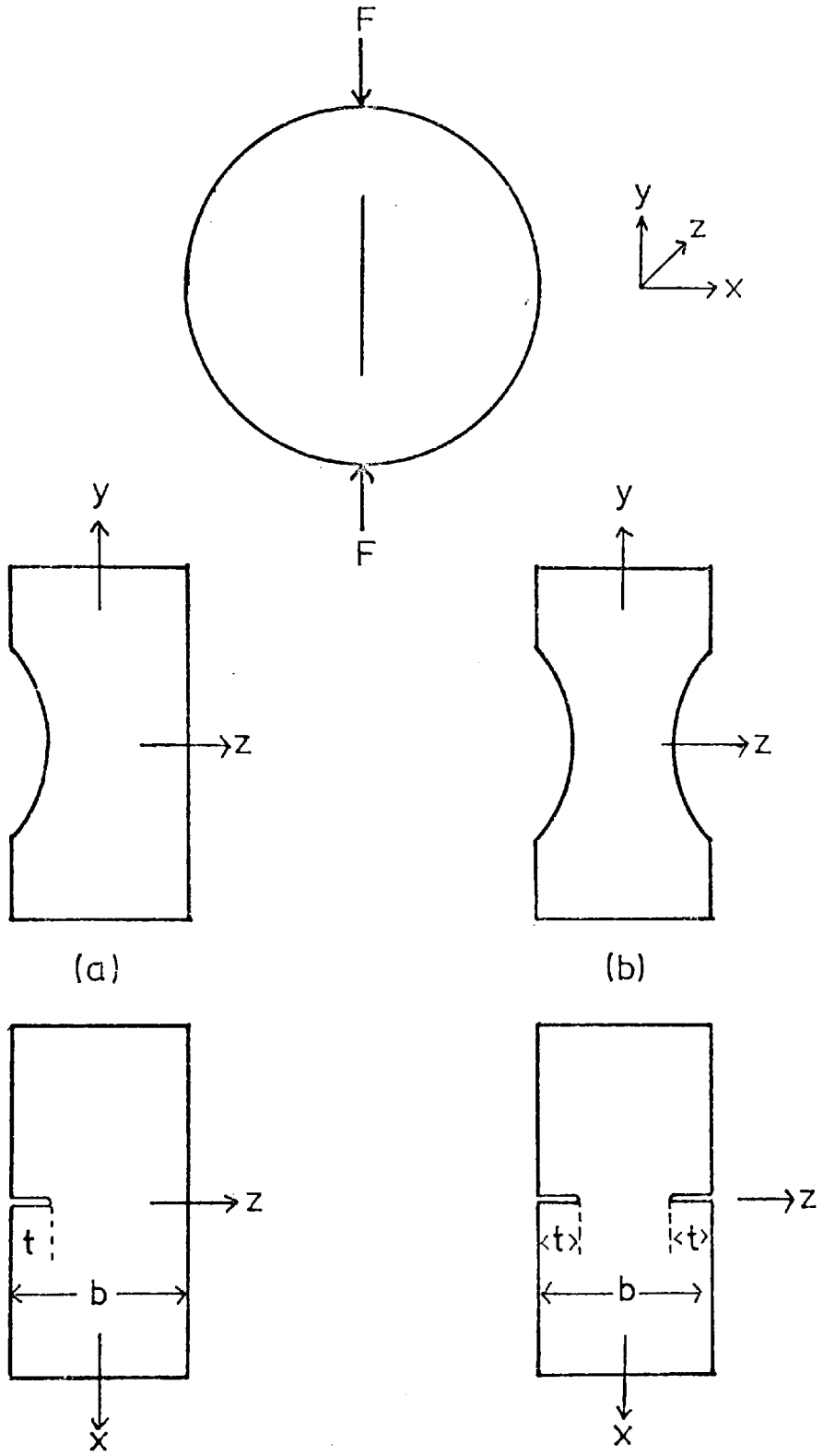

Fig 3.9 The slotted disc under diametral loading (SDDL) specimen, and cross-sections for a) one slot, and b) two slots.

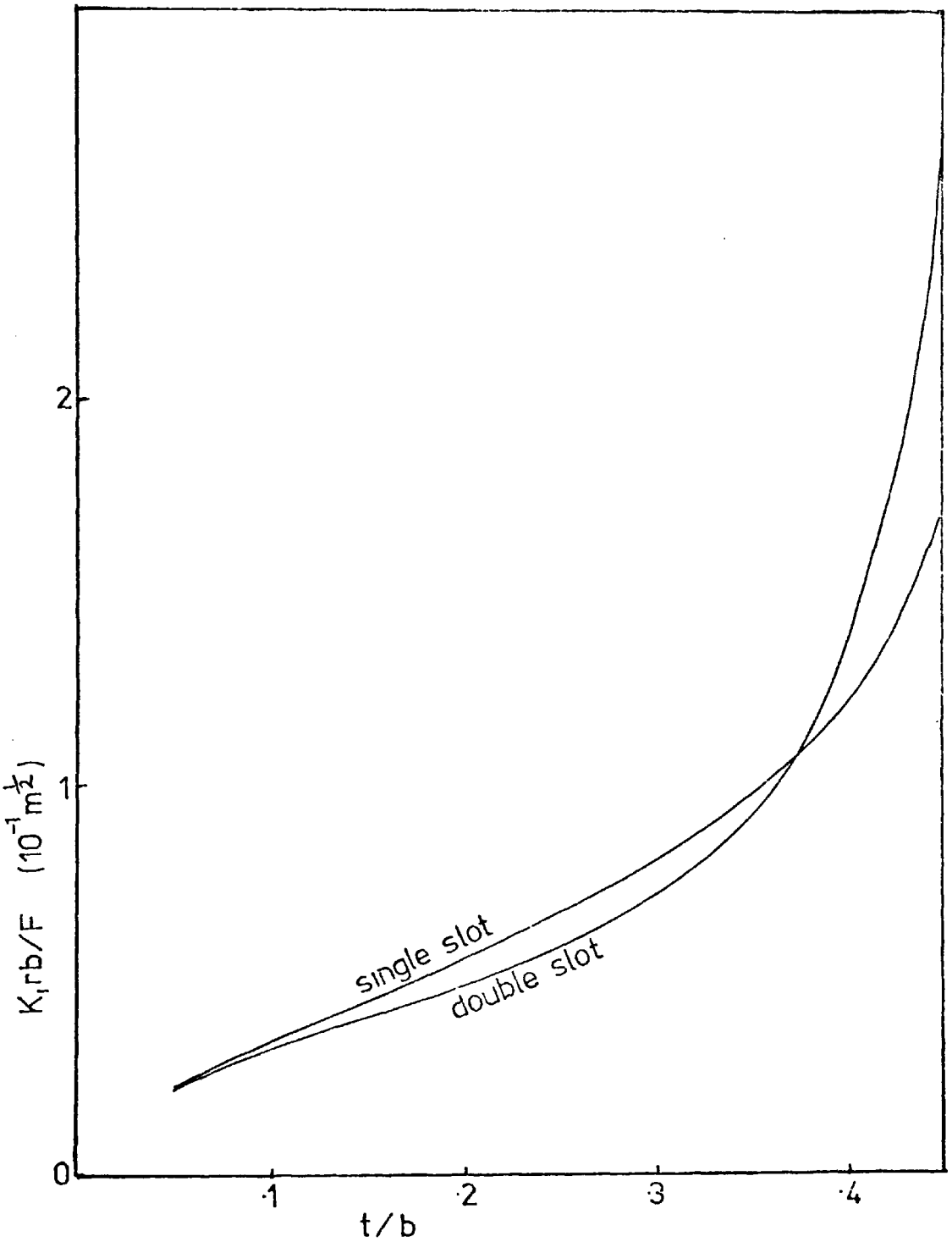

Fig 3.10 Graph of $K_1 rb/F$ vs t/b for SDDL specimens with one or two slots.

where r is the radius of the specimen. If a crack were present along the diameter of the specimen, parallel to the loading direction, it would open under mode 1 conditions.

A slot, simulating a crack, can be cut either on one, or both sides of a disc of rock or concrete. Figure 3.9 illustrates the two possibilities, and also depicts cross-sections taken along the diameter of the specimens, perpendicular to the direction of loading. The resultant sections are similar to the stress situations for finite, notched sheets under a tensile load.

The stress intensity factors for a single or double cracked sheet are given by Paris and Sih (1964) and will be denoted by K_{1S} and K_{1D} respectively. Using the notation of figure 3.9:-

$$K_{1S} = \sigma_T(\pi)^{\frac{1}{2}} g(\frac{t}{b}) \qquad (3.18)$$

$$K_{1D} = \sigma_T(\pi t)^{\frac{1}{2}} (\frac{b}{\pi t} \tan \frac{\pi t}{b})^{\frac{1}{2}} h(\frac{t}{b}) \qquad (3.19)$$

where g(t/b), h(t/b) are polynomial functions of t/b. The functions $K_{1S}rb/F$ and $K_{1D}rb/F$ are plotted against t/b for an arbitrary disc thickness of 25 mm in figure 3.10.

The expressions for K_1, derived above, assume that $\rho \to 0$ as in equation (3.1), but in practical specimens ρ is finite because the notches are cut with a saw. However, there is evidence to suggest that, for a brittle material, the difference between a finite and 'zero' radius is small. Brown (1972) measured K_{1c} for concrete and found the values for a finite radius notch, as cut by a saw, and those for a fatigue crack (a natural crack) were identical. Shoemaker (1964)

experimented with notches in mild steel at very low temperatures (-164 C). At low temperatures, steel behaves as a very brittle material and his results showed that the failure load of steel specimens was independent of notch radius for radii less than 0.02 cm.

Evans (1946) showed that cracking occurred in concrete at loads very much less than the failure load. It is likely that a finite radius notch acts as a nucleus for microcracking so that when the failure load is reached the crack is propagating from a 'zero' radius notch, and equation (3.1) is then valid.

Appendices

Derivation of the stress intensity factors for the CNRBB and CNRBEL testing arrangements.

3a Derivation of the stress intensity factor for CNRBB specimens

Substitution of equation (3.5) into (3.2) gives:-

$$K_1 = \lim_{\rho \to 0} \frac{1}{2}\sigma(\pi\rho)^{\frac{1}{2}} \quad 1 + \frac{(S_1-1)(S_2-1)}{\sqrt{(S_1-1)^2+(S_2-1)^2}} \qquad (3a.1)$$

$$= \lim_{\rho \to 0} \frac{1}{2}\sigma\pi^{\frac{1}{2}} \; \rho^{\frac{1}{2}}+\rho^{\frac{1}{2}}.\frac{\rho^{\frac{1}{2}}}{\rho^{\frac{1}{2}}\sqrt{(S_1-1)^2+(S_2-1)^2}} \; \frac{(S_1-1)(S_2-1)}{} \qquad (3a.2)$$

$$= \lim_{\rho \to 0} \frac{1}{2}\sigma\pi^{\frac{1}{2}}. \quad \frac{S_1\rho^{\frac{1}{2}}, S_2\rho^{\frac{1}{2}}}{\sqrt{(S_1\rho^{\frac{1}{2}})^2+(S_2\rho^{\frac{1}{2}})^2}} \qquad (3a.3)$$

Note that terms in $\rho^{\frac{1}{2}} \to 0$ as $\rho \to 0$.

From equation (3.9)

$$S_1\rho^{\frac{1}{2}} = \rho^{\frac{1}{2}}+2.24\rho^{\frac{1}{2}}\sqrt{\frac{t}{\rho}}$$

and:-

$$\lim_{\rho \to 0} S_1\rho^{\frac{1}{2}} = 2.24t^{\frac{1}{2}} \qquad (3a.4)$$

Also:-

$$S_2\rho^{\frac{1}{2}} = S_2\rho^{\frac{1}{2}}.\frac{\rho}{\rho} = \frac{3\rho^{\frac{1}{2}}}{4}.\frac{\rho}{N\rho}\left(\sqrt{\frac{a}{\rho}+1}\right)\left(\frac{3a}{\rho}-\left(1-\frac{2}{m}\right)\sqrt{\frac{a}{\rho}+1}+4+\frac{1}{m}\right) \qquad (3a.5)$$

$$N\rho = 3(a+\rho) + (\rho+\frac{4\rho}{m})\sqrt{\frac{a}{\rho}+1} + \frac{\rho+\frac{\rho}{m}}{1+\sqrt{\frac{a}{\rho}+1}}$$

$$\therefore \quad \lim_{\rho\to 0} N\rho = 3a. \qquad (3a.6)$$

Substituting for N

$$S_2\rho^{\frac{1}{2}} = \frac{3\rho^{\frac{1}{2}}}{4.3a}\left(\sqrt{a+\rho}\right)\left(\frac{3a}{\rho^{\frac{1}{2}}}-\left(1-\frac{2}{m}\right)\sqrt{a+\rho}+4\rho^{\frac{1}{2}}+\frac{\rho^{\frac{1}{2}}}{m}\right)$$

and

$$\lim_{\rho\to 0} S_2\rho^{\frac{1}{2}} = \frac{3a^{\frac{1}{2}}}{4} \qquad (3a.7)$$

Substitution of equations (3a.4) and (3a.7) into (3a.3) gives:-

$$K_1 = \frac{1}{2}\sigma\pi^{\frac{1}{2}} \cdot \frac{2.24.\frac{3}{4}\sqrt{at}}{\sqrt{2.24^2 t+\frac{9a}{16}}}$$

or:-

$$K_1 = \frac{1}{2}\sigma\pi^{\frac{1}{2}}.\frac{3}{4}\sqrt{\frac{4a}{4+.448\frac{a}{t}}} \qquad (3a.8)$$

which is the result appearing in equation (3.10).

3b Derivation of the stress intensity factor for CNRBEL specimens

Neuber (1937) assumed that, for a shallow notch, the stress concentration factor, S_1, for a circumferentially notched round specimen under tension was the same as that for one under bending, i.e.:-

$$S_1 = 1 + 2.24\sqrt{\frac{t}{\rho}} \qquad (3b.1)$$

For a deep notch, S_2 is given by:-

$$S_2 = \frac{1}{N}\left[\frac{a}{\rho}\sqrt{\frac{a}{\rho}+1} + \left(\frac{1}{2}+\frac{1}{m}\right)\frac{a}{\rho} + \left(1+\frac{1}{m}\right)\left(\sqrt{\frac{a}{\rho}+1}+1\right)\right] \qquad (3b.2)$$

where

$$N = \frac{a}{\rho} + \frac{2}{m}\sqrt{\frac{a}{\rho}+1} + 2$$

and the notation is the same as for CNRBB specimens. Using equation (3a.3) from appendix 3a:-

$$K_1 = \lim_{\rho\to 0} \frac{\sigma\pi^{\frac{1}{2}}}{2} \frac{S_1\rho^{\frac{1}{2}}.S_2\rho^{\frac{1}{2}}}{\sqrt{(S_1\rho^{\frac{1}{2}})^2+(S_2\rho^{\frac{1}{2}})^2}} \qquad (3b.3)$$

Again,

$$\lim_{\rho\to 0} S_1\rho^{\frac{1}{2}} = 2.24\sqrt{t} \qquad (3b.4)$$

$$\lim_{\rho\to 0} S_2\rho^{\frac{1}{2}} = \frac{1}{N\rho}\left[a\sqrt{a+\rho}+\left(\frac{1}{2}+\frac{1}{m}\right)a\rho^{\frac{1}{2}}+\left(\rho+\frac{\rho}{m}\right)\left(\sqrt{a+\rho}+\rho^{\frac{1}{2}}\right)\right] \qquad (3b.5)$$

$$\lim_{\rho\to 0} N\rho = a \qquad (3b.6)$$

Therefore,

$$\lim_{\rho \to 0} S_2 \rho^{\frac{1}{2}} = \sqrt{a} \qquad (3b.7)$$

Substituting equations (3b.4) and (3b.7) into equation (3b.3) gives:-

$$K_1 = \frac{\sigma \pi^{\frac{1}{2}}}{2} \sqrt{\frac{2.24\sqrt{ta}}{2.24^2 t + a}}$$

or,

$$K_1 = \sigma \sqrt{\frac{\pi t a}{4t + 0.8a}} \qquad (3b.8)$$

which is the result appearing in equation (3.15).

CHAPTER 4

Three new experimental methods are described in which K_{Ic} is measured for concrete and rocks. The results from the three methods are compared, and the relative merits of the tests are discussed.

4.1 Introduction

The objective of the experimental work described in the thesis was to develop suitable fracture tests for rock. Three new testing arrangements, as described in chapter 3, were investigated and developed to varying degrees.

The expressions for K_I for all three proposed testing arrangements have many variables in them. For example, for the CNRBB test (equation 3.12), K_I is a function of specimen diameter and notch depth. There are also variables which might affect the measured value of K_{Ic}, and are not implied in the expression. These are testing speed, mode of test (load, strain or displacement control), condition of sample (wet or dry), temperature, loading span, and other variables which affect any mechanical testing.

It would obviously need a very large development program, well outside the scope of this project, to assess the effect of all these parameters and to formulate a standard test procedure. Instead, the test program described in this chapter was designed to investigate some of the variables, and to establish the applicability of the new tests to rock.

To investigate the effect of some of the test variables described above, it is necessary to use a material which has relatively constant fracture properties, but behaves in a manner similar to rock. Such a material is concrete. The review of literature in chapter 2 illustrates the close connection between the properties of rock and concrete. Furthermore, concrete can be very easily prepared in large quantities and with reasonably reproducible properties. The results from fracture tests on rocks and concrete show that concrete is a far more homogeneous

material and is more suitable for a test development program.

4.2 Specimen Preparation

The mixes of concrete used in the experimental program was considered to be unimportant. To study the effect of a change in one experimental variable, all samples were taken from the same concrete mix, and tested in batches, each batch with one change in variable. Because only changes in the measured K_{1c} were important, and not K_{1c} itself, the actual value for any particular mix was irrelevant to the present test program.

The grain size of most rocks is very small compared to a typical concrete. Therefore, very fine aggregates (0.6 - 2.4 mm) were used so that the concrete would most closely simulate the behaviour of most rocks. Furthermore, by using a fine-grained material the size of the specimens can be kept to a minimum and ensures economy of material. The expression for K_1 derived in chapter 3 assumes an homogeneous, isotropic material. A fine-grained material more closely approaches this ideal. If, for example, a large piece of aggregate were positioned at the notch root, at the point of initiation of a crack, then the resulting measurement of K_{1c} would not necessarily be that of the specimen as a whole.

The concrete was a mixture of 4.5:2.7:1 aggregate:cement:water. The aggregate size was varied for each mix and depended upon the availability of a particular size. The concrete was cast into standard beam moulds (15 x 15 x 75 cm) and compacted on a vibrating table. Care was taken to remove most air bubbles, but inevitably some were visible in all specimens. The concrete was cured, under water, for 28 days.

The first set of experiments were conducted on specimens of approximately 4.1 cm diameter, and the data showed that the deviations of the results for such specimens was acceptable. Using such a specimen size, at least 30 samples could be taken from one concrete mix.

Cores were cut from the concrete beams using a Qualters & Smith R3 radial drill (plate 4.1). The diamond-tipped corers were rotated at 260 r.p.m. and water was used as a lubricant. The water was filtered through gravel in a box under the beam and recirculated. Each core was cut in the same direction, relative to the beam, to ensure that the effects of any anisotropy would be minimised.

The cylindrical cores were notched on a lathe using a tool-post grinder (plate 4.2). Six inch diameter diamond-tipped saw blades were used, rotating at 975 r.p.m. and the cores were simultaneously turned at 125 r.p.m. For most experiments, a 0.022" (0.056 cm) wide blade was used but for some later experiments it was superceded by a 0.01" (0.025 cm) wide blade. For the first three concrete mixes, additional notches were cut 0.06 cm deep and 2.5 cm either side of the central deep notch. The extra notches were to facilitate attachment of a strain extensometer. Water, with a small amount of soluble oil, was used as a lubricant, and the specimens were left for at least 7 days to dry at room temperature.

4.3 Testing Rig

Because of the small size of the specimens, a rig was designed to ensure that the specimens were loaded in the same way for each experiment (plate 4.3). Two pieces of 0.25" thick Perspex

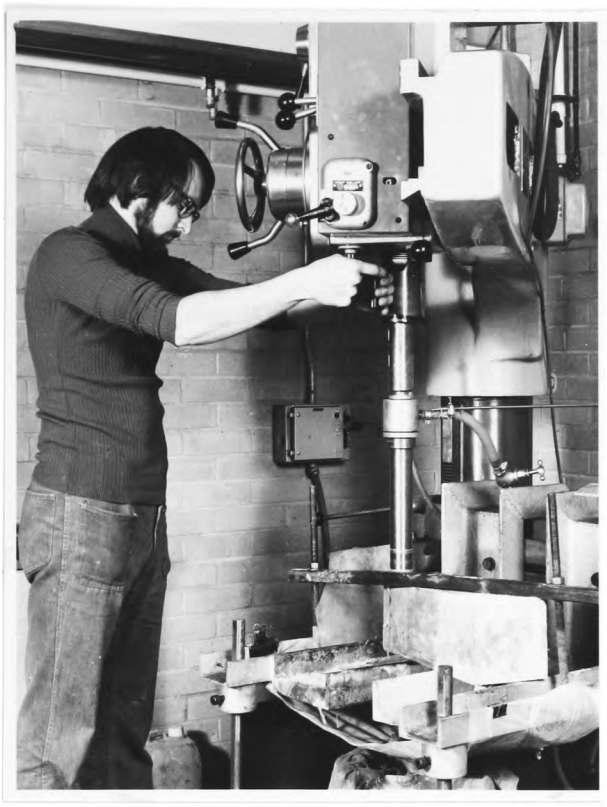

Plate 4.1

Plate 4.2

were drilled to hold steel rollers in place for 4-point loading. It is not possible to use 3-point loading for CNRBB tests because one of the loading points would be on the circumferential notch, causing local failure. The four 0.375" steel rods were held in place to give a major loading span of 10 cm and a minor one of 0.8 cm. The spans were chosen arbitrarily to suit the size of cores drilled from the concrete beams.

The holes in the Perspex holders were slightly elongated horizontally so that the rollers were free to move as the specimens deformed. Elastic bands, threaded through small holes in the Perspex were used to hold the rollers in place at the start of the experiment. The top two rollers were free to move horizontally (towards each other) and vertically, and had two notches ground in each as shown in plate 4.3 The notches ensured that the elastic bands were not loaded by the machine and thereby absorb energy.

An apparatus was designed to facilitate measurement of the diameter of a CNRBB specimen inside the notch. Two pieces of 0.5" thick Perspex were bolted together to form a channel for two sliding blocks (plate 4.4). The two blocks hold razor blades which are fixed vertically and can be clamped any distance apart. The specimen is placed between the two blocks, as shown in the photograph, and the razor blades inserted in the notch. A micrometer is then placed on the outside of the blocks and a measurement made. To calibrate the apparatus, a metal bar of known diameter was put in between the two razor blades and a conversion factor was obtained. For a 4.1 cm diameter specimen, a 75-100 mm micrometer is used and the distance between the razor blades is given as the micrometer reading plus 2.44 cm.

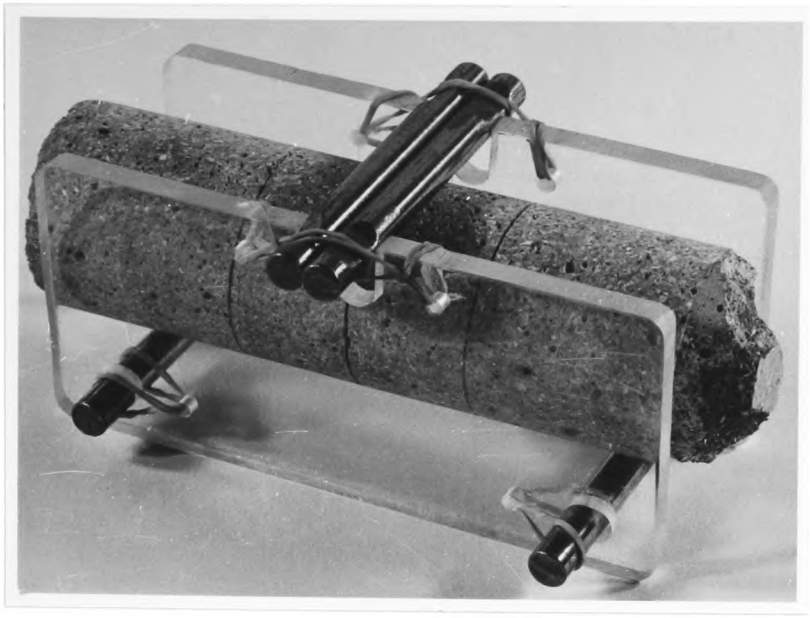

Plate 4.3

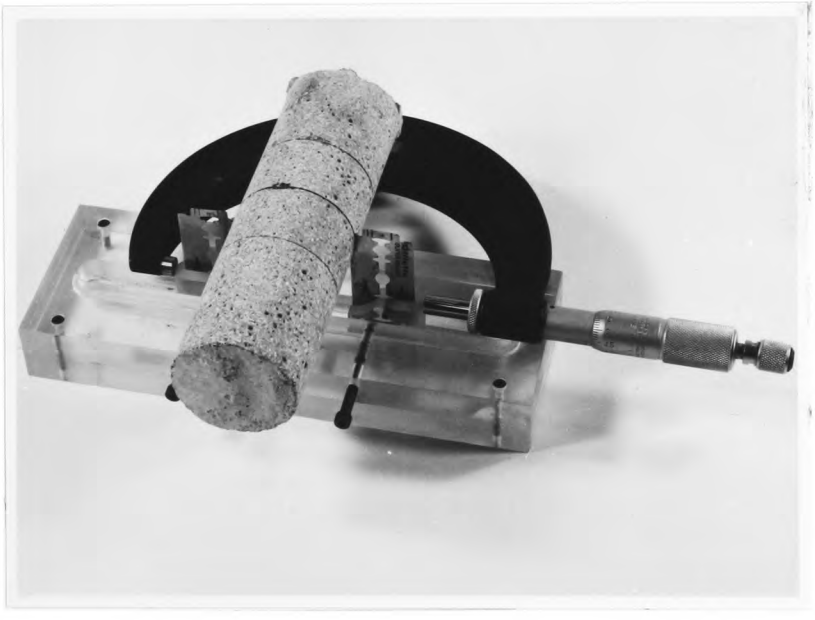

Plate 4.4

4.4 Testing Procedure for CNRBB

To conduct a CNRBB fracture test, a specimen is positioned in the Perspex rig as shown in plate 4.5. A vertical line has been scribed on the centre of the rig which can be used to centralise the deep notch. The whole apparatus is then placed in the testing machine between two flat platens. The two bottom rollers are supported on two billets of steel as shown in the photograph.

An Instron 1251 testing machine was used for all experiments (plate 4.6), but because of the relatively low failure load (less than 1 kN), it was necessary to use a more sensitive load cell than that normally used. It is a long and tedious process to replace the fitted load cell by another, and so fitments were made so that a sensitive load cell can be simply clamped in the jaws of the machine. An extension lead was made so that the lead which is normally connected to the fitted load cell can be connected to the sensitive cell. The modifications greatly expedited CNRBB testing.

Preliminary experiments showed that CNRBB specimens failed catastrophically, or very nearly so, when the Instron was used as a 'stiff' testing machine. Moavenzadeh and Kuguel (1969) pointed out that if the specimen failed catastrophically, then the measured fracture energy (i.e. the area under the load-deflection curve) would be excessive. Therefore, the CNRBB experiments were carried out using servo-controlled loading.

4.5 Servo-controlled Testing

Nakayama (1965), Friedman, Handin & Alani (1971) and others emphasised that crack propagation has to be stable to make a valid

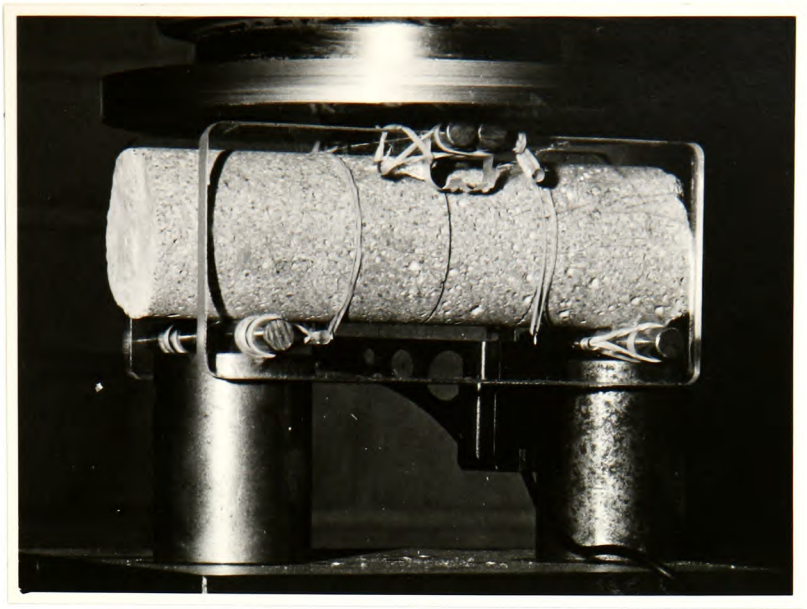

Plate 4.5

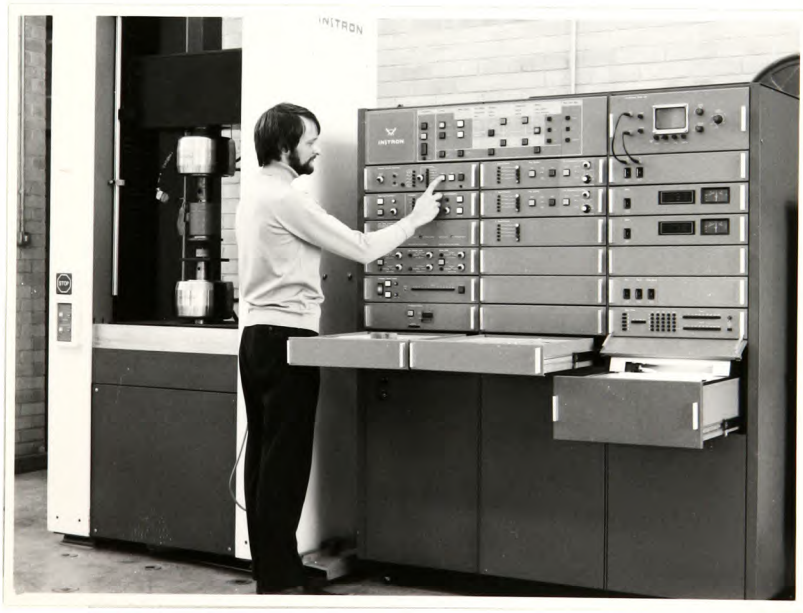

Plate 4.6

measurement of fracture surface energies. The theory of 'soft', 'stiff' and servo-controlled testing machines has been well explained by Hudson, Crouch & Fairhurst (1972).

For any testing machine, let k_m be the machine stiffness, (i.e. the slope of the load-deflection graph in the absence of any specimen), and $f'(d_s)$ the slope of the load-deflection graph for any specimen, as defined in Figure 4.1. Then the system is stable if:-

$$k_m + f'(d_s) > 0 \qquad (4.1)$$

The machine stiffness k_m is always positive, so the stability of the system largely depends upon the sign of $f'(d_s)$. Figure 4.2 shows load-deflection graphs for two test specimens, A and B. Specimen A is described by Hudson et al as of Class I type, and B as Class II. After failure, the slopes $f'(d_s)$ of the graphs are negative. Also included in the figure is the machine stiffness k_m. For an infinitely stiff machine, $k_m \to \alpha$ and the specimen can unload along the line C-D. For specimen A, $|f'(d_s)| < k_m$ and the system is stable. For specimen B, $|f'(d_s)| > k_m$ and the system is unstable. The shaded area in the figure denotes the energy measured on the load-deflection graph in excess of the true amount.

For a beam, the load-deflection graph as shown by Hardy, Hudson and Fairhurst (1973) is of Class II behaviour, and so even a stiff testing machine cannot provide stability. Hudson et al showed that if the strain across an opening crack is used to control the rate of loading of a specimen then stability can be obtained. Figure 4.3 is a block diagram of a servo-controlled testing system. For strain control, the feedback signal (s) is the output from a strain extensometer. This system was used to control the loading of CNRBB specimens for the first group of experiments.

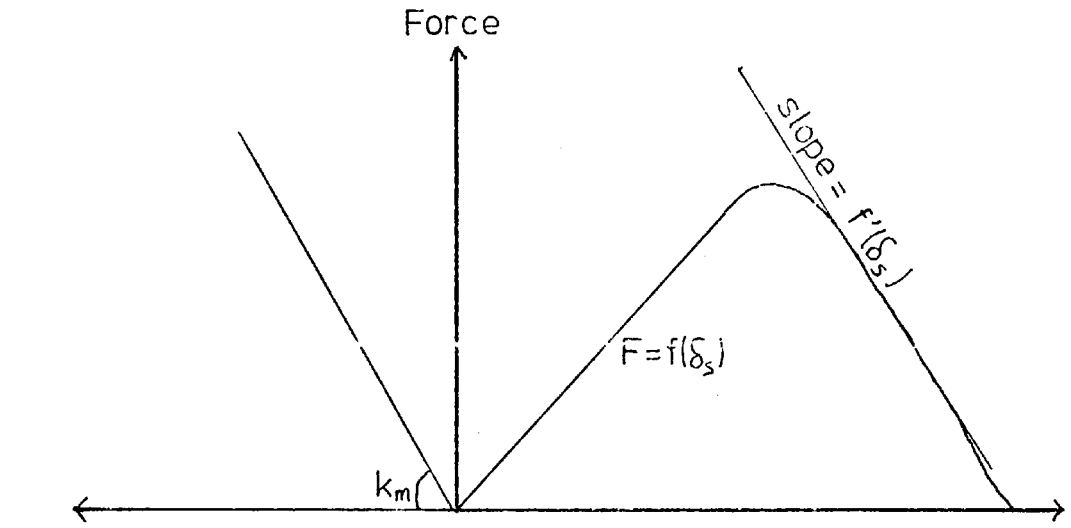

Fig4·1 Machine and specimen force-displacement curves.

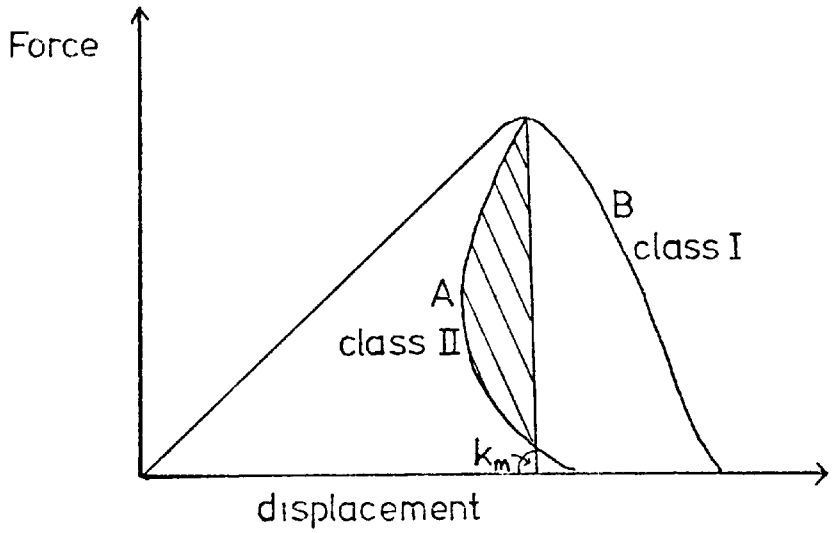

Fig4·2 Classification of specimen failure behaviour.

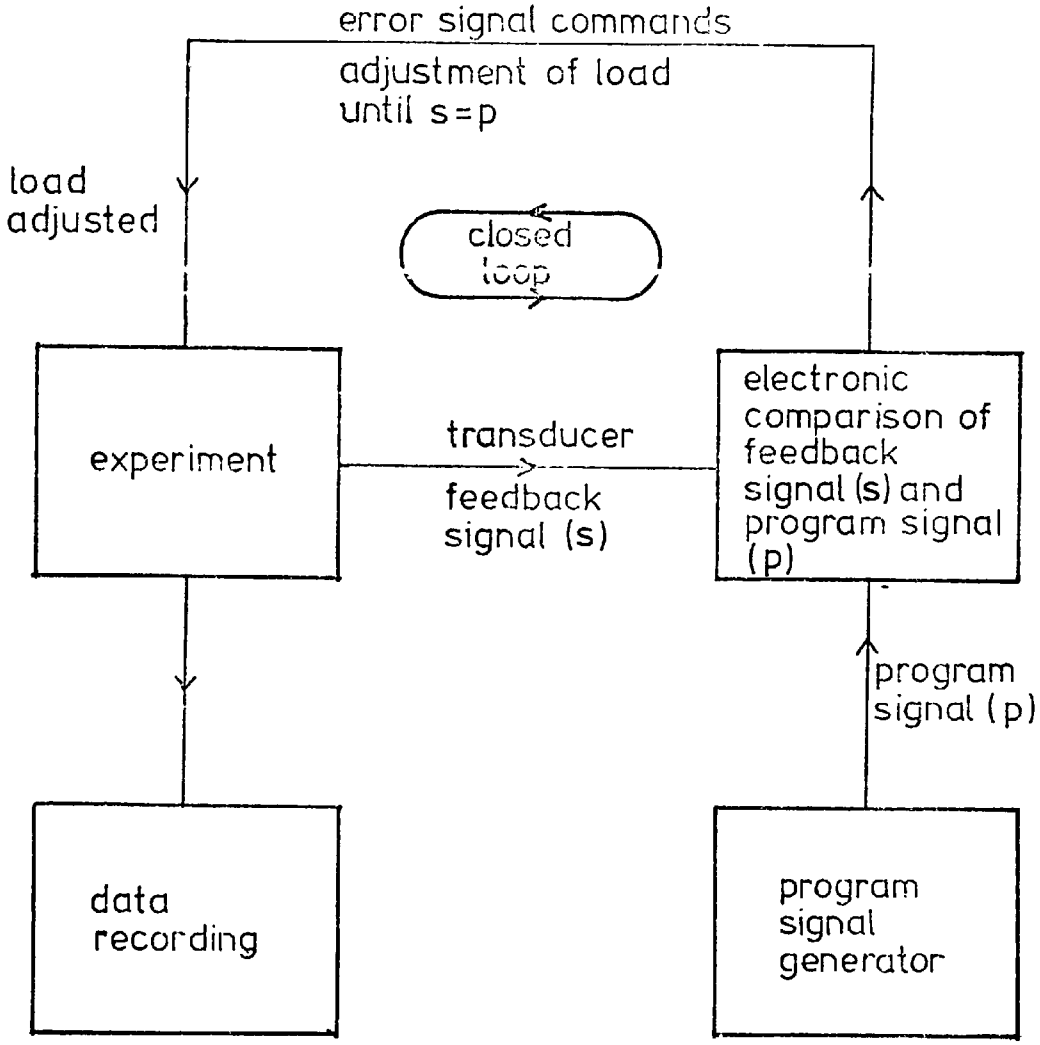

Fig 4·3 Block diagram of servo-controlled testing machine [after Hudson et al (1972)].

The strain extensometer was fitted, by elastic bands, to the tensile side of the CNRBB specimens, as shown in plate 4.5. The Instron generated a program signal (p) of a ramp function. If a crack were suddenly to try to propagate through a specimen during a test, the strain extensometer detected the rapid crack opening and the signal automatically reduced the load, and the crack was then arrested. The CNRBB samples from the first three concrete mixes were loaded to give a crack opening displacement (COD) rate of 1.2×10^{-4} mm/sec.

Subsequent specimens were tested with the machine in displacement control. In this mode, the machine acts as an infinitely stiff testing rig. Several displacement rates were used for these experiments. All experiments were conducted at nominal room temperature and results were plotted autographically.

The Instron testing machine was connected to a data-logger (plate 4.7) and computer so that results could be monitored and stored. This system allowed instantaneous calculation of the area under the load-deflection graphs and K_{1c}.

4.6 Results from the Concrete CNRBB Tests

Figure 4.4 shows two typical load-deflection graphs for two geometrically similar CNRBB specimens. Graph A is from an experiment conducted in strain control, and B is from one in displacement control. The graphs show that deformation is nearly linear until crack propagation occurs, and the graph finally approaches zero asymptotically. It can be seen that, for graph A, it is concave during crack propagation, i.e. the displacement has been automatically reduced to allow stable

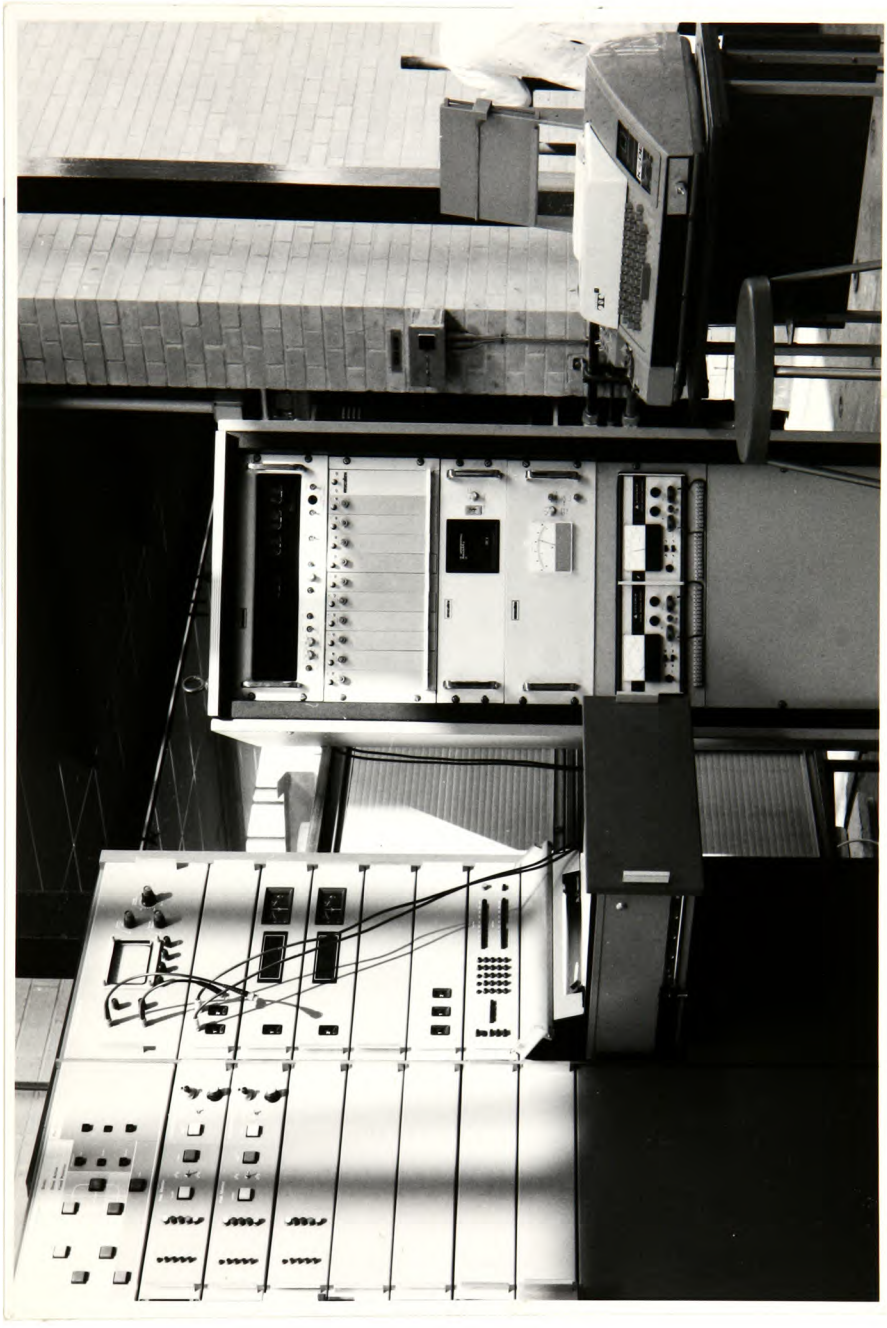

Plate 4.7

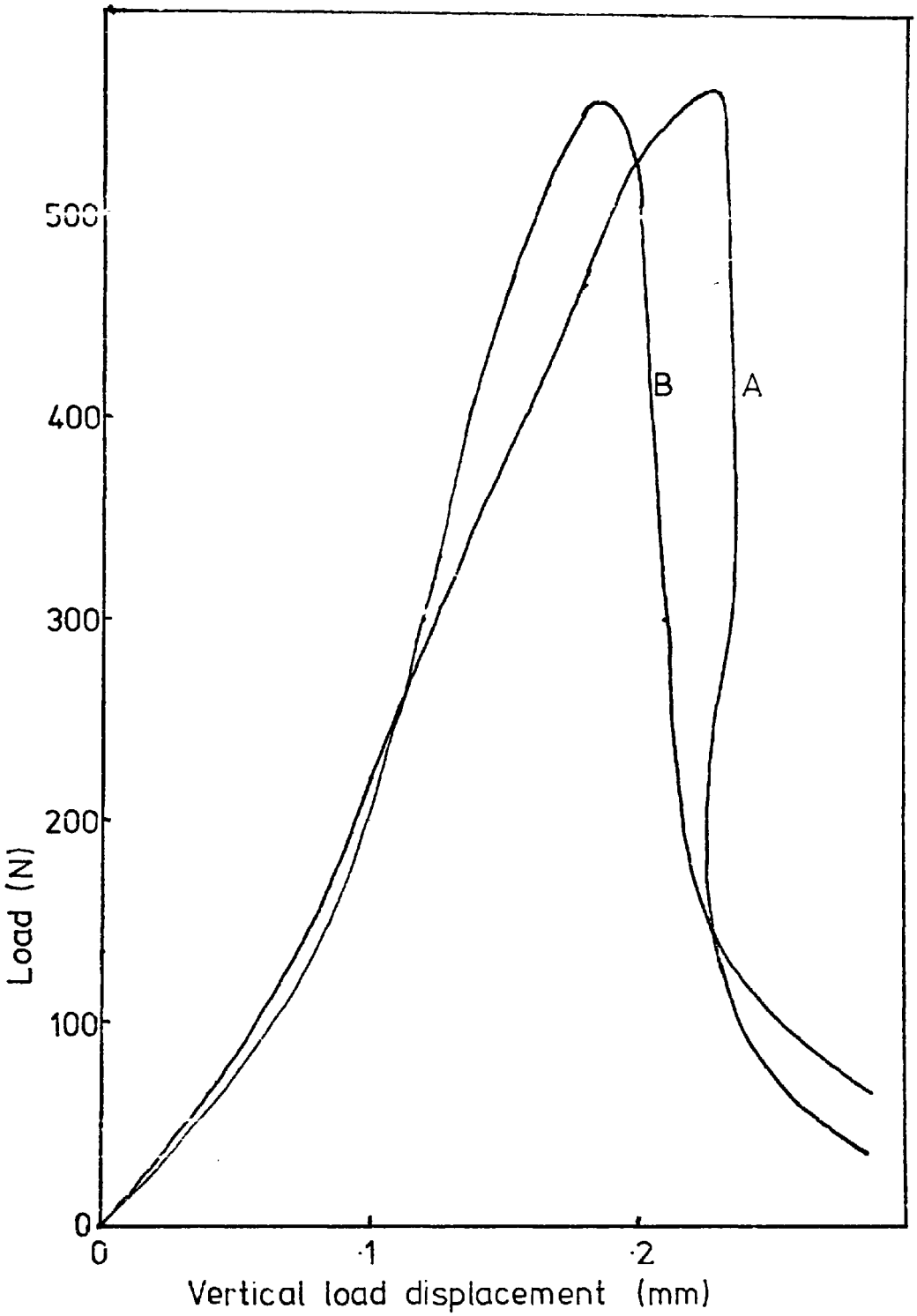

Fig 4.4 Load-deflection graphs for CNRBB specimens under strain control (A), and displacement control (B).

crack propagation. Graph B shows no such concavity as the cracking proceeds. The sharp drop in load after failure is not instantaneous, but takes place over a period of 2 or 3 seconds. This suggests that the system is semi-stable, or referring to inequality (4.1) $k_m = f'(d_s)$. The similarity of the shapes of the graphs indicate that the measured fracture energies are similar whether strain or displacement control is used. Graph A was derived at a slower rate of vertical displacement than graph B, hence the slope of the curves prior to failure is different.

At failure, the graphs are quite smooth (c.f. figure 2.6) and shows that crack initiation was a gradual process. Some sub-critical crack growth must have occurred, as previousiy demonstrated by Evans (1946). Using the concepts of Bieniawski (1967a) crack initiation has occurred prior to crack propagation. However, it was emphasised in chapter 3 that the expression for the stress intensity factor, K_1, is only valid for a 'zero' radius notch. The load-displacement graphs support the assumption that failure occurs by crack propagation from a 'zero' radius notch rather than a blunt one. The failure load in calculations of K_{1c} was taken as the maximum load on the graphs.

The effective fracture surface energy, $\mathcal{G}_{1c}$, was measured as the total area under a graph, divided by the nominal crack area πa^2. The area under each graph was automatically calculated by computer using the trapezoid rule, and the details of the computer program are given in appendix 4a.

CNRBB specimens from two concrete beams were tested in strain control to develop a testing technique and to prove the feasability of the new testing arrangement. The results from the two beams are

summarised in table 4.1 and detailed results are given in appendix 4b. The results from the second beam indicate that K_{1c} for the CNRBB test is independent of notch depth for 0.57 and 0.76 cm deep notches. The same series of experiments was repeated on a third beam, and the results are given in table 4.2. Analysis of this table shows that a random sample of 5 specimens gives an average value for K_{1c} very close to the average for 15. Indeed, if the 5 highest values of K_{1c} are averaged, the result is within 5% of the average for all results. Also, for the last series of results, the mode of testing was changed from strain to displacement control, with no appreciable effect on K_{1c} values. The last 9 specimens were tested in displacement control at a rate of 1.3×10^{-3} mm/sec.

The average value of K_{1c} obtained from the first beam for a 0.25 cm deep notch suggested that K_{1c} is not independent of notch depth for shallow notches. A fourth beam was cast and cured to provide specimens to investigate the relation between K_{1c} and notch depth, t, for 4.1 cm diameter specimens. The results are illustrated in figure 4.5. The error on each data point is the standard deviation of the average value for 5 specimens. The experiments were conducted in displacement control at a rate of 1.5×10^{-3} mm/sec.

The graph shows that K_{1c} increases for small notch depths to a limiting value for deep notches. These results, taken in conjunction with those from previous beams, show that for a 4.1 cm diameter CNRBB specimen, a notch depth of 0.6 cm will give a K_{1c} value very close to the limiting value for a deep notch.

Experiments were conducted to investigate the variation of K_{1c} with testing speed. All tests were carried out in the manner

BEAM 1

Series A. 8 specimens.

Average specimen diameter = 4.07 cm.

Average notch depth = 0.253cm.

K_{1c} = 3.49 ± 0.2 x 10^5 N/$m^{3/2}$ (5.9% var)

G_{1c} = 76.6 ± 10.2 N/m (13.3% var)

Series B. 8 specimens.

Average specimen diameter = 4.06 cm.

Average notch depth = 0.5 cm.

K_{1c} = 4.35 ± 0.15 x 10^5 N/$m^{3/2}$ (3.4% var)

G_{1c} = 68.4 ± 13 N/m (19% var)

Series C. 7 specimens.

Average specimen diameter = 4.1 cm.

Average notch depth = 0.77cm.

K_{1c} = 4.32 ± 0.44 x 10^5 N/$m^{3/2}$ (10.3% var)

G_{1c} = 44 ± 11.3 N/m (25% var)

BEAM 2

Series A. 14 specimens.

Average specimen diameter = 4.08 cm.

Average notch depth = 0.51 cm.

K_{1c} = 5.24 ± 0.34 x 10^5 N/$m^{3/2}$ (6.4% var)

G_{1c} = 85.3 ± 12.3 N/m (14.4% var)

Series B. 15 specimens.

Average specimen diameter = 4.08 cm.

Average notch depth = 0.76 cm.

K_{1c} = 5.38 ± 0.51 x 10^5 N/$m^{3/2}$ (9.6% var)

G_{1c} = 76.3 ± 10.2 N/m (13.3% var)

All experiments were conducted in strain control, using COD rates of 1.2×10^{-4} and 2.4×10^{-4} mm/sec for beams 1 and 2 respectively.

Table 4.1 Summary of results from fracture tests on samples from 2 concrete beams.

spec. number	external diam. cm	internal diam. cm	failure load N	K_{1c} $\times 10^5$ N/m$^{3/2}$	$\mathcal{G}_{1c}$ N/m
1A	4.09	3.09	1025	5.79	-
2A	4.09	3.08	1030	5.88	-
3A	4.09	3.07	970	5.59	105
4A	4.09	3.07	981	5.66	105
5A	4.09	3.07	1030	5.94	117
6A	4.09	3.07	966	5.57	87.3
7A	4.09	3.07	974	5.61	101
8A	4.09	3.07	942	5.43	93.6
9A	4.09	3.07	1025	5.91	97.2
10A	4.09	3.07	954	5.5	110
11A	4.09	3.07	896	5.16	75.9
12A	4.09	3.07	915	5.27	102
13A	4.09	3.07	1021	5.89	103
14A	4.09	3.07	1010	5.77	106
15A	4.09	3.07	1018	5.82	103
Average K_{1c} = 5.65 ± 0.24x10^5 N/m$^{3/2}$ (4.2% var)					
Average $\mathcal{G}_{1c}$ = 101 ± 10.4 N/m (10.4% var)					
1B	4.11	2.58	586	5.53	-
2B	4.09	2.57	577	5.5	-
3B	4.09	2.59	582	5.44	-
4B	4.1	2.57	556	5.3	70.4
5B	4.09	2.57	660	6.29*	83.9
6B	4.09	2.57	554	5.28	71.1
7B	4.09	2.57	627	5.98	91.8
8B	4.09	2.57	605	5.77	77.6
9B	4.1	2.57	604	5.72	83.7
10B	4.1	2.57	562	5.36	76.6
11B	4.1	2.57	624	5.95	72.2
12B	4.1	2.56	564	5.44	70.2
13B	4.1	2.57	586	5.59	97.5
14B	4.1	2.57	547	5.22	64.8
Average K_{1c} = 5.54 ± 0.25x10^5 N/m$^{3/2}$ (4.4% var)					
Average $\mathcal{G}_{1c}$ = 72.0 ± 9.6 N/M (12.2% var)					

Table 4.2 Results from fracture tests on concrete beam number 3. The result marked * was not used in the calculation of the average K_{1c} value. The specimens 6B to 14B were tested in displacement control at a rate of 1.3×10^{-3} mm/sec, and the remainder, in strain control, using a COD rate of 2.4×10^{-4} mm/sec.

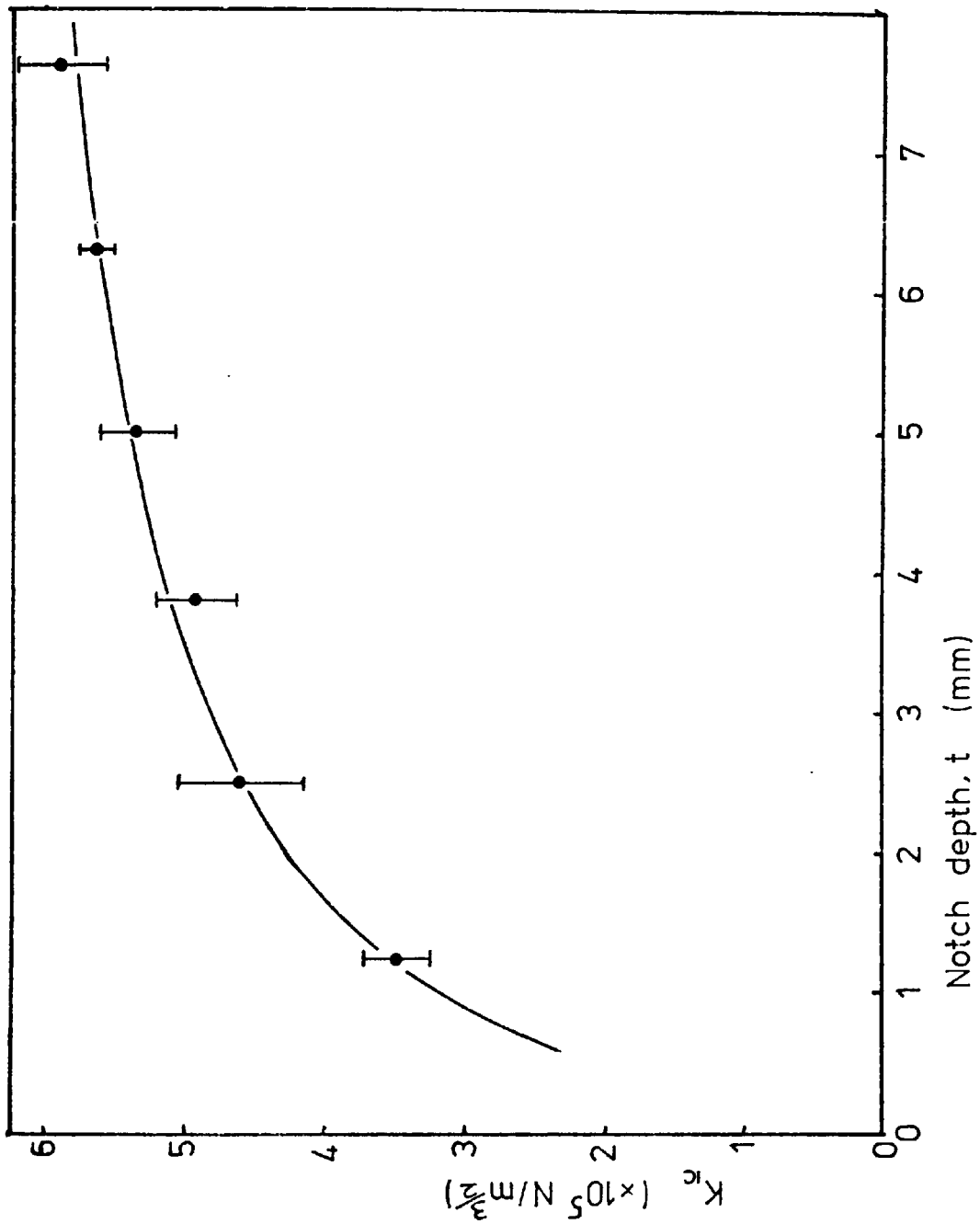

Fig 4.5 Variation of K_{ic} with notch depth for 4·1 cm diameter CNRBB specimens.

described above. Figure 4.6 shows K_{1c} plotted against the log of the displacement rate. Five specimens were tested at each displacement rate, and the errors are again the standard deviation of the mean. All points, with the exception of A, are measurements for 0.056 cm wide notches. Point A is the equivalent value for a 0.025 cm wide notch. The similarity of points A and B indicate that K_{1c} is independent of notch width for thin notches. The graph shows that K_{1c} is independent of load displacement rate for speeds less than 2×10^{-3} mm/sec.

For the CNRBB test to be a useful measure of K_{1c}, it has to be relatively independent of specimen size. A series of experiments were carried out to compare results from specimens with different diameters. Because of the size of corers available, the specimen diameters used were 4.1 and 5.35 cm (approximately).

Table 4.3 compares the K_{1c} measurements for 4.1 and 5.35 cm diameter specimens, and it can be seen that the average values are similar. Experiments were conducted to investigate the effect of notch depth on K_{1c} measurement for 5.35 cm diameter specimens. Tables 4.4 and 4.5 give the results from such experiments (table 4.4 is detailed in appendix 4b). Both tables show that K_{1c} is largely unaffected by increasing the notch depth from 1.01 to 1.27 cm, but a larger increase in depth caused a reduction in K_{1c} measurements. Also, the deep notch produced a very large deviation in the data (table 4.5).

One disadvantage of the CNRBB test, using present techniques, is that it requires a specimen of at least 11 cm long. An attempt was made to reduce this required length by attaching metal collars to

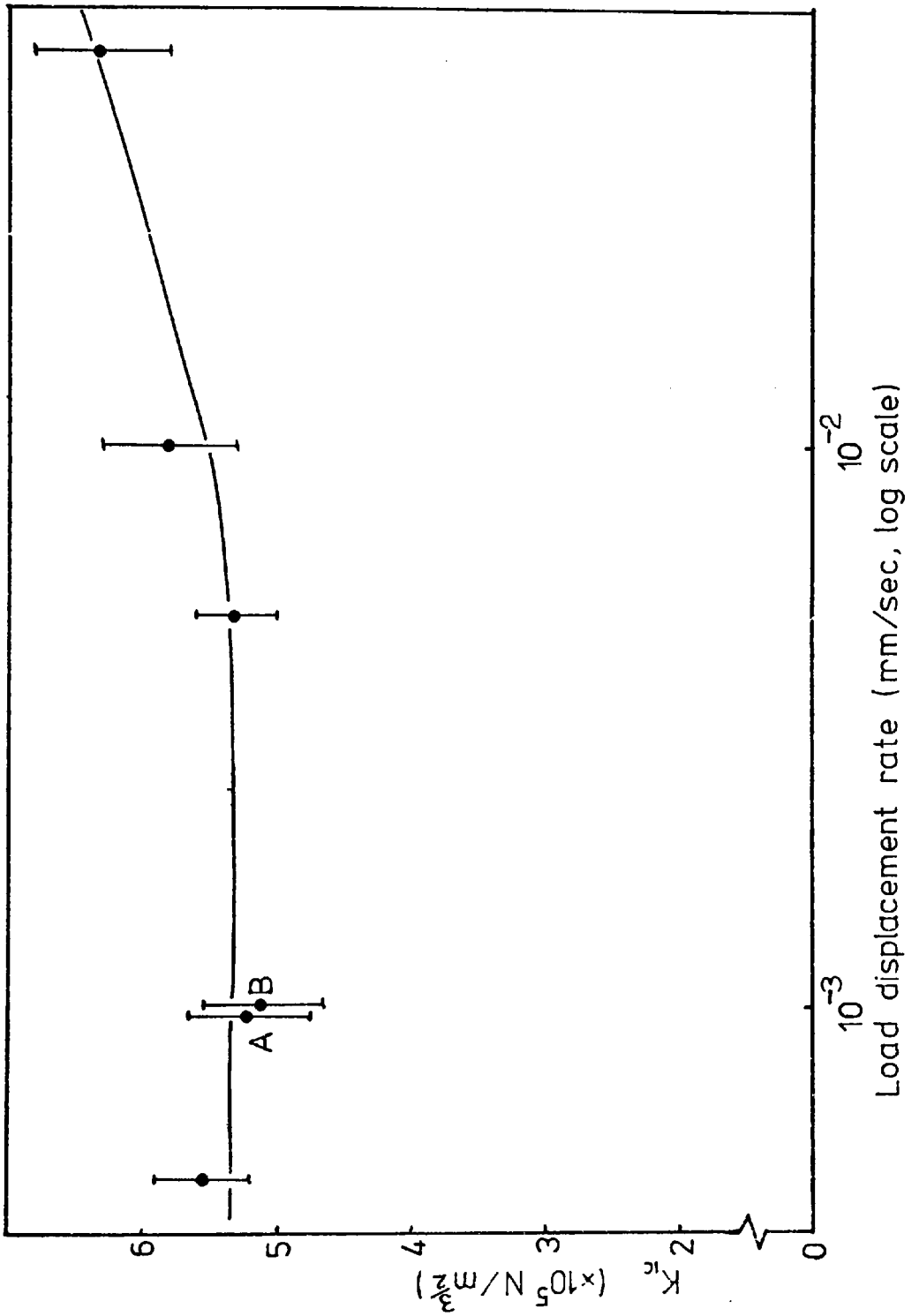

Fig 4-6 Variation of K_{ic} with load displacement rate for 4·1 cm diameter CNRBB specimens.

spec. number	external diam. cm	internal diam. cm	failure load N	K_{1c} $x10^5$ $N/m^{3/2}$
1A	4.08	2.56	584	5.64
2A	4.08	2.57	610	5.83
3A	4.08	2.56	619	5.98
4A	4.08	2.56	689	6.65*
5A	4.08	2.56	626	6.05
Average K_{1c} = 5.87 ± .18 $x10^5$ $N/m^{3/2}$ (3.1% var)				
1B	5.33	3.33	1205	6.03
2B	5.34	3.33	1062	5.32
3B	5.35	3.33	1190	5.94
4B	5.32	3.31	1307	6.65*
5B	5.33	3.32	1257	6.32
Average K_{1c} = 5.90 ± .42 $x10^5$ $N/m^{3/2}$ (7.1% var)				

Table 4.3 Comparison of K_{1c} results from fracture tests for two different sample diameters. The results marked * were not used in the calculations of the average K_{1c} values.

BEAM A

5 specimens.
Average specimen diameter = 4.05 cm.
Average notch depth = 0.76 cm.
$K_{1c} = 4.04 \pm 0.23 \times 10^5$ N/m$^{3/2}$ (5.6% var)

4 specimens.
Average specimen diameter = 4.05 cm.
Average notch depth = 0.88 cm.
$K_{1c} = 4.16 \pm 0.17 \times 10^5$ N/m$^{3/2}$ (4.1% var)

6 specimens.
Average specimen diameter = 5.35 cm.
Average notch depth = 0.76 cm.
$K_{1c} = 3.81 \pm 0.33 \times 10^5$ N/m$^{3/2}$ (8.8% var)

7 specimens.
Average specimen diameter = 5.35 cm.
Average notch depth = 1.0 cm.
$K_{1c} = 4.24 \pm 0.47 \times 10^5$ N/m$^{3/2}$ (11.1% var)

7 specimens.
Average specimen diameter = 5.35 cm.
Average notch depth = 1.26 cm.
$K_{1c} = 4.74 \pm 0.31 \times 10^5$ N/m$^{3/2}$ (6.6% var)

BEAM B

6 specimens.
Average specimen diameter = 5.35 cm.
Average notch depth = 1.01 cm.
$K_{1c} = 6.36 \pm 0.6 \times 10^5$ N/m$^{3/2}$ (9.5% var)

6 specimens.
Average specimen diameter = 5.35 cm.
Average notch depth = 1.27 cm.
$K_{1c} = 6.27 \pm 0.45 \times 10^5$ N/m$^{3/2}$ (7.2%)

Table 4.4 Comparison of K_{1c} results from fracture tests on two different sample diameters, and the variation of K_{1c} with notch depth for 5.35 cm diameter specimens.

spec. no.	external diam. cm	internal diam. cm	failure load N	K_{1c} $x10^5 N/m^{\frac{3}{2}}$
1	5.37	3.33	1088	5.44
2	5.37	3.33	1270	6.35
3	5.37	3.33	1260	6.30
4	5.37	3.34	1315	6.53
5	5.37	3.36	1262	6.16
6	5.37	3.34	1295	6.43
7	5.37	3.36	1375	6.71
8	5.37	3.34	1180	5.86
$K_{1c} = 6.22 \pm 0.4$ $x10^5$ $N/m^{\frac{3}{2}}$ (6.5% var)				
9	5.37	2.83	850	6.55
10	5.37	2.82	792	6.16
11	5.37	2.83	705	5.43
12	5.37	2.81	850	6.67
13	5.37	2.83	925	7.13
14	5.37	2.82	1062	8.26*
15	5.37	2.83	775	5.97
16	5.37	2.84	803	6.13
17	5.37	2.82	833	6.48
$K_{1c} = 6.31 \pm 0.51$ $x10^5$ $N/m^{\frac{3}{2}}$ (8.1% var)				
18	5.37	2.32	537	6.92
19	5.37	2.31	481	6.27
20	5.37	2.34	369	4.65
21	5.37	2.32	578	7.45*
22	5.37	2.32	358	4.61
23	5.37	2.34	381	4.78
24	5.37	2.31	300	3.91
$K_{1c} = 5.19 \pm 1.15$ $x10^5$ $N/m^{\frac{3}{2}}$ (22% var)				

Table 4.5 Comparison of CNRBB test results for 5.37 cm diameter concrete cores with three different notch depths. Results marked * were not used in the calculation of averages.

smaller specimens and extending it. Plate 4.8 illustrates such an arrangement. The core size used was 7.5 cm long and 4.1 cm diameter (the resultant halves from previous tests). The metal collars were 5.5 cm long, 0.315 cm thick and 4.1 cm internal diameter. The collars were heated and melted Canada Balsam smeared inside them. The collars were then slid over each end of a concrete core and allowed to cool. The specimens were tested in the same manner as for previous CNRBB tests.

Table 4.6 summarises the results from CNRBB tests, with and without metal collars, using the same concrete mix. The results indicate that the collars reduced the measured K_{1c} by about 22%, and also increased the standard deviation of the data.

4.7 Discussion of CNRBB Test Results

The series of experiments described above have shown the CNRBB test to be a reproducible and convenient method to determine K_{1c} for concrete. There are several advantages of the test, especially when compared to the more common Notched Beam under Bending (chapter 2). The advantages are:-

1. The specimens are quickly and easily prepared, and experience shows that a specimen can be prepared in less than 30 minutes.

2. Specimens can be prepared from in situ concrete whereas the notched beams have to be moulded.

3. The test is economic of material.

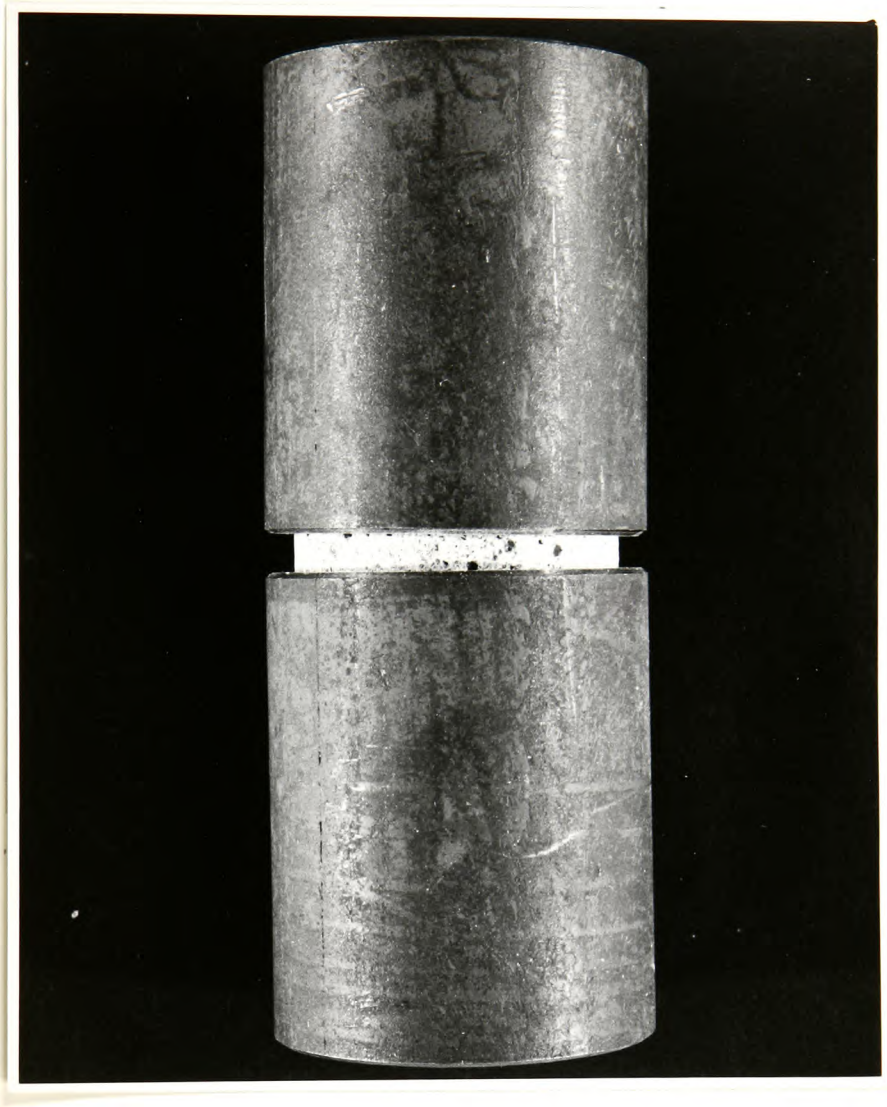

Plate 4.8

BEAM A

5 specimens, without metal collars.

Average specimen diameter = 4.07 cm.

Average notch depth = 0.76 cm.

$K_{1c} = 1.04 \pm 0.07 \times 10^{6}$ N/m$^{\frac{3}{2}}$ (7.1% var)

12 specimens, with metal collars.

Average specimen diameter = 4.07 cm.

Average notch depth = 0.76 cm.

$K_{1c} = 7.77 \pm 1.08 \times 10^{5}$ N/m$^{\frac{3}{2}}$ (13.9% var)

Beam B

5 specimens, without metal collars.

Average specimen diameter = 4.09 cm.

Average notch depth = 0.76 cm.

$K_{1c} = 7.14 \pm 0.64 \times 10^{5}$ N/m$^{\frac{3}{2}}$ (8.9% var)

7 specimens, with metal collars.

Average specimen diameter = 4.07 cm.

Average notch depth = 0.76 cm.

$K_{1c} = 6.03 \pm 1.03 \times 10^{5}$ N/m$^{\frac{3}{2}}$ (17.1% var)

Table 4.6 Comparison of average K_{1c} results from CNRBB tests on concrete with, and without, metal collars to extend specimen length.

4. The loading of the cylindrical specimens is easy; there is no problem of non-alignment of opposing faces as with the Notched Beam test.

5. The plane of propagation of the crack is governed by the circumferential notch.

6. The point of initiation of the crack can be predetermined by rotating the specimen to give the desired point on the tensile side.

7. The crack propagation starts from a very small area. The last point can be a disadvantage under certain circumstances. Wiess & Yukawa (1964) have pointed out that the measured fracture strength decreases as the length of the crack front increases. This result is true for an inhomogeneous material containing flaws. The longer the crack front is, the greater the likelihood of the crack initiating at a weakness in the material.

For a CNRBB specimen, the crack theoretically starts at a tangent to the base of the circumferential notch, and so the length of the crack front approaches zero. Therefore, the size effect should be zero for CNRBB tests. However, because the crack front is so small, it could be located in a piece of aggregate or matrix, and the deviations of the data reflect the properties of the component materials in a specimen. In a notched beam, the crack front is usually over the width of the beam, and so the measure K_{1c} is an average of all the materials at the crack front.

The sensitivity of K_{1c} measurements to inhomogeneities in a specimen can be judged by two anomalous readings in table 4.3. The two values were omitted from calculations of the averages. Examination of the crack surfaces from the two specimens, shown in plates 4.9 and 4.10 explain the high values of K_{1c}. There are large regions of mortar in the crack surfaces which give higher K_{1c} readings than the concrete as a whole.

To relate the measurement of K_{1c} to the crack surfaces, it is advisable to mark the position of the tensile side of a specimen prior to testing. If the test gives an anomalous result, compared to the average from other tests, it is possible to observe the area in which crack initiation occurred. It is often possible to relate a low K_{1c} measurement to an air bubble at the notch base, or a high value to a large piece of aggregate.

The average K_{1c} value from several CNRBB tests migh be expected to correspond to the value derived from one notched beam test. If individual components of a material need to be tested, the CNRBB test is advantageous. Later experiments on rock, described elsewhere in this thesis emphasise this advantage.

Figure 4.4 shows that the load-deflection graph is similar for experiments conducted under strain or displacement control. For these experiments, therefore, it is not necessary to use expensive, servo-controlled testing machines to measure the fracture energy. Probably the most limiting factor in the choice of testing machines is the necessity for very low speeds.

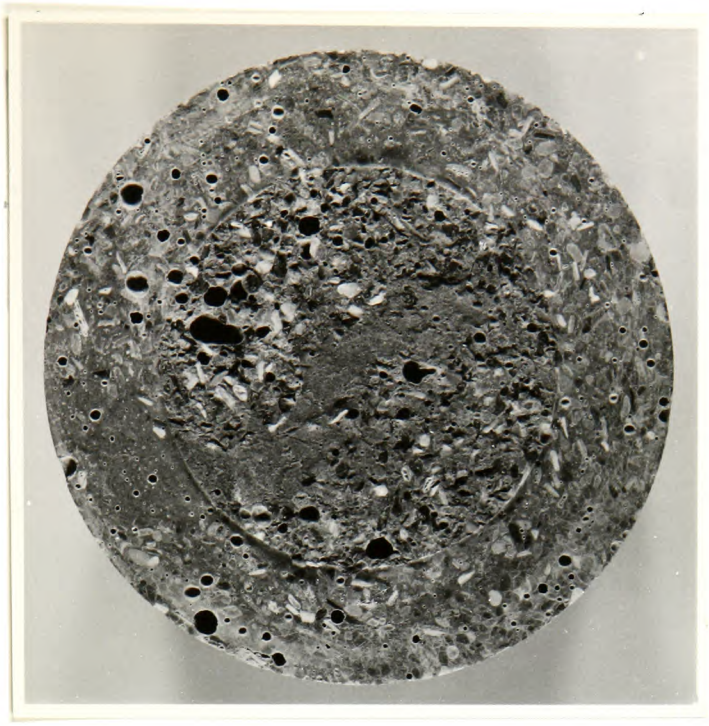

Plate 4.9

Plate 4.10

The variation of K_{1c} with notch depth, as shown in figure 4.5, has an interesting parallel with results published by Brown (1972). He used the Double Cantilever Beam (DCB) method, as discussed in chapter 2. The beam shape was designed to give a constant K_1 as the crack propagated. Brown's results show an apparent K_{1c} increase with increasing crack length, and approached an asymptotic value. Brown thought this effect to be surprising but offered no explanation for it. The mechanism of the apparent increase in K_{1c} is different for the DCB than for CNRBB because in the former case the crack is a natural one.

For the CNRBB test, K_{1c} apparently increases with increasing notch depth, but it is not considered that this detracts in any way from the usefulness of the test. If the notch is made deep, relative to the diameter, then the measured K_{1c} will approach the limiting value. The experiments described in this chapter (e.g. tables 4.1 and 4.2) support this view.

Figure 4.6 shows that K_{1c} is not critically dependent upon testing speeds for load displacement rates less than 2×10^{-3} mm/sec. It is well known in metallurgical fracture testing that a fatigue-produced crack gives a low K_{1c} measurement compared to an artificially produced one. Evans (1946) showed that cracks are produced in concrete at sub-critical loads. The cracks might be caused by the relaxation of strains around a notch tip, and that time is required for relaxation to occur. Therefore, for slow testing speeds, relaxation can cause cracks to be formed at low loads. At high speeds little relaxation has time to occur, and the crack propagates from a blunt notch at a higher load.

For one of the beams (the results of which are given in figure 4.5), the modulus of elasticity was measured (according to BS 1881 part 5 (1970)) as 3.84×10^{10} N/m^2. Assuming K_{1c} to be 5.89×10^5 N/m$^{3/2}$, the fracture energy $\mathcal{G}_{1c}$ can be calculated from equation (2.13):-

$$\mathcal{G}_{1c} = \frac{K_{1c}^2}{E} = \frac{5.89^2 \times 10^{10}}{3.84 \times 10^{10}} = 9$$

For all results from the same concrete mix, $\mathcal{G}_{1c}$ was measured as 87.6 ± 16.6 N/m, which is approximately ten times the value calculated above.

The discrepancy is due to the underestimate of the true crack area. Because of the meandering crack path and microcracking, the nominal crack area, πa^2, is only a fraction of the true area. Moavenzadeh and Kuguel (1969) used quantitative microscopy to show that, in concrete, the true crack area is up to 12 times the nominal one. By assuming a multiplication factor of ten for the crack area of the CNRBB, then the relation between $\mathcal{G}_{1c}$ and K_{1c} approaches that given by equation (2.13).

Table 4.2 shows that the effective fracture surface energy $\mathcal{G}_{1c}$, is not a constant for CNRBB tests. It is possible that the actual crack area is dependent upon the stress field in a specimen. This stress field is dependent upon the notch depth, and so $\mathcal{G}_{1c}$ will also depend upon the notch depth. Consequently, the measurement of $\mathcal{G}_{1c}$ from CNRBB tests on small diameter specimens seem to be of little value.

A change in specimen diameter from 4.1 to 5.35 cm has little effect on K_{1c} measurements. For the larger size, however, the relation between K_{1c} and notch depth seems to be less obvious than that for the

smaller size.

The results shown in tables 4.4 and 4.5 show that 1.0 and 1.27 cm deep notches gave similar K_{1c} measurements, but a 1.52 cm notch gave a much lower value. This contradicts earlier results on smaller specimens, as shown in figure 4.5. Also the deviations of the data is much higher for the deep notches.

One explanation of the anomalous result for a deep notch in 5.35 cm specimens is that the low readings are due to imperfections in the concrete mix. Precautions were taken to ensure that there were few air bubbles in a mix, but inevitably some remained. If there were a high proportion of voids, especially near the point of crack initiation, then anomalously low readings might result. As a notch is made deeper, the volume of material at a notch root is reduced, and the effect of an air bubble would be greatly increased. This explanation assumes that the concrete mix for the larger CNRBB specimens had more entrapped air than for the small specimens.

The particularly high deviation of K_{1c} values for very deep notches in the CNRBB test make these results less useful. It is advisable, therefore, to use a 1.0 to 1.27 cm deep notch for 5.35 cm diameter specimens.

The use of metal collars to extend the length of the CNRBB specimens results in a 20% decrease in measurements of K_{1c}. A similar effect has been reported by Glucklich & Cohen (1968). The introduction of springs in series with gypsum beams under bending reduced the failure load considerably. They also found that the failure load was a function of specimen size. Glucklich and Cohen

postulated that these effects were due to the inhomogeneity of the tested material.

When a crack propagates, it encounters regions of material which have a higher K_{1c} than their surroundings. In a stiff system, the specimen needs an input of energy to allow the crack to propagate through this region. If, however, there is strain energy stored in the system, the crack can spontaneously propagate through the high K_{1c} region, and the net effect is that there is a lower failure load measured. Therefore, any procedure which increases a specimen's capacity to store strain energy, such as attaching metal collars (which are more flexible than an equivalent length of concrete) should reduce the failure load.

Unfortunately, there seems to be no quantitative relation available between the failure load of a specimen and its flexibility. Consequently, the use of metal collars to extend a specimen's length is not recommended. Indeed, the procedure has been superceded by the introduction of the CNRBEL test.

The CNRBB test has only been investigated for one span of 4-point loading. It is possible that the measured K_{1c} will vary for different spans, and this variation will have to be investigated before a standard CNRBB test can be established.

4.8 Summary of Results from CNRBB Tests

From the experiments described above, for concrete, a testing technique has been established. The depth of notch for a CNRBB specimen is not critical as long as it is greater than 0.6 cm for a 4.1 cm diameter specimen, and 1.0 cm deep for a 5.35 cm one. The

testing speed can be any value up to 2×10^{-3} mm/sec. A 4.1 and 5.35 cm diameter specimen gives similar K_{1c} results. The experiment can be carried out in either strain or displacement control with little change in results.

4.9 The Circumferentially Notched Round Bar under Eccentric Loading (CNRBEL). Experimental details.

The CNRBEL specimens were prepared in the same way as they were for the CNRBB test. Whereas CNRBB specimens do not need preparation of the ends of the cylinders, the CNRBEL ones have to be cut cleanly to provide a flat loading surface. As the loading is limited to the outside 6mm of a specimen, it is not necessary to prepare the ends completely. For example, the two halves of a CNRBB specimen can be notched and used as CNRBEL without preparing the ends containing the crack surfaces (see plate 4.9).

The expression for K_1 for CNRBEL (equation (3.16)) contains the term, e, which is the eccentricity of the load. For a small diameter specimen, any error in the measurement of the point of application of the load would result in a large error in K_{1c} measurements. For this reason, CNRBEL tests were only carried out on 5.35 cm diameter specimens. The CNRBEL tests were conducted on the same testing machine as for CNRBB, using displacement control. The load was applied by means of two 5 cm lengths of 6 mm square steel. Two opposing faces of each length of steel were ground flat. The steel bars were positioned, parallel to each other, on the edges of the CNRBEL specimen as shown in plate 4.11. A small piece of Plasticine was placed under the specimen to support it prior to loading (plate 4.12).

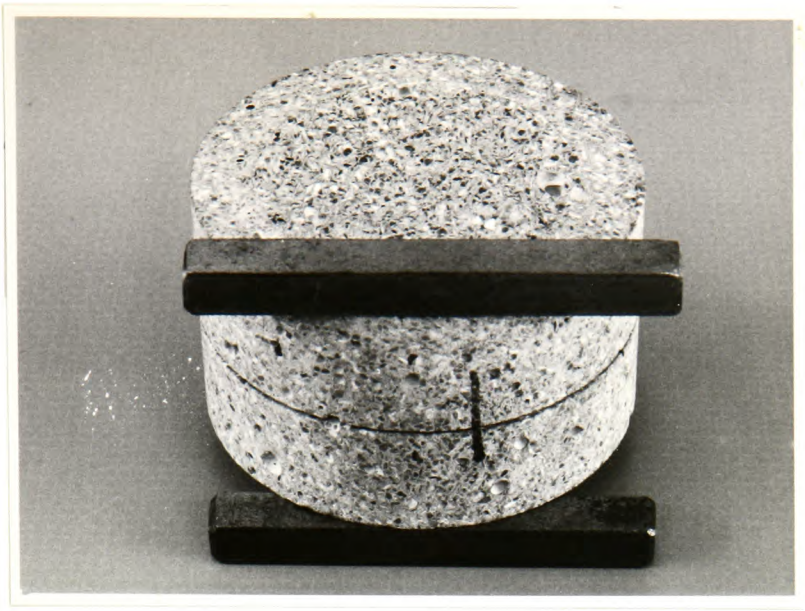

Plate 4.11

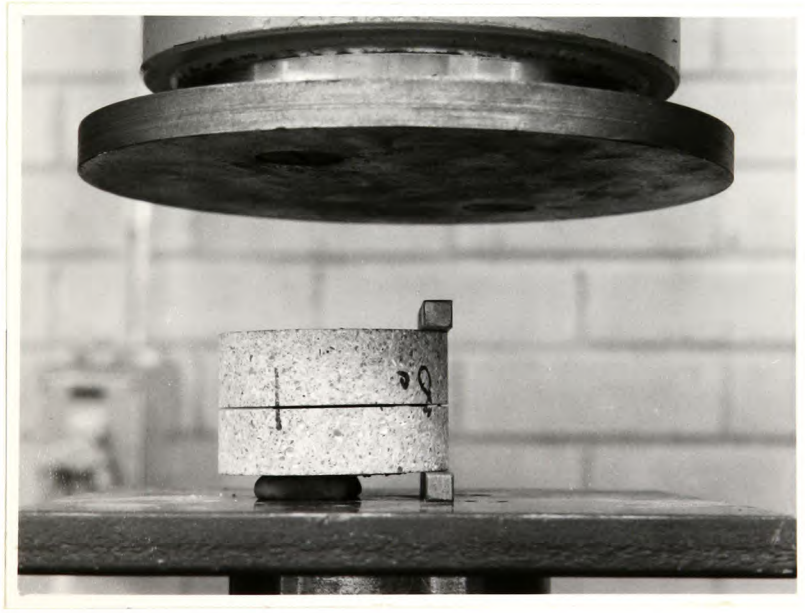

Plate 4.12

The points of application of the load were taken as the inside edges of the steel bars (i.e. e = r - 6 mm). As the load was applied, the side of the specimen under the bars was compressed, and all the load transferred to the inside edge of the bars.

All CNRBEL experiments were carried out under the same environmental conditions as for CNRBB.

4.10 Results from CNRBEL Tests

The first CNRBEL experiments were designed to compare the results with those obtained from CNRBB tests. Ten CNRBB specimens were prepared and tested, and each half of these was then notched and tested as CNRBEL.

The comparison between the two tests is given in table 4.7. The average values for K_{1c} are similar for both methods of testing. The CNRBEL measurement of K_{1c} for a 1.26 cm notch is less than that for a shallower notch. This is a different result to that derived for CNRBB (see figure 4.5).

Another series of CNRBEL tests was carried out to investigate the variation in K_{1c} measurements with notch depth. The results are summarised in table 4.8, and detailed in appendix 4b. The results show that there is a trend towards a decreasing K_{1c} with increasing notch depth, but there are not enough results to draw definite conclusions. Apart from the result for a 1.02 cm deep notch there is little variation in the average K_{1c} values.

4.11 Discussion of CNRBEL Results

There are several practical advantages to the CNRBEL test, compared

spec. no.	external diam cm.	internal diam cm.	failure load N	K_{1c} x10^5 N/$m^{3/2}$
CNRBB				
1	5.36	3.34	1587	7.87
2	5.36	3.34	2025	10.04*
3	5.36	3.33	1487	7.44
4	5.36	3.28	1575	8.20
5	5.36	3.35	1700	8.36
6	5.36	3.36	1675	8.17
7	5.36	3.37	1550	7.50
8	5.36	3.36	1762	8.60
9	5.36	3.36	1575	7.69
10	5.36	3.36	1750	8.54
K_{1c} = 8.04 ± 0.43 x10^5 N/$m^{3/2}$ (5.4% var)				
CNRBEL				
11	5.36	3.38	2700	8.74
12	5.36	3.34	2180	7.31
13	5.36	3.37	2575	8.40
14	5.36	3.33	2460	8.32
15	5.36	3.34	2250	7.54
16	5.36	3.34	3050	10.2*
17	5.36	3.34	2550	8.55
18	5.36	3.34	2550	8.55
19	5.36	3.34	2130	7.14
20	5.36	3.34	2800	9.39*
K_{1c} = 8.06 ± 0.63 x10^5 N/$m^{3/2}$ (7.8% var)				

Table 4.7 Results from fracture toughness tests on samples from a concrete beam. Specimens 1-10 were tested by the CNRBB method, and 11-20 by the CNRBEL method. Results marked * were not used in the calculation of the averages.

12 specimens.

Average specimen diameter = 5.37 cm.

Average notch depth = 0.78 cm.

$K_{1c} = 7.06 \pm 0.46 \times 10^5$ N/m$^{3/2}$ (6.5% var)

12 specimens.

Average specimen diameter = 5.37 cm.

Average notch depth = 1.02 cm.

$K_{1c} = 7.70 \pm 0.46 \times 10^5$ N/m$^{3/2}$ (6% var)

12 specimens.

Average specimen diameter = 5.37 cm.

Average notch depth = 1.28 cm.

$K_{1c} = 6.88 \pm 0.59 \times 10^5$ N/m$^{3/2}$ (8.6% var)

12 specimens.

Average specimen diameter = 5.37 cm.

Average notch depth = 1.54 cm.

$K_{1c} = 6.42 \pm 0.57 \times 10^5$ N/m$^{3/2}$ (8.8% var)

Table 4.8 Summary of results from CNRBEL tests on specimens from a concrete beam, showing the variation of K_{1c} with notch depth.

with CNRBB. The advantages are:-

1. The specimens are much smaller than for the CNRBB test, but without losing any of the advantages of the ease of preparation.

2. The experimental method is easier, and no special loading rig is required.

3. The failure load is relatively high. This is particularly important for some testing machines. A 4.1 cm diameter CNRBB specimen, with a deep notch, failed at loads near to the limits of sensitivity of an Instron 1251 machine.

A disadvantage of the test is that a little extra preparation is required for the ends of the core. Even so, only a small area of the ends needs to be prepared, as can be seen from plate 4.11.

The limiting factor to the size of the CNRBEL specimens is the space required for holding in the jaws of the lathe (plate 4.13). If the tool-post grinder is too near to the rotating chuck, there is a danger that the saw blade will hit the jaws. The smallest specimen which can be safely prepared is about 3 cm long.

For a short specimen, it is important that the circumferential notch is made a deep one. If a shallow notch is used, shear failure occurs under the loading bars before crack propagation occurs at the notch base. For the concrete used in these experiments, the notch had to be greater than 1 cm deep for a 5.35 cm diameter CNRBEL specimen.

The CNRBEL K_{1c} results are consistently higher than for the CNRBB

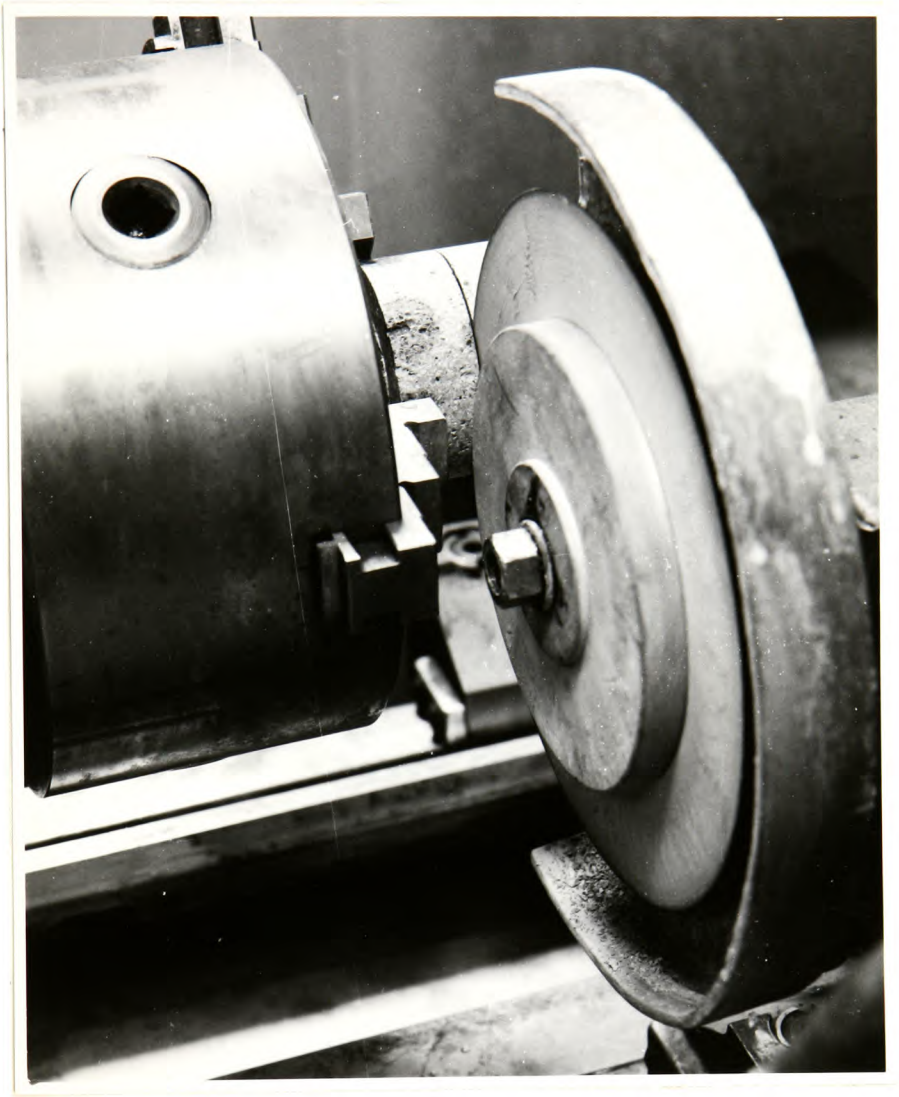

Plate 4.13

test, but this is to be expected from the discussion in section 4.7. The flexibility of the CNRBEL specimen is less than that for the CNRBB test, and this results in a smaller store of strain energy in the system and the failure load is higher.

4.12 The Slotted Disc under Diametral Loading (SDDL). Specimen Preparation

It must be emphasised that the purpose of experiments on the SDDL arrangement was merely to determine the feasibility of such a test. No attempt was made to investigate the effect of parameter changes on K_{1c} measurements. Consequently, few results are available for this test, but they do show the potential usefulness of the SDDL test.

The size of the SDDL specimens was determined by the diameter of the saw blade used to make the notches. The smallest practical blade diameter was 5 cm, and to obtain a deep notch it was necessary to use large diameter discs.

A concrete beam was cast and cured in the same mannner as for previous tests. The beam was drilled and the resultant cores were then sliced to give 7.5 cm diameter and approximately 2.5 cm thick discs. The discs were mounted, on a lathe, in a 4-jaw chuck and a slot was machined in one or two faces, as shown in plate 4.14. The saw blade was fixed to the end of an internal grinder arbor as shown in the photograph. This allowed the tool-post grinder to clear the edge of the disc. The depths of the slots were set by the scale on the cross-slide of the lathe.

To cut slots on opposite sides of a disc, it is important to

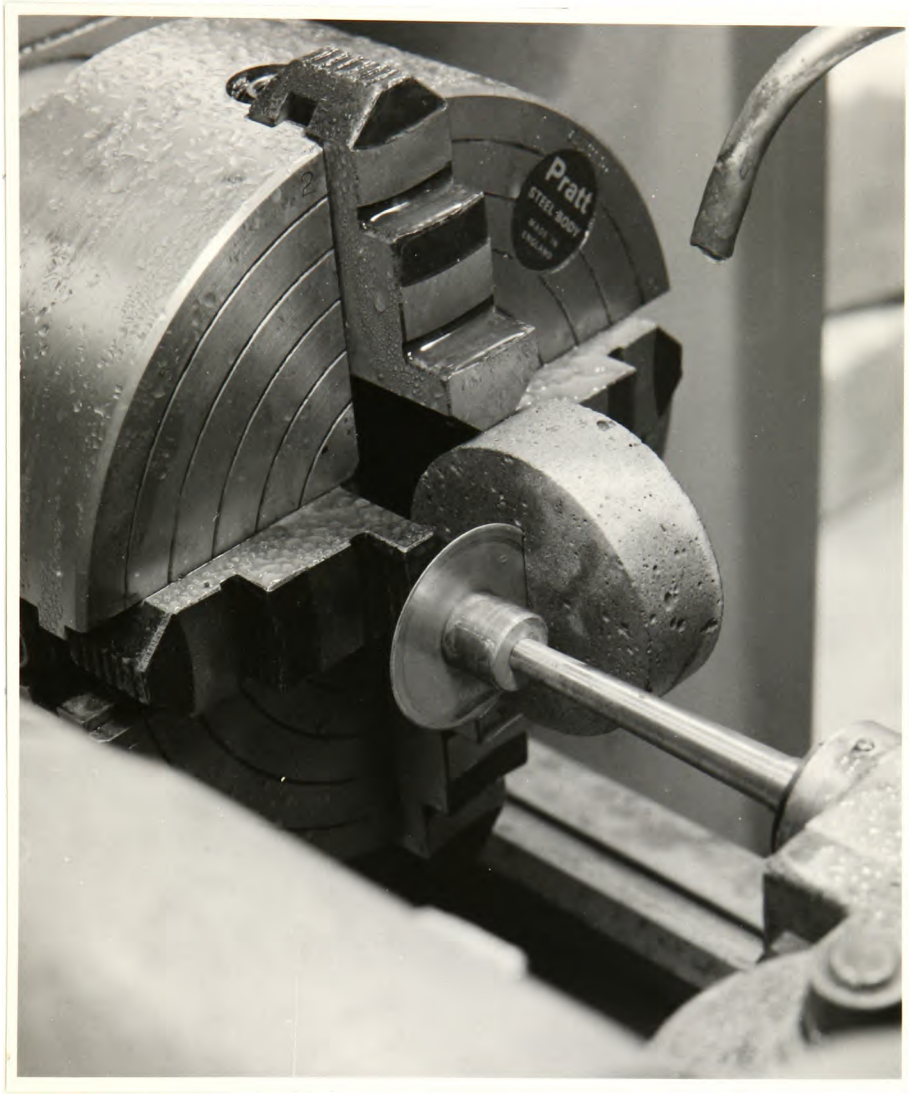

Plate 4.14

ensure that a disc is centrally gripped in the 4-jaw chuck. When the chuck is rotated through 180 degrees it is essential that the second slot is cut opposite.

4.13 Experimental Details for the SDDL Test

The discs were loaded in the same testing machine as was used for previous tests. It was important to ensure that the discs were positioned so that the slots were vertical (plate 4.15). It was sometimes necessary to use small pieces of Plasticine to stop a disc rolling out of position whilst the load was being applied. The failure load was taken as the maximum on the load-displacement graphs.

4.14 Results from the SDDL Test

From the initial tests, it became apparent that SDDL specimens with only one slot were not suitable for fracture tests. The failure load was found to be largely independent of the slot depth, and the stress concentration at the base of the notch was not sufficient to ensure failure along the plane of the slot (plate 4.16). No valid K_{1c} measurements were obtained from single-slotted discs.

Two opposite slots in a disc ensured that a disc failed through the plane of the slots. A typical cross-section of a tested specimen is shown in plate 4.17. Several disc thicknesses were used in the tests, and K_{1c} was calculated from equation (3.19). Six SDDL tests were carried out and compared with 6 CNRBEL tests from the same concrete beam. The results are given in table 4.9.

4.15 Discussion of SDDL Results

Specimens for the SDDL test are more difficult to prepare than for

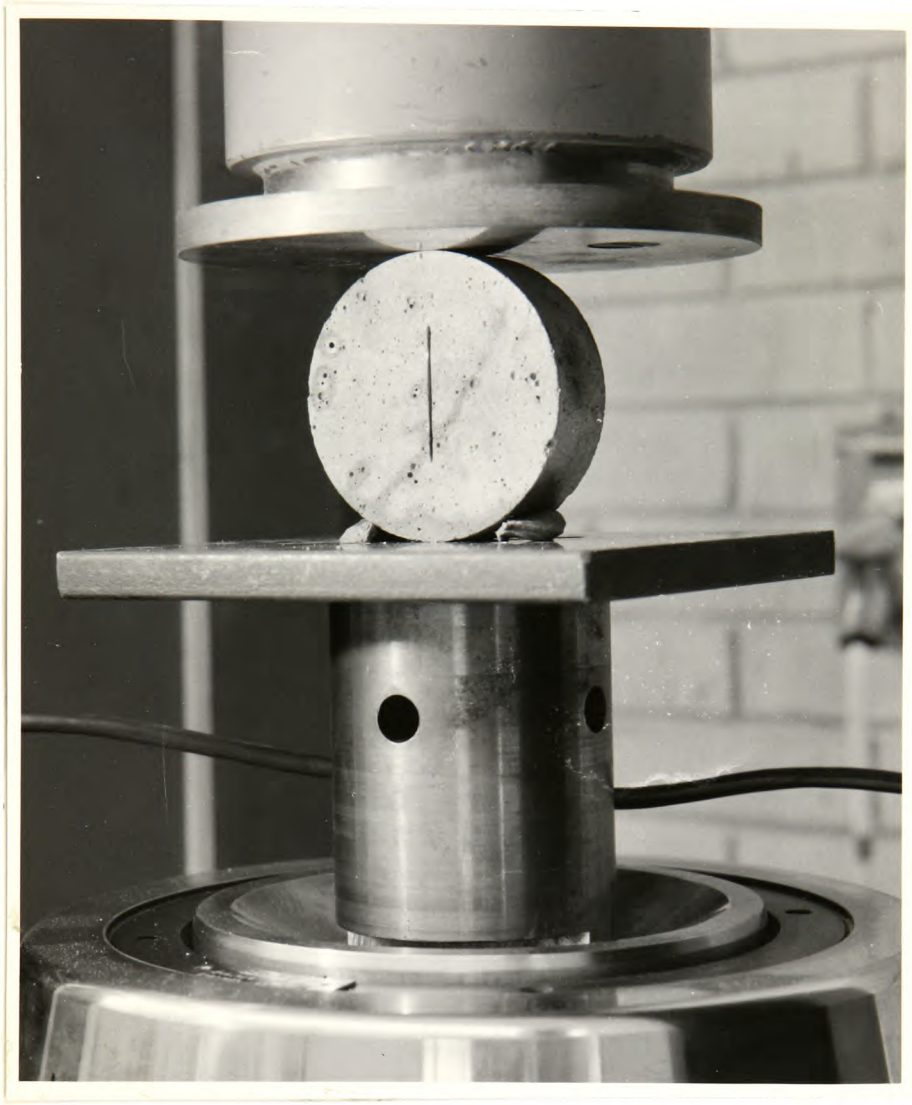

Plate 4.15

Plate 4.16

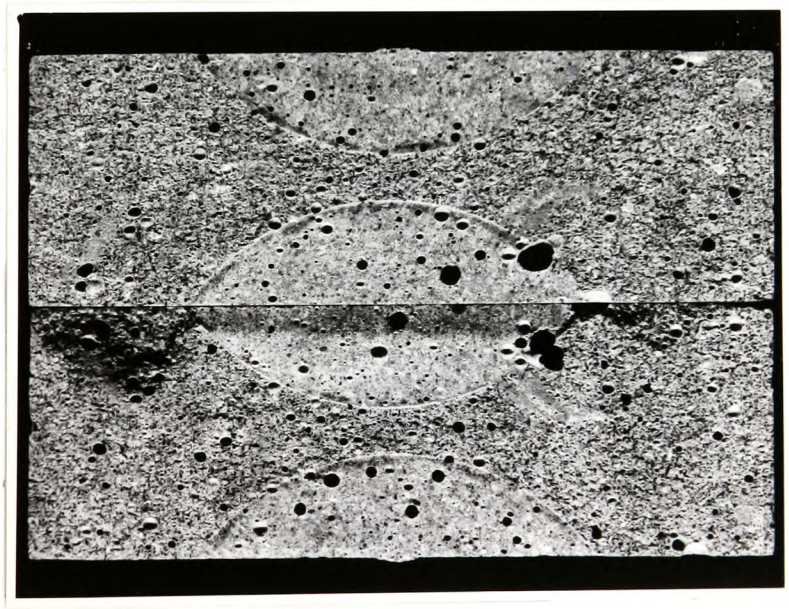

Plate 4.17

SDDL spec. no.	breadth cm.	notch depth cm	failure load kN	K_{1c} $\times 10^5$ N/m$^{3/2}$
Specimen diameter = 7.5 cm.				
1	2.53	1.02	8.0	7.43
2	2.50	0.89	8.58	6.52
3	2.48	1.02	7.91	7.75
4	2.47	1.02	6.62	6.56
5	2.56	1.02	8.0	7.21
6	2.51	1.02	7.3	6.92
$K_{1c} = 7.06 \pm 0.8 \times 10^5$ N/m$^{3/2}$ (11.3% var)				
CNRBEL spec. no.	external diam cm.	internal diam cm.	failure load N	K_{1c} $\times 10^5$ N/m$^{3/2}$
1	5.37	2.30	590	5.80
2	5.37	2.30	653	6.42
3	5.37	2.30	848	8.34*
4	5.37	2.29	663	6.60
5	5.37	2.29	550	5.47
6	5.37	2.28	550	5.54
7	5.37	2.30	585	5.75
$K_{1c} = 5.92 \pm 0.48 \times 10^5$ N/m$^{3/2}$ (8.1% var)				

Table 4.9 Comparison of fracture toughness results for concrete, using SDDL and CNRBEL specimens. Result marked * was not used in the calculation of the average.

CNRBB or CNRBEL. The main difficulty lies in holding a disc in a 4-jaw chuck sufficiently accurately for two opposite slots to be cut. There are, however, two big advantages to the test. It is often easier to produce large, flat discs of rock rather than longer cores of smaller diameter. For example, when coring slate, the rock often breaks off inside a corer to give flat discs. Therefore, for certain rocks, the SDDL test might be the only one suitable.

The direction of fracture of SDDL is easy to predetermine, which is important when testing anisotropic rocks such as slate. By simply choosing the direction in which the slots are cut, it is possible to measure K_{1c} relative to any direction in the rock. It is expected that the SDDL test will prove to be useful for testing the variation of K_{1c} with directions of anisotropy in rock.

The SDDL test gave 19% higher values for K_{1c} than did the CNRBEL test. This is to be expected for the reason given in section 4.7. The flexibility of the SDDL testing arrangement is less than that for CNRBEL.

The difference in results between the two tests is small when put into perspective with differences in other fracture tests or more conventional tests on rock and concrete. For example, Kaplan (1961) reported that $\mathcal{G}_{1c}$ values, calculated from stress intensity factors, were 15% lower for 4-point loading compared with 3-point. Hardy and Jayaraman (1970) showed that the variation in tensile strength measurements between several modes of testing was often very much larger than 20%. In the light of other methods of testing, a 19% difference between SDDL and CNRBEL results is considered to be of little consequence. Note also that the difference in results is based on a

very small sample, and more extensive experiments could point to a different conclusion.

Very much more work has to be carried out on the SDDL method of fracture toughness testing before it can be used as a measure of K_{1c}, but the few results gained so far show it to be a potentially useful method.

4.16 CNRBB Tests on Dolomite Rock

Fracture toughness tests were conducted on dolomite rock to assess the applicability of the CNRBB method to rock. Dolomite was chosen as the first rock to be tested because it is relatively isotropic with no discernable bedding.

The rock was obtained from a local quarry, at Miskin, where it is worked for road-stone. It is a very fine-grained rock, but contains extensive calcite veins.

Fifteen cores were cut from a single block of dolomite; three sets of 5 were taken perpendicular to each other to test for any anisotropy. The minimum length of core needed for a CNRBB test is about 12 cm. It was found that cores greater than 18 cm long could be taken, and so 2 notches, 6 cm apart were cut in each long specimen. The long specimens were then tested across each notch in turn. A total of 20 results were possible from the 15 cores. The tests were conducted in the same manner as for the concrete tests, and the results are shown in table 4.10, series A, B and C.

Analysis of the results show that there was no appreciable difference in the measured K_{1c} values for the three sets, but the scatter of the results was greater than might be expected from

Spec. no.	External diam cm	Internal diam cm	Failure load N	K_{1c} $\times 10^6$ $N/m^{\frac{3}{2}}$
1Aa	4.1	2.59	1362	1.27
1Ab	4.1	2.07	1100	1.86
2Aa	4.1	2.56	1385	1.33
2Ab	4.09	2.56	965	0.93
3Aa	4.1	2.59	1185	1.11
3Ab	4.1	2.56	1990	1.91
4Aa	4.1	2.67	1747	1.50
4Ab	4.1	2.59	2005	1.87
5Aa	4.1	2.55	1405	1.37
5Ab	4.1	2.59	1847	1.72
1B	4.1	2.55	2010	1.96
2B	4.07	2.55	2077	2.02
3B	4.1	2.05	1060	1.84
4B	4.1	2.55	1365	1.33
5B	4.1	2.56	1217	1.17
1C	4.1	2.54	1847	1.82
2C	4.1	2.56	1850	1.78
3C	4.09	2.59	1837	1.71
4Ca	4.09	2.56	1245	1.20
4Cb	4.09	2.58	1847	1.74
5C	4.09	2.59	2018	1.88
1	4.1	2.56	1137	1.09
2	4.09	2.57	1258	1.20
3	4.09	2.56	1460	1.40
4	4.09	2.57	965	0.92
5	4.09	2.57	827	0.79
6	4.1	2.05	888	1.53
7	4.1	2.56	1782	1.71
8	4.1	2.56	1435	1.38
9	4.1	2.56	1328	1.28
10	4.1	2.55	1787	1.73
11	4.09	2.56	1265	1.21
12	4.1	2.55	1492	1.44
13	4.09	2.55	1413	1.37

Table 4.10 Results from CNRBB tests on dolomite rock. In series A, B and C the cores were cut, from a single block, mutually perpendicular. The rest were cut with no regard to direction.

consideration of the results from concrete tests. Consequently, another 20 specimens were prepared from another block, and the cores were taken at random with no regard for direction.

The samples from the second dolomite block had more calcite veins in them, and were therefore weaker. Seven specimens broke in places other than through the notch, and had to be discarded. The results from the second block are also given in table 4.10.

Again, the scatter of results was large, and so a histogram of the frequency of occurrence of K_{1c} values was drawn (figure 4.7). It can be seen immediately that there are two peaks to the histogram, one at 1.35×10^6 N/m$^{3/2}$ and one at 1.75×10^6 N/m$^{3/2}$. The histogram suggested that the results were from two populations, and possibly three. Consequently, the results were divided into three groups (table 4.11) and the average and standard deviation for each group was calculated. The scatter of the results for each K_{1c} value was low and more consistent with the results obtained from concrete specimens.

The distribution of the K_{1c} values can be explained as being from the different mineral components in the rock. The high value (1.82×10^6 N/m$^{3/2}$) is the fracture toughness of pure Dolomite. The lower K_{1c} (1.3×10^6 N/m$^{3/2}$) is that of pure calcite in the veins. The lowest value may tentatively be attributed to weathered calcite, the same component which caused several specimens to break distant from the notch. Inspection of several fracture surfaces lends credence to the above explanation (see plates 4.18 and 4.19).

If the average values for the two highest sets of K_{1c} had been calculated from one beam only, they would have been within 5% of the averages for both beams. However, the low K_{1c} value would not have

Plate 4.18

Plate 4.19

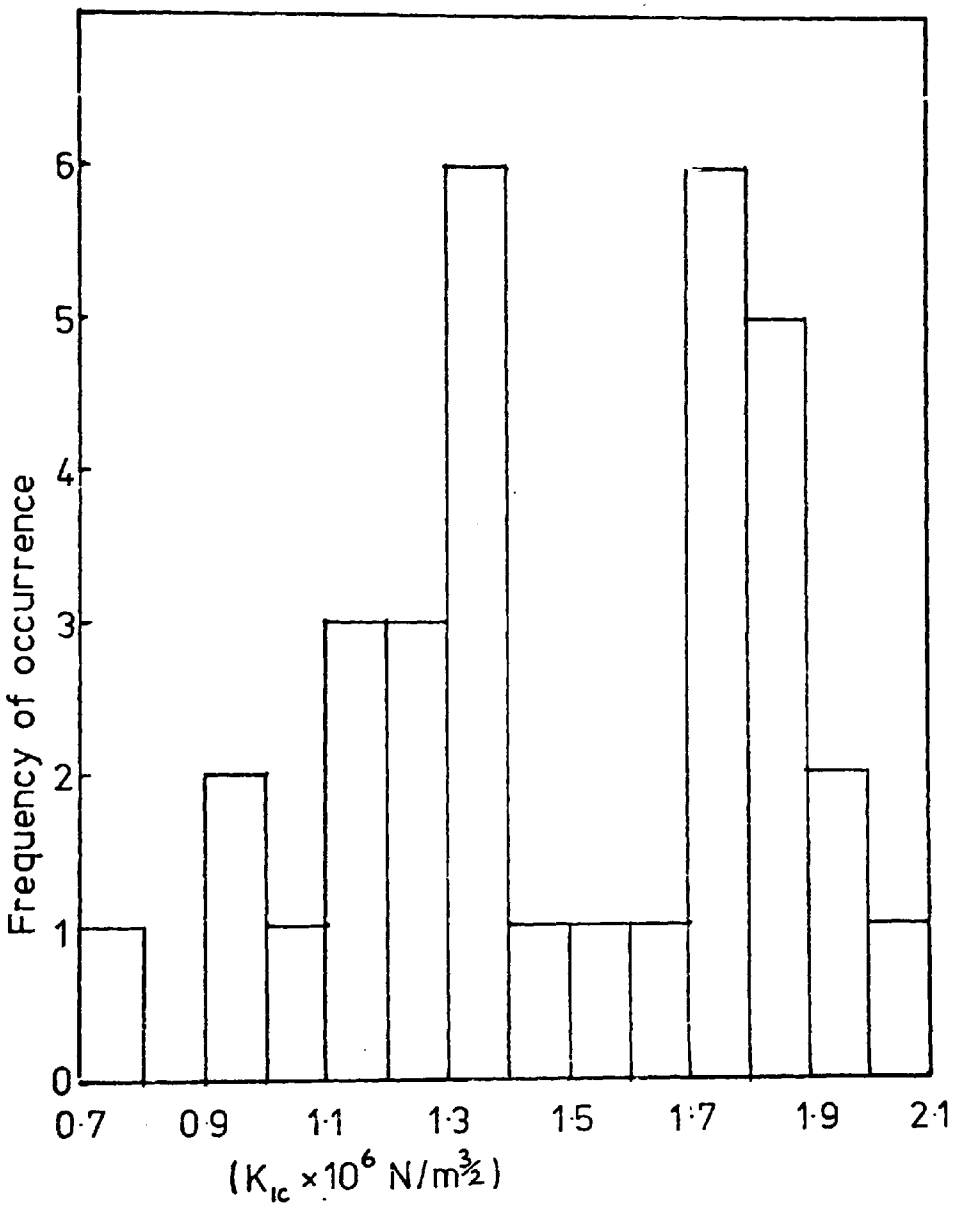

Fig 4.7 Histogram of the frequency of occurrence of K_{IC} values for dolomite rock.

K_{1c} ($x10^5$ $N/m^{\frac{3}{2}}$)	K_{1c} ($x10^6$ $N/m^{\frac{3}{2}}$)	K_{1c} ($x10^6$ $N/m^{\frac{3}{2}}$)
9.3	1.27	1.86
9.2	1.33	1.91
7.9	1.11	1.87
	1.50	1.72
	1.37	1.96
	1.33	2.02
	1.17	1.84
	1.20	1.82
	1.09	1.78
	1.20	1.71
	1.40	1.74
	1.53	1.88
	1.38	1.71
	1.28	1.73
	1.21	
	1.44	
	1.37	
K_{1c}=8.8±0.08 ($x10^5$ $N/m^{\frac{3}{2}}$) var.=8.9%	K_{1c}=1.3±0.13 ($x10^6$ $N/m^{\frac{3}{2}}$) var.=9.9%	K_{1c}=1.82±0.1 ($x10^6$ $N/m^{\frac{3}{2}}$) var.=5.4%

Table 4.11 Results from CNRBB fracture toughness tests on samples from two dolomite blocks, divided into three groups, showing the average and standard deviation for each group.

been recognised as being separate from the two higher values.

Preliminary experiments have shown the CNRBB test to be suitable for dolomite rock. The test is sensitive enough to separate the fracture toughness values for various mineral components within the rock.

4.17 CNRBEL Tests on Slate

To assess the applicability of fracture toughness testing to anisotropic materials, CNRBEL tests were conducted on slate.

The slate was taken from a quarry at Corris, in North Wales, where it is still worked. The rock has a well-defined cleavage, but it is not very friable, and is a suitable test material. As the rock was drilled perpendicular to the bedding plane (PEB), the cores broke off at about 5 cm intervals, and so were not long enough for CNRBB testing. However, CNRBEL tests were possible and the rock was prepared as for concrete described previously. Cores were cut parallel to the bedding plane (PAB) from the same rock. Twelve specimens were prepared from each coring direction.

The samples were tested in the same manner as for concrete, described in section 4.9. There were two problems associated with CNRBEL testing of slate which had not been encountered before.

It was important, with PEB specimens, to ensure that the loading bar was also PEB. Because of the weakness of the bedding plane, shear failure along it can easily occur, as shown in plate 4.20. As long as the loading bar was placed across the bedding plane, shear failure did not occur.

Plate 4.20

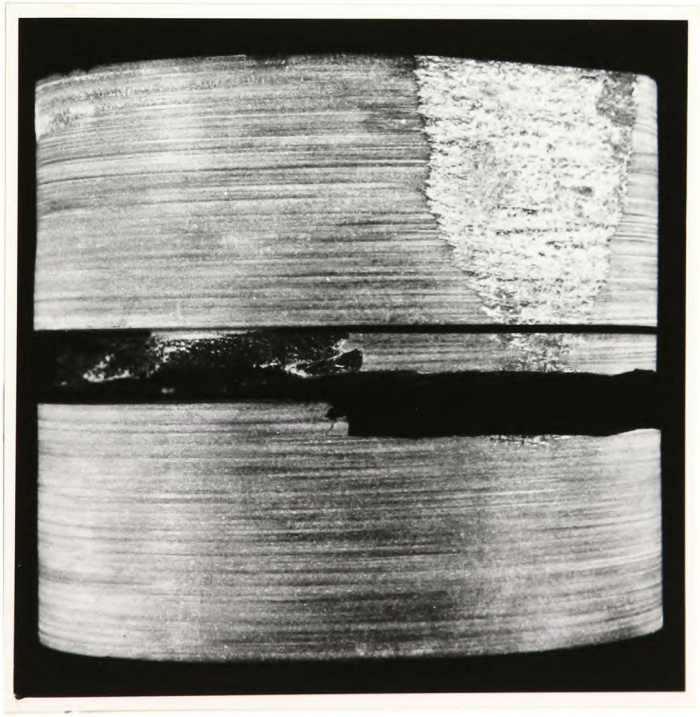

Plate 4.21

When the specimens were tested with the notch PAB, failure sometimes occurred along a plane other than at the notch (plate 4.21), and no fracture toughness results were obtained. The only information which can be gained from such an occurrence is that the fracture toughness is greater than a value determined from the failure load.

The results from CNRBEL tests on slate are given in table 4.12.

4.18 Discussion of Fracture Toughness Results for Slate

The most obvious difference in results between the two sets of data in table 4.12 is that K_{1c} for PEB specimens is more than twice that for PAB. The deviation of the latter set of data is larger, but note that the smaller number of results would tend to make for a greater scatter.

Plates 4.22 and 4.23 are photographs of fracture surfaces perpendicular and parallel to the bedding plane. The appearance of the surfaces illustrates why the deviations of the data are so different. The irregular topography of the second photograph shows that the specimen had failed across a bedding plane rather than through the circumferential notch. The rock probably did not fail at the base of the notch but to one side. This means that the expression for K_1 for a slate specimen is only an approximation of the condition under which a crack initiated.

For design purposes, the minimum K_{1c} value might be the most appropriate. For K_{1c} measurements PAB, the minimum value is only 60% of the average. If a large mass of slate were to fail, it might do so at the point where K_{1c} is a minimum.

Plate 4.22

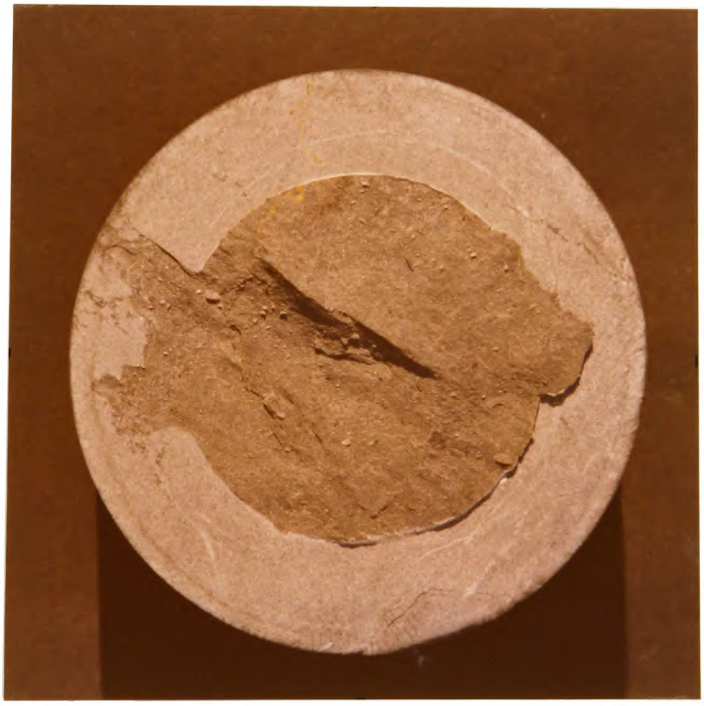

Plate 4.23

spec. no.	external diam cm.	internal diam cm.	failure load kN	K_{1c} $x10^5$ $N/m^{\frac{3}{2}}$
1	5.35	3.33	5.98	2.02
2	5.35	3.34	6.62	2.21
3	5.35	3.32	6.25	2.13
4	5.35	3.34	6.62	2.21
5	5.35	3.33	6.37	2.13
6	5.35	3.34	7.13	2.38
7	5.35	3.34	7.39	2.47
8	5.35	3.10	0.60	-
9	5.35	3.33	6.86	2.31
10	5.35	3.34	6.20	2.07
11	5.35	3.34	7.70	2.57
K_{1c} = 2.25 ± 0.18 $x10^5$ $N/m^{\frac{3}{2}}$ (8% var)				
12	5.35	3.34	1.30	-
13	5.35	3.36	1.97	0.65
14	5.35	3.35	2.19	0.72
15	5.35	3.35	2.65	-
16	5.35	3.33	1.69	-
17	5.35	3.33	3.33	1.12
18	5.35	3.35	3.25	1.08
19	5.35	3.32	0.95	-
20	5.35	3.32	3.92	1.33
21	5.35	3.37	3.95	1.28
22	5.35	3.34	2.78	0.93
23	5.35	3.32	1.27	-
24	5.35	3.35	4.6	1.52
K_{1c} = 1.08 ± 0.03 $x10^5$ $N/m^{\frac{3}{2}}$ (28% var)				

Table 4.12 Fracture toughness results from CNRBEL tests on slate. Specimens 1-11 were tested perpendicular to the bedding plane, 12-24 were tested parallel to it. Results marked - indicate that the specimen broke at a place other than at the notch.

The problem of the slate breaking at a place other than at the notch could be reduced by making the circumferential notch deeper, and this would ensure that failure occurred at the notch root. However, as CNRBEL results from concrete show (section 4.10), a deep notch gives a much higher deviation of the data, and this has to be considered against the advantage which might be gained.

The expression for K_1 for CNRBEL tests has been derived for an elastically isotropic material. Slate only poorly approximates to such a material, but within this limitation, the CNRBEL test can give reproducible K_{1c} results with acceptable deviations of the data.

Appendices

Computer program to analyse load-deflection graphs, and detailed results from fracture toughness tests on concrete.

4a Computer program to calculate the area under a load-deflection graph, and K_{1c} for CNRBB tests

The load and displacement channels of an Instron 1251 model testing machine were connected to one unit of a Mycalex Series 5 computer system. The system consists of three data-loggers, with teletypes, connected to a central Data General Nova 1220 computer. Each data-logger can take up to 100 signals, and can be accessed by the computer.

The computer uses the interactive language 'BASIC', and the program described in this appendix is relatively simple and self-explanatory. There are two instructions which are peculiar to the Mycalex system. Statements of the form 'Call 9,A1,A2,A3' (e.g. 0010) access a clock in the computer, and gives the time where A1 is in hours, A2 in minutes, and A3 in seconds. Statements of the form 'Call 10,C1, A2,A3' access a data channel (e.g. 0600), where C1 is the required channel, A2 is the voltage on the channel (in microvolts), and A3 is the channel accessed. In the absence of errors, A3 = C1.

In the computer system there was an intrinsic problem with accessing the clock, and it was found to be necessary to insert dummy statements (e.g. 0550) and time delays (e.g. 0020 - 0040) to ensure correct time readings. As the clock and computer were remote from the testing machine and computer terminal, a check was written into the program (statements 0010 - 0090) to ensure that the clock was switched on.

The computer sampled the load-deflection graph (i.e. the voltage outputs) from the Instron at N second intervals, where N was set at the beginning of a series of experiments (statements 0170 & 0180). The sampling was stopped if one of two conditions was satisfied.

The maximum dimension which can be given to any array is 225 (statement 0100), so that when a maximum of 225 data points were gathered, the sampling stopped (statement 0690). More normally, the sampling stopped when the voltage on the load channel was within 10 mV of the zero line (see for example figure 4.4), and the graph was assumed to be completed (statement 0680). To prevent the program from stopping immediately if the load did not increase at the start of the experiment, a delay was introduced of 20 sample points (statement 0670). The maximum load used in the expression for K_{1c} was simply derived from a comparison of all load sample points (statements 0800 - 0830).

```
0010 CALL 9,A1,A2,A3
0020 FOR I=1 TO 1000
0030   LET Z=10
0040 NEXT I
0050 CALL 9,A1,A2,A3
0060 LET T=A2*60+A3
0070 CALL 9,A1,A2,A3
0080 IF A2*60+A3<T+5 GOTO 0070
0090 PRINT T,A2*60+A3
0100 DIM A$[50],U[225],X[225]
0110 PRINT "PROGRAM TO MEASURE X-U GRAPHS"
0120 PRINT "FOR CYLINDRICAL NOTCHED SPECIMENS"
0130 PRINT
0140 PRINT "WHICH CHANNELS ARE YOU USING (LOAD CHANNEL FIRST)";
0150 INPUT C1,C2
0160 PRINT
0170 PRINT "WHAT SAMPLE INTERVAL DO YOU WANT (IN SECS.)";
0180 INPUT N
0190 PRINT
0200 PRINT "ARE ALL SCALE FACTORS CONSTANT (TYPE Y OR N)";
0210 INPUT A$
0220 IF A$="N" GOTO 0270
0230 PRINT
0240 PRINT "INPUT HOR. AND VERT. SCALE FACTORS (MM/V,N/V)";
0250 INPUT P5,P6
0260 PRINT
0270 PRINT
0280 PRINT "EXPERIMENT NUMBER";
0290 INPUT J
0300 PRINT
0310 PRINT "INPUT MAX. AND MIN. SPEC. DIAM. (IN CM.)";
0320 INPUT D1,D2
0330 IF D2>=D1 GOTO 0310
0340 PRINT
0350 IF A$="N" GOTO 0390
0360 LET F1=P5
0370 LET F2=P6
0380 GOTO 0420
0390 PRINT "INPUT HOR. AND VERT. SCALE FACTORS (MM/V,N/V)";
0400 INPUT F1,F2
0410 PRINT
0420 LET F1=F1/1000
0430 PRINT "TO START PROGRAM TYPE 1";
0440 INPUT Z9
```

```
0450 PRINT
0460 IF Z9<>1 GOTO  0430
0470 CALL 9,A1,A2,A3
0480 FOR Z=1 TO 1000
0490   LET K5=8
0500 NEXT Z
0510 CALL 9,A1,A2,A3
0520 LET T1=3600*A1+60*A2+A3
0530 LET I=0
0540 LET I=I+1
0550 CALL 9,A1,A2,A3
0560 CALL 9,A1,A2,A3
0570 LET T2=3600*A1+60*A2+A3
0580 IF T2-T1<N GOTO  0550
0590 LET T1=3600*A1+60*A2+A3
0600 CALL 10,C1,A2,A3
0610 LET X[I]=ABS(A2)
0620 CALL 10,C2,A2,A3
0630 LET U[I]=ABS(A2)
0640 IF I=1 GOTO  0660
0650 LET X[I]=X[1]-X[I]
0660 LET U[I]=U[1]-U[I]
0670 IF I<20 GOTO 0540
0680 IF ABS(X[I])<10000 GOTO  0700
0690 IF I<225 GOTO  0540
0700 GOTO 0710
0710 LET S=0
0720 LET X[1]=0
0730 FOR K=1 TO I
0740   LET S=S+.5*1E-12*(U[K]-U[K-1])*(X[K]+X[K-1])
0750 NEXT K
0760 PRINT "AREA UNDER THE CURVE = ";S*F1*F2;"NM"
0770 LET W=4*S*F1*F2*10000/3.1416/D2↑2
0780 PRINT "WORK OF FRACTURE = ";W;"N/M"
0790 LET L=0
0800 FOR K=1 TO I
0810   IF ABS(X[K])<L GOTO  0830
0820   LET L=X[K]
0830 NEXT K
0840 PRINT "MAXIMUM LOAD = ";L*F2/1E+6;"N"
0850 LET A=D2*.01/2
0860 LET T=.01*(D1-D2)/2
0870 LET A5=A↑5
0880 LET K=4.139*.01*SQR(T/A5/(4.48*T+.502*A))
0890 LET K=K*L*F2/1E+6
0900 PRINT "KIC = ";K;"N/M↑3/2"
0910 PRINT
0920 PRINT "IF YOU WANT ANOTHER EXPERIMENT TYPE 2";
0930 INPUT H
0940 PRINT
0950 IF H=2 GO TO  0270
0960 END
```

```
RUN
 3Ø97          31Ø2
PROGRAM TO MEASURE X-U GRAPHS
FOR CYLINDRICAL NOTCHED SPECIMENS

WHICH CHANNELS ARE YOU USING (LOAD CHANNEL FIRST)? 2Ø7,2Ø9
WHAT SAMPLE INTERVAL DO YOU WANT (IN SECS.)? 2
ARE ALL SCALE FACTORS CONSTANT (TYPE Y OR N)? Y
INPUT HOR. AND VERT. SCALE FACTORS (MM/V,N/V)? .75,25ØØ

EXPERIMENT NUMBER? 1
INPUT MAX. AND MIN. SPEC. DIAM. (IN CM.)? 4.1,2.56
TO START PROGRAM TYPE 1? 1
AREA UNDER THE CURVE =  6.7ØØ59E-2 NM
WORK OF FRACTURE =  259.345 N/M
MAXIMUM LOAD =  1137.5 N
KIC =  1.Ø8569E+6 N/M↑3/2

IF YOU WANT ANOTHER EXPERIMENT TYPE 2
? 2

EXPERIMENT NUMBER? 2
INPUT MAX. AND MIN. SPEC. DIAM. (IN CM.)? 4.Ø9,2.57

TO START PROGRAM TYPE 1? 1
AREA UNDER THE CURVE =  .123828 NM
WORK OF FRACTURE =  477.411 N/M
MAXIMUM LOAD =  1257.75 N
KIC =  1.19341E+6 N/M↑3/2

IF YOU WANT ANOTHER EXPERIMENT TYPE 2
? 3

*READY
```

4b Detailed results from fracture toughness tests.

spec. no.	external diam. cm	internal diam. cm	failure load N	K_{Ic} $\times 10^5$ N/m$^{\frac{3}{2}}$	$\mathcal{G}_{Ic}$ J/m
1	4.07	3.56	1015	3.5	74.3
2	4.07	3.58	980	3.3	94.9
3	4.01	3.5	858	3.1	62.9
4	4.11	3.62	1120	3.66	-
5	4.0	3.49	1017	3.7	81.7
6	4.11	3.6	1088	3.64	75.0
7	4.08	3.55	1020	3.57	78.7
8	4.08	3.58	1017	3.44	68.5
9	4.02	2.99	739	4.57	82.0
10	4.0	3.04	737	4.33	77.0
11	4.06	3.1	802	4.47	86.7
12	4.06	3.08	770	4.38	69.9
13	4.08	3.05	676	4.47	53.0
14	4.05	3.04	729	4.3	68.1
15	4.1	3.09	740	4.19	54.5
16	4.07	3.04	695	4.12	55.6
17	4.12	2.58	452	4.28	39.9
18	4.12	2.59	530	4.93	59.9
19	4.11	2.59	501	4.69	57.0
20	4.11	2.58	429	4.03	34.7
21	4.11	2.59	388	3.62	40.3
22	4.11	2.59	441	4.16	47.0
23	4.11	2.58	485	4.59	29.4

Table b4.1 Detailed results from fracture toughness tests conducted on samples from concrete beam number 1, as summarised in table 4.1.

spec. number	external diam. cm	internal diam. cm	failure load N	K_{1c} $\times 10^5$ N/m$^{3/2}$	$\mathcal{G}_{1c}$ N/m
1	4.08	3.05	947	5.56	103
2	4.08	3.06	941	5.47	100
3	4.08	3.06	870	5.06	77.5
4	4.08	3.05	861	5.06	79.1
5	4.08	3.06	962	5.6	81.6
6	-	-	-	-	-
7	4.09	3.06	785	4.57	82.5
8	4.07	3.06	967	5.62	98.6
9	4.08	3.05	837	4.92	69.1
10	4.09	3.06	867	5.05	88.0
11	4.09	3.06	895	5.21	86.5
12	4.09	3.05	949	5.58	94.5
13	4.09	3.06	737	4.29*	58.3
14	4.09	3.06	847	4.93	91.7
15	4.1	3.06	945	5.51	83.2
16	4.1	2.55	585	5.7	76.8
17	4.09	2.56	571	5.5	77.5
18	4.09	2.56	560	5.39	77.3
19	4.09	2.56	611	5.89	73.5
20	4.08	2.56	640	6.16	94.4
21	4.08	2.56	594	5.72	72.8
22	4.08	2.56	541	5.21	77.9
23	4.08	2.56	539	5.19	71.7
24	4.08	2.56	547	5.27	82.9
25	4.09	2.56	471	4.54	56.6
26	4.08	2.56	672	6.21	98.6
27	4.08	2.56	565	5.44	68.3
28	4.09	2.56	515	4.96	68.3
29	4.08	2.56	522	5.03	73.7
30	4.08	2.56	464	4.47	73.7

Table b4.2 Detailed results for fracture tests conducted on specimens from concrete beam number 2. There are no results for specimen number 6 because it broke at a place other than the notch. K_{1c} value marked * was not used in the calculation of averages because it is abnormally low.

spec. no.	external diam. cm	internal diam. cm	failure load N	K_{1c} $x10^5$ $N/m^{\frac{3}{2}}$
1	4.04	2.525	440	4.39
2	4.04	2.575	400	4.03
3	4.05	2.505	400	4.08
4	4.04	2.52	381	3.82
5	4.04	2.525	387	3.86
K_{1c} = 4.04 ± 0.23 $x10^5$ $N/m^{\frac{3}{2}}$ (5.6% var)				
6	4.06	2.257	300	4.04
7	4.06	2.28	-	-
8	4.06	2.275	317	4.18
9	4.06	2.295	341	4.40
10	4.06	2.295	313	4.04
K_{1c} = 4.16 ± 0.17 $x10^5$ $N/m^{\frac{3}{2}}$ (4.1% var)				
11	5.35	3.83	1125	3.81
12	5.35	3.83	1062	3.60
13	5.35	3.83	1110	3.76
14	5.35	3.815	1300	4.45
15	5.35	3.855	1050	3.49
16	5.35	3.815	1100	3.71
K_{1c} = 3.81 ± 0.33 $x10^5$ $N/m^{\frac{3}{2}}$ (8.8% var)				
17	5.35	3.35	800	3.93
18	5.35	3.31	1175	5.97*
19	5.35	3.31	780	3.96
20	5.35	3.31	750	3.81
21	5.35	3.31	1000	5.08
22	5.35	3.34	855	4.24
23	5.35	3.345	900	4.44
K_{1c} = 4.24 ± 0.47 $x10^5$ $N/m^{\frac{3}{2}}$ (11.1% var)				
24	5.35	2.825	650	5.03
25	5.35	2.82	590	4.59
26	5.35	2.81	650	5.10
27	5.35	2.84	581	4.43
28	5.35	2.82	656	4.10
29	5.35	2.82	575	4.47
30	5.35	2.84	600	4.58
K_{1c} = 4.74 ± 0.31 $x10^5$ $N/m^{\frac{3}{2}}$ (6.6% var)				

Table b4.3 Detailed results from CNRBB tests on concrete with two sample diameters (Beam A in table 4.4). Result marked * was not used in the calculation of the average.

spec. no.	external diam. cm	internal diam. cm	failure load N	K_{1c} $x10^5$ $N/m^{3/2}$
1	5.35	3.315	1840	6.29
2	5.35	3.315	1680	5.74
3	5.35	3.3	2025	7.01
4	5.35	3.28	1975	6.97
5	5.35	3.325	1650	5.59
6	5.35	3.32	1925	6.55
$K_{1c} = 6.36 \pm 0.6$ $x10^5$ $N/m^{3/2}$ (9.5% var)				
7	5.35	2.81	1085	6.02
8	5.35	2.8	1225	6.86
9	5.35	2.805	1025	5.71
10	5.35	2.805	1112	6.20
11	5.35	2.805	1175	6.55
12	5.35	2.805	912	5.08*
$K_{1c} = 6.27 \pm 0.45$ $x10^5$ $N/m^{3/2}$ (7.2% var)				

Table b 4.4 Results from CNRBB tests on concrete with two sample notch depths (Beam B in table 4.4). Result marked * was not used in tha calculation of the average.

spec. no.	external diam. cm	internal diam. cm	failure load N	K_{1c} $\times 10^5$ $N/m^{3/2}$
1A	4.07	2.555	1030	9.97
2A	4.08	2.55	1092	10.63
3A	4.08	2.55	1110	10.80
4A	4.07	2.545	1145	11.2
5A	4.07	2.54	950	9.34
$K_{1c} = 10.4 \pm 0.73 \times 10^5$ $N/m^{3/2}$ (7.1% var)				
6A	4.08	2.54	930	9.15
7A	4.08	2.56	1210	11.65*
8A	4.06	2.54	875	8.6
9A	4.06	2.55	700	6.80
10A	4.07	2.53	877	8.71
11A	4.06	2.54	620	6.09
12A	4.07	2.56	685	6.59
13A	4.075	2.57	787	7.5
14A	4.075	2.56	720	6.93
15A	4.08	2.56	820	7.90
16A	4.06	2.54	945	9.28
17A	4.085	2.57	827	7.88
$K_{1c} = 7.77 \pm 1.08 \times 10^5$ $N/m^{3/2}$ (13.9% var)				
1B	4.09	2.56	747.5	7.2
2B	4.09	2.56	665	6.41
3B	4.09	2.56	742.5	7.15
4B	4.09	2.55	835	8.13
5B	4.09	2.565	710	6.8
$K_{1c} = 7.14 \pm 0.64 \times 10^5$ $N/m^{3/2}$ (8.9% var)				
6B	4.08	2.54	605	5.95
7B	4.05	2.54	685	6.73
8B	4.06	2.53	630	6.26
9B	4.06	2.535	547.5	5.41
10B	4.07	2.56	510	4.91
11B	4.06	2.56	800	7.69
12B	4.07	2.57	435	4.14
$K_{1c} = 6.03 \pm 1.03 \times 10^5$ $N/m^{3/2}$ (17.1% var)				

Table b4.5 Detailed results from comparisons of CNRBB tests on concrete, with and without metal collars (beams A and B in table 4.6). Samples 6A - 17A and 6B - 12B were tested with metal collars. Result marked * was not used in the calculation of the average K_{1c}.

spec. no.	external diam. cm	internal diam. cm	failure load N	K_{1c} $\times 10^5$ N/m$^{\frac{3}{2}}$
1	5.37	3.83	2850	6.3
2	5.37	3.82	3925	8.64*
3	5.37	3.81	3180	7.14
4	5.37	3.81	2740	6.16
5	5.37	3.82	2875	6.40
6	5.37	3.82	3360	7.49
7	5.37	3.82	3190	7.11
8	5.37	3.82	3500	7.80
9	5.37	3.81	3500	7.86
10	5.37	3.82	3625	8.08
11	5.37	3.82	3090	6.88
12	5.37	3.81	2890	6.49
$K_{1c} = 7.06 \pm 0.46 \times 10^5$ N/m$^{\frac{3}{2}}$ (6.5% var)				
1A	5.37	3.32	1762	6.05*
2A	5.37	3.33	2050	6.97
3A	5.37	3.31	2125	7.36
4A	5.37	3.31	2285	7.91
5A	5.37	3.31	2425	8.40
6A	5.37	3.29	2125	7.49
7A	5.37	3.33	2400	8.16
8A	5.37	3.32	2350	8.07
9A	5.37	3.31	2325	8.05
10A	5.37	3.33	2175	7.40
11A	5.37	3.31	2238	7.75
12A	5.37	3.35	2125	7.10
$K_{1c} = 7.70 \pm 0.46 \times 10^5$ N/m$^{\frac{3}{2}}$ (6% var)				

Table b4.6 Detailed results from CNRBEL tests on concrete, as summarised in table 4.8. Results marked * were not used in the calculation of the averages.

spec. no.	external diam. cm	internal diam. cm	failure load N	K_{1c} $\times 10^5$ $N/m^{\frac{3}{2}}$
1B	5.37	2.81	1335	7.46
2B	5.37	2.82	1362	7.54
3B	5.37	2.82	1230	6.81
4B	5.37	2.82	1262	6.98
5B	5.37	2.81	1355	7.58
6B	5.37	2.81	1062	5.94
7B	5.37	2.82	925	5.12*
8B	5.37	2.84	1175	6.37
9B	5.37	2.81	1288	7.28
10B	5.37	2.80	1103	6.17
11B	5.37	2.81	1186	6.63
12B	5.37	2.81	-	-
K_{1c} = 6.88 ± 0.59 $\times 10^5$ $N/m^{\frac{3}{2}}$ (8.6% var)				
1C	5.37	2.30	525	5.16
2C	5.37	2.31	694	6.74
3C	5.37	2.29	712	7.04
4C	5.37	2.29	594	5.88
5C	5.37	2.29	684	6.77
6C	5.37	2.29	696	6.88
7C	5.37	2.31	696	6.76
8C	5.37	2.31	674	6.55
9C	5.37	2.30	862	8.47*
10C	5.37	2.30	662	6.51
11C	5.37	2.30	662	6.51
12C	5.37	2.29	588	5.82
K_{1c} = 6.42 ± 0.57 $\times 10^5$ $N/m^{\frac{3}{2}}$ (8.8% var)				

Table b4.7 Detailed results from CNRBTL tests on concrete, as summarised in table 4.8. Results marked * were not used in the calculation of the averages.

CHAPTER 5

Failure criteria are derived for simple rock structures, using the K_{1c} measurements from the new fracture toughness tests. The results are compared with conventional tensile strength criteria.

5.1 Introduction

As pointed out in chapter 1, the theoretical content of this thesis concentrates on situations in which the tensile failure of rock is involved. In tension, crack initiation and crack propagation are usually simultaneous, and fracture criteria are then failure criteria. This is a different situation from compressive failure where considerable crack propagation occurs prior to failure.

This chapter can only give design criteria for very simple, and perhaps limited structures. For most real circumstances, more complicated numerical techniques, such as finite elements, would have to be used. However, the purpose of this thesis is to illustrate how fracture mechanics can be used to give useful design guidance, and the concepts introduced can then be extended to more complicated situations.

There are two methods by which fracture toughness measurements can be used to predict strength failure. These are by consideration of either the stresses at a crack tip, or energy changes in a system during the cracking process.

The first method assumes a relation of the form:-

$$K_1 = k.\sigma\sqrt{\pi a} \qquad (5.1)$$

where σ is the nominal stress around a crack of length t, and k is a factor which depends upon the loading arrangement of the system. The structure is assumed to fail when K_1 reaches a critical value K_{1c}. The principal advantage of a failure criterion of the form (5.1) is its simplicity. Perhaps the biggest disadvantage is that an arbitrary decision has to be made as to how large a crack, t, can become before

it is considered intolerable.

The second method of calculating fracture failure criteria assumes a relation of the form expressed earlier in section 2.3, i.e.:-

$$\mathcal{G}_{1c} = \frac{d}{dA}\left(\frac{1}{2}yF\right)_F \qquad (5.2)$$

This equation is for quasi-static crack propagation and can be simply expressed in words; 'a crack will extend when the rate of change of strain energy caused by the extension of the crack is greater than the rate of energy absorption by the crack surfaces'. If U_s is the energy absorbed by the crack, and W is the strain energy in a body containing the crack, then (5.2) at failure can be written as:-

$$\frac{dW}{dA} = \frac{dU_s}{dA} \qquad (5.3)$$

It will be shown in this chapter that failure criteria in the form of (5.3) can be used successfully to derive design criteria for rock structures. Furthermore, in most cases, these criteria will assume no crack lengths, as is needed for equation (5.1).

5.2 Tensile Stress Situations

The main circumstances in which tensile stresses occur is in a tunnel of rectangular profile (Obert & Duvall 1967). For most situations, tensile stresses are avoided by having a tunnel of circular or oval cross-section. However, rectangular profiles are found in mines, especially for roadways and where longwall mining is used.

This chapter will consider three cases in which tensile stresses

are important. These cases are shown in figure 5.1. They are a simple cantilever, an immediate roof detaching from the main roof, and buckling of near-surface rock layers (spalling). The analysis will also consider the effect of roof supports, either from props or bolts.

5.3 Assumptions

The deformation of the structures in figure 5.1 will be calculated on the basis of simple beam theory. It is worth enumerating the assumptions of the theory, and compare them with the real properties of rocks. Figure 5.1 also shows the coordinate system used, and the sign convention for bending moments.

1. Conditions in the beams will be assumed to be of plane stress. This means that there are no stresses in the z direction (see figure 5.1). This is not a very limiting assumption for rock. If there were stresses in the z direction, normal stresses in the x direction would be modified by a factor of $1/(1 - \nu^2)$. For rock, $\nu < 0.3$ and the error in assuming plane stress is less than 10%, which is more than compensated by the relative ease of the mathematics.

2. The beam is composed of homogeneous, isotropic, and elastic material. However, it will not be assumed that K_{1c} for rock is isotropic. For layered material, such as slate, this anisotropy is important.

3. The beam has a uniform cross-section and a longitudinal plane of symmetry, and is subjected to transverse loading.

4. Deflections of the beam are small.

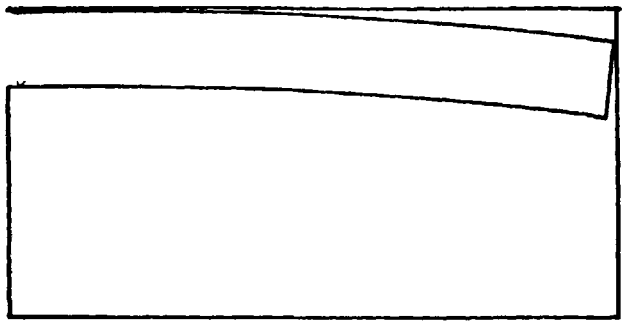

a) simple cantilever

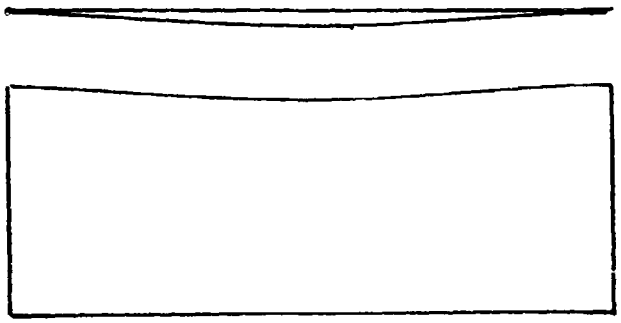

b) detachment of immediate roof

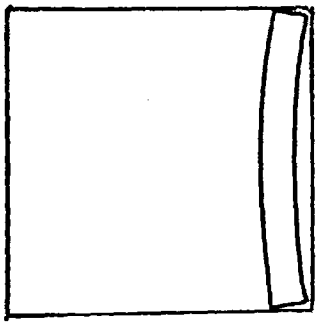

c) buckling of side walls

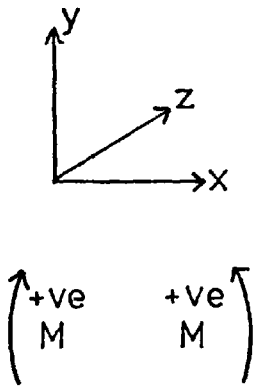

d) coordinate axes and bending moment sign convention,

Fig 5.1 Situations of possible rock failure which will be analysed using fracture mechanics, and coordinate system

5. The shear stresses in any section of the beam have a parabolic distribution through the section, and for a rectangular section the shear coefficient is 6/5.

6. Where two planes are touching, the coefficient of friction between the two planes is zero. This is obviously an unrealistic assumption, but for this analysis it errs on the side of safety. When considering anergy changes in a system, it is assumed that none is absorbed by friction. In real circumstances, any energy which is absorbed by friction will reduce the amount available to cause failure, i.e. in equation (5.3) dW/dA will be an overestimate.

7. Cracks initiate in the regions of highest tensile stress, and propagate perpendicular to the direction of this maximum stress. This assumption is justified if it is assumed that rock is an isotropic, granular material, with a grain size of 't'. Brace (1961) showed that the grain boundaries in a material could be associated with 'Griffith cracks', i.e. the grain boundaries are nuclei for crack initiation. For a circular crack of diameter 2t, K_1 is given by Paris and Sih (1965):-

$$K_1 = 2\sigma\sqrt{\frac{t}{\pi}} \qquad (5.4)$$

For an isotropic body, failure will occur in a region where σ is a maximum.

5.4 Rock Cantilever

A simple example of a rock cantilever is shown in figure 5.2. Such a structure might be found in the roof of an opening in which there

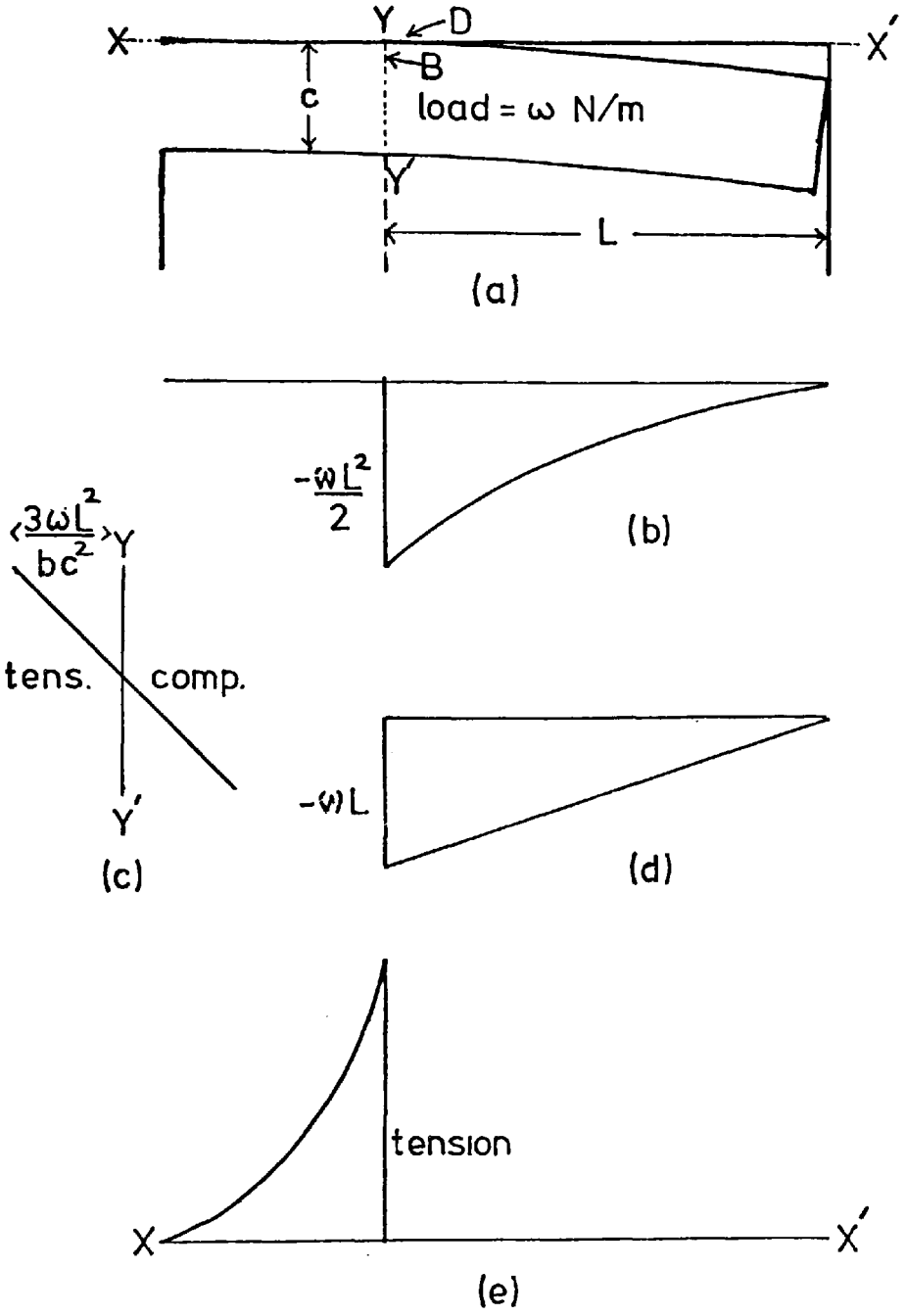

Fig 5.2 a) Rock cantilever detaching from the main roof.

b) Bending moment diagram

c) Horizontal stresses along the vertical section Y-Y′.

d) Shear-force diagram.

e) Vertical stresses along the horizontal section X-X′ (idealised)

is a joint at one side. Also, the roof of a tunnel after the advance of hydraulic jacks might be modelled by such a structure (Thomas 1973). Also included in the figure are the distribution of bending moments, shear and normal stresses. It can be seen that there are two regions of high tensile stress, as marked D and B in the figure. These are between the cantilever and the main roof, and at the top of the beam. If the beam is stressed by an overlying pressure, rather than by its own weight, then there will be no tensile stress at D.

This analysis will consider two failure conditions; when the beam is detaching from the main roof (at D) and when a crack appears in the upper side of the beam (at B). It is easier to calculate the potential energy in a beam, P, from the beam deflections than the strain energy, W, from the bending moments. By substitution of $W = P/2$ (section 2.1), the strain energy can be calculated from the potential energy. Because of the coordinate system used in this thesis, the deflections are negative, and the calculated potential energy is also negative. Therefore, the substitution $W = -P/2$ is used in subsequent calculations and:-

$$W = \frac{1}{2}\int_0^L \omega y dx \qquad (5.5)$$

where ω is the force/unit length on the beam, and y is the deflection at any point.

The deflection of the beam is given by:-

$$y = \frac{\omega}{EI}\left(\frac{Lx^3}{6} - \frac{L^2x^2}{4} - \frac{x^4}{24}\right) + \frac{6}{5}\frac{\omega x}{GA}\left(\frac{x}{2} - L\right) \qquad (5.6)$$

where E = Young's modulus, A = cross-sectional area, G = shear modulus, I = second moment of area, $bc^3/12$, L = beam length.

The first major term in (5.5) represents the deflection due to bending, and the second term is that due to shear and is only important for short beams. Substitution of (5.6) into (5.5) gives the result:-

$$W = \frac{\omega^2}{2}\left(\frac{L^5}{20EI} + \frac{2L^3}{5Gbc}\right) \qquad (5.7)$$

The crack area increment (dA) = bdL where b is the beam width, and:-

$$\frac{dW}{dA} = \frac{\omega^2}{2b}\left(\frac{L^4}{4EI} + \frac{6L^2}{5Gbc}\right) \qquad (5.8)$$

Using equation (5.3), and noting that $\mathcal{G}_{1c} = dU_s/dA$, the failure condition is:-

$$\mathcal{G}_{1c} = \frac{\omega^2}{2b}\left(\frac{L^4}{4EI} + \frac{6L^2}{5Gbc}\right) \qquad (5.9)$$

For a beam deflecting under its own weight, $\omega = dbc$, where d is the rock beam density. Substituting $G = E/2(1+\nu)$, $I = bc^3/12$, and $\mathcal{G}_{1c} = K_1^2/E$ gives at failure:-

$$K_{1c}^{\ 2} = \frac{d^2cL^2}{2}\left(\frac{3L^2}{c^2} + \frac{12(1+\nu)}{5}\right) \qquad (5.10)$$

Figure 5.3 is a graphical representation of equation (5.10) for various roof thicknesses, and can be used as design criteria for the width of a tunnel. For a given tunnel width, and roof thickness, K_{1c}/d has to be greater than the value given by the appropriate curve for failure not to occur. There is not an equivalent failure criterion in terms of tensile stresses because a crack is already assumed to

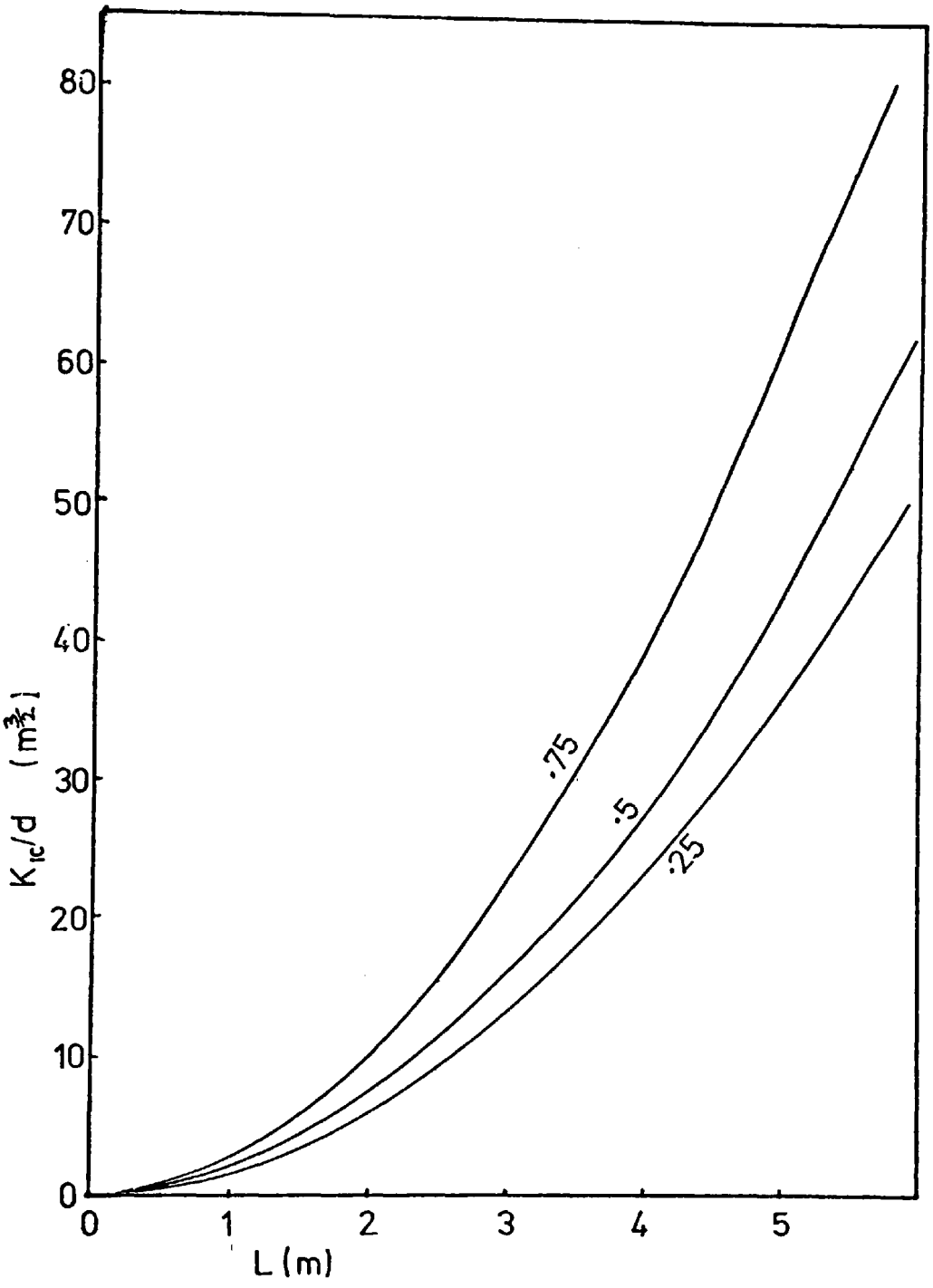

Fig 5.3 Graphical representation of equation (5·10) for $\nu = 0{\cdot}25$. The numbers on the curves indicate the beam thickness, c (in m).

exist in the structure, and the tensile stress at the tip of a crack is theoretically infinite.

The failure condition (5.10) is only for the situation in which a beam is becoming detached from the main roof (point D in figure 5.2). It is possible that the beam will fail at point B before conditions at D become critical.

The most convenient way of representing failure across the beam is to assume that, as a crack propagates, the beam breaks up into layers (figure 5.4). In this case, it is assumed that the force per unit length of beam, ω, remains constant, while the thickness, c, is reduced to (c-t). Because the length of the beam does not change for this mode of failure, the strain energy due to shear remains constant throughout the cracking process. Therefore, equation (5.7) becomes:-

$$W = \frac{\omega^2 L^5}{40EI} \qquad (5.11)$$

Substituing $I = b(c - t^3)/12$, and differentiating with respect to t gives:-

$$\frac{dW}{dt} = \frac{9\omega^2 L^5}{10Eb(c-t)^4} \qquad (5.12)$$

The incremental crack area (dA) = bdt, and substitution of (5.12) into (5.3) gives, at failure:-

$$\mathcal{G}_{1c} = \frac{9\omega^2 L^5}{10Eb^2(c-t)^4} \qquad (5.13)$$

At the start of the cracking process, t = 0, and substituting for $\mathcal{G}_{1c}$ gives the failure condition:-

$$K_{1c} = \frac{3\omega}{bc^2}\sqrt{\frac{L^5}{10}} \qquad (5.14)$$

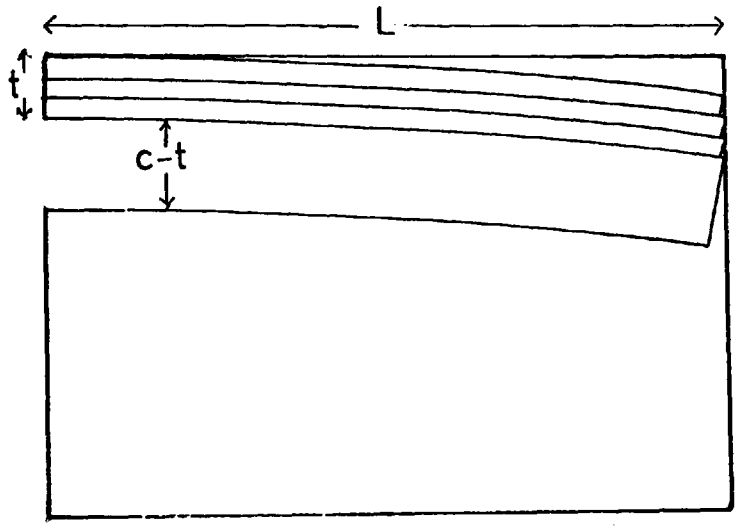

Fig5.4 Hypothetical mode of failure of a rock cantilever

Figure 5.5 is a graphical representation of equation (5.14) for a beam of unit breadth and various thicknesses. Again, these curves can be used to give design guidance for the width of a tunnel. The force per unit length of beam, ω, can be due to the self-weight of the beam or from the pressure of overlying strata.

It is interesting to compare the stability condition (5.14) with the conventional tensile strength one. The tensile stress, σ, at the point B in figure 5.2 is given by:-

$$\sigma = \frac{3\omega L^2}{bc^2} \qquad (5.15)$$

or, at failure

$$T_0 = \frac{3\omega L^2}{bc^2} \qquad (5.16)$$

where T_0 is the tensile strength of the beam material.

The equation (5.14) can be differentiated, with respect to K_{1c}, to give the error in the calculation of the length, dL, corresponding to an error in the measurement of K_{1c}, dK_{1c}. It can be simply derived that, at failure:-

$$\frac{dL}{L} = \frac{2}{5} \frac{dK_{1c}}{K_{1c}} \qquad (5.17)$$

and similarly, from equation (5.16):-

$$\frac{dL}{L} = \frac{1}{2} \frac{dT_0}{T_0} \qquad (5.18)$$

Comparison of these two equations shows that, even if K_{1c} and T_0 were known to the same accuracy, the fracture failure criterion is 20%

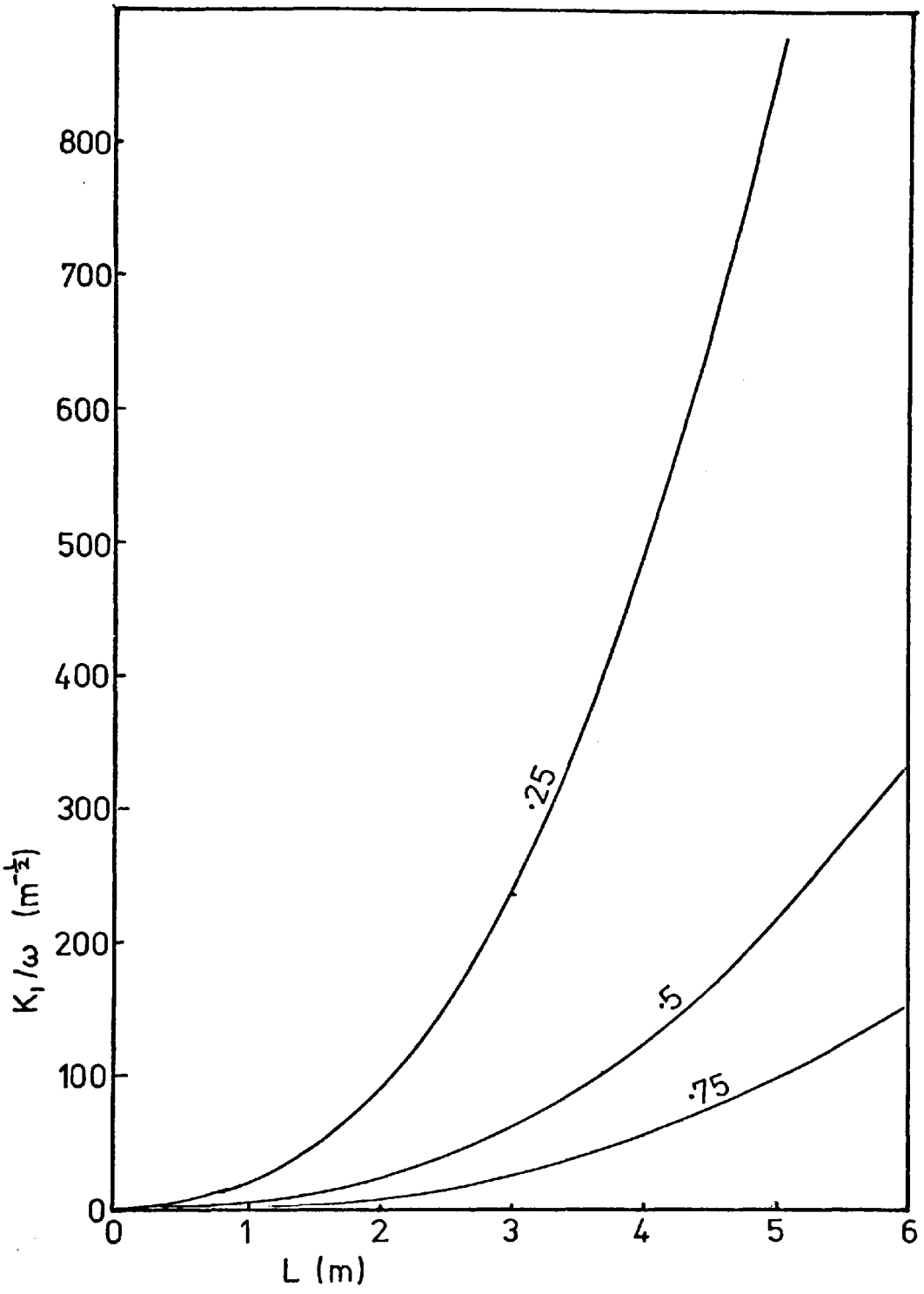

Fig 5.5 Graphical representation of equation (5.14) for a beam of unit breadth. The numbers on the curves indicate the beam thickness, c (in m).

more accurate than the tensile strength one; i.e. the estimation of the beam length at failure is less critically dependent upon the measurement of K_{1c} than upon T_0. However, experiments described elsewhere in this thesis show that K_{1c} is more easily measured than T_0, so that the advantage of the fracture failure criterion becomes even more obvious.

The criterion of failure, equivalent to (5.14), can also be derived from consideration of the stress intensity factor in the form of equation (5.1). The stress intensity factor for a notched beam is given by Paris and Sih (1965) as:-

$$K_1 = \frac{6M}{b(c-t)^{3/2}} \; g\left(\frac{t}{c}\right) \qquad (5.19)$$

where g(t/c) is a polynomial function of t/c and is plotted in figure 5.6, together with a definition of the parameters M, c and t.

From equation (5.14), failure occurs when K_{1c} is a value given by the equation. By making (5.14) and (5.19) equal, the crack length, t, for which the two expressions are equal can be determined. The equality between the two equations is independent of ω and b. The value of t for which the two expressions is equivalent is about 0.18c when L = 3m and c = 0.5m; i.e. if there is a crack (at point B in figure 5.2) of less than 0.18c for a 3m long cantilever, then the failure condition (5.14) is a conservative estimate. The real advantage of fracture failure criteria, of the form of (5.14) over conventional tensile strength ones, is that a crack can be catered for in the calculations instead of assuming a homogeneous, flawless material.

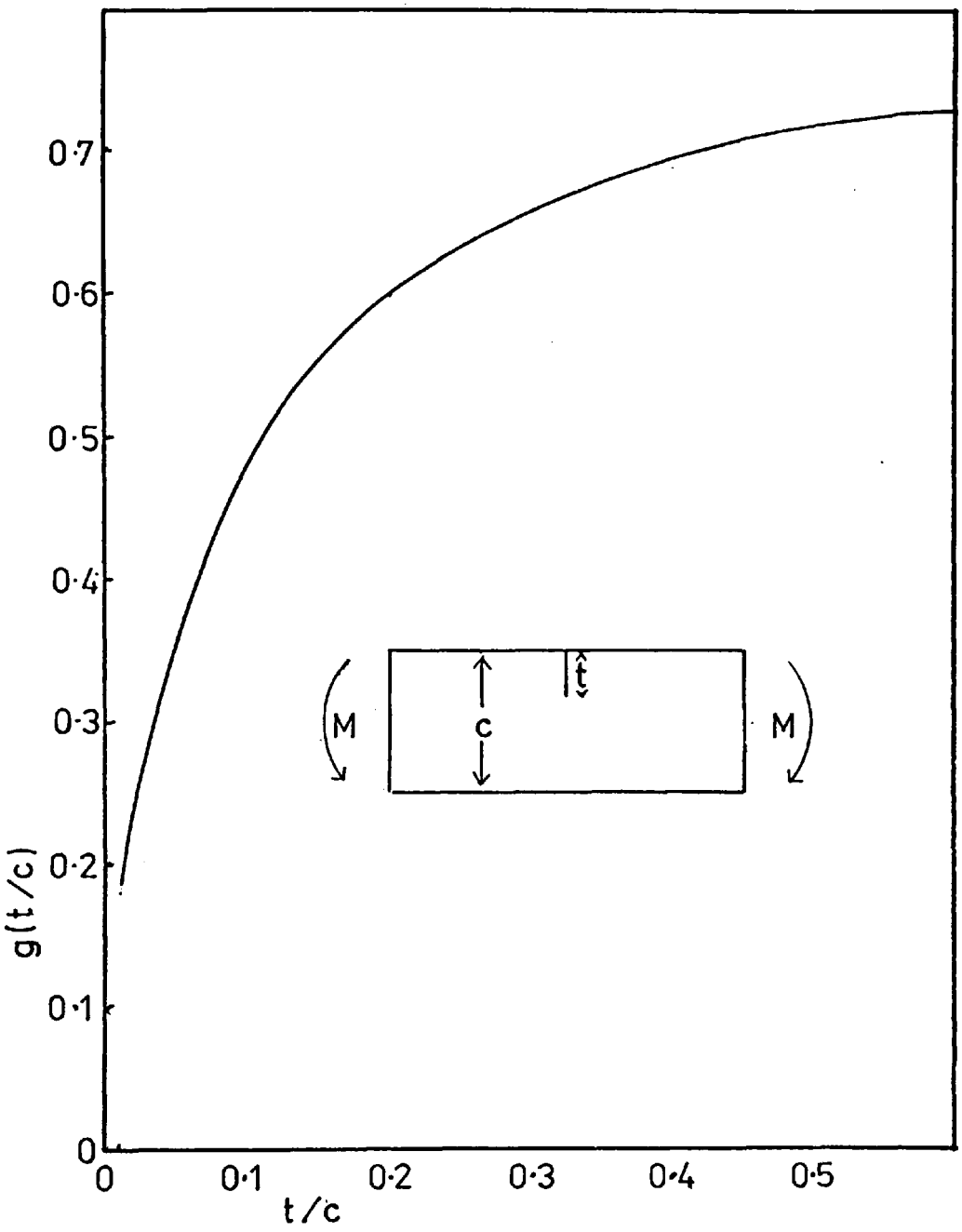

Fig 5·6 Graph of the polynomial function g(t/c), and definition of parameters used in equation (5-19).

Figure 5.7 is a comparison of the three failure conditions (5.10), (5.14) and (5.19). $K_{1c}b/\omega$ is plotted against L for a beam thickness of 0.5 m and $\nu = 0.25$. The condition (5.19) is calculated for a crack length of 0.18c. It can be seen that (5.14) and (5.19) are similar until L > 3m, when the former failure condition becomes the most critical.

Although the failure condition (5.14) gives the largest estimate of K_{1c} necessary for stability, it must be remembered that for some rocks K_{1c} is anisotropic. For example, in chapter in this thesis, experiments on slate showed K_{1c}, measured perpendicular to the bedding plane, to be twice that parallel to the bedding plane. Consider a 4.5 m long slate cantilever and deflected under its own weight. Figure 5.7 shows that if the beam were to detach from the main roof, it would also fail perpendicular to the bedding plane, i.e. K_{1c} from (5.19) is greater than twice that from (5.14) necessary to prevent failure.

5.5 A Propped Cantilever

The design criteria described above assumes that the cantilever is freely hanging. In fact, it might be propped at one end, and the support might change the stability conditions considerably and make the beam less likely to fail. An estimate of the conditions under which a beam is propped, can be derived from very simple considerations.

The top end of the beam rotates relative to the horizontal, causing an extension of the edge, as shown in figure 5.8. At the same time, the overall deflection of the beam has the effect of reducing its horizontal length.

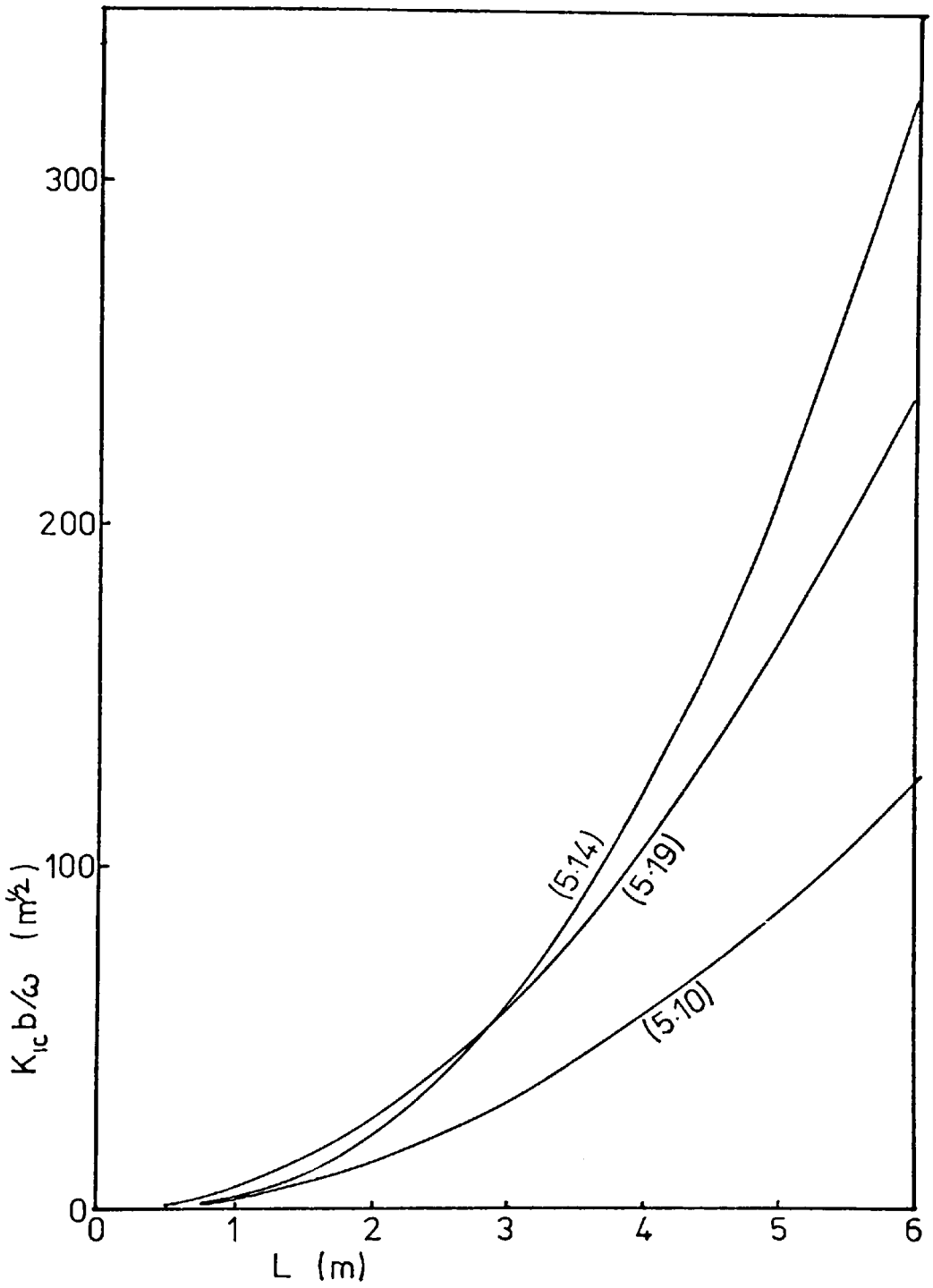

Fig 5.7 A comparison of the three failure conditions (5.10), (5.14) and (5.19).

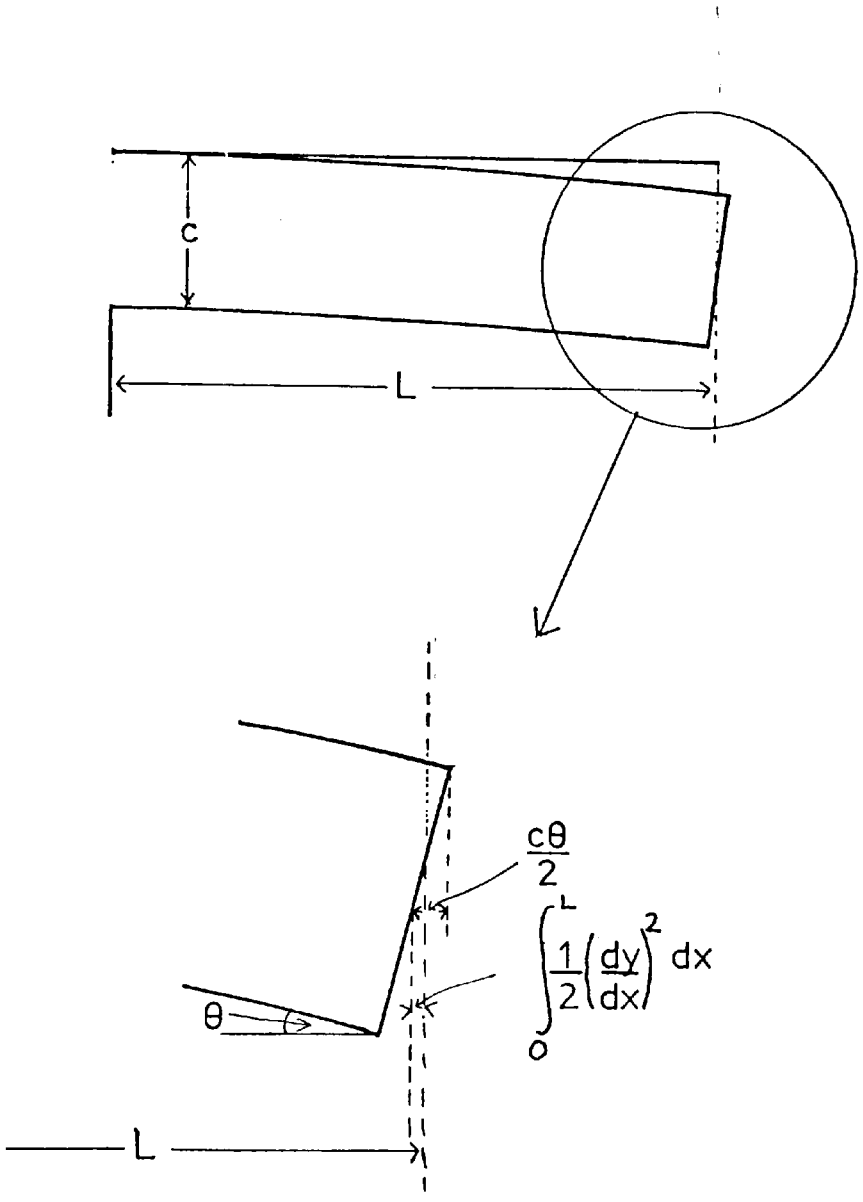

Fig 5.8 The factors contributing to the apparent expansion or contraction of a cantilever

The deflection of the beam is given by:-

$$y = \frac{\omega}{EI}\left(\frac{Lx^3}{6} - \frac{L^2x^2}{4} - \frac{x^4}{24}\right) \qquad (5.20)$$

where the shear term is neglected for simplicity.

The extension of the top edge of the beam is given by:-

$$dx_1 = \frac{c}{2}\left(\frac{dy}{dx}\right)_{x=L} \qquad (5.21)$$

By differentiating (5.20) and substituting x = L, gives:-

$$dx_1 = \frac{c\omega L^3}{12EI} \qquad (5.22)$$

The contraction of the beam is given by:-

$$dx_2 = \int_0^L \frac{1}{2}\left(\frac{dy}{dx}\right)^2 dx \qquad (5.23)$$

and the calculation of this term results in:-

$$dx_2 = \frac{\omega^2 L^7}{112E^2I^2} \qquad (5.24)$$

The condition that there is no propping of the beam is that $dx_2 > dx_1$ or:-

$$\frac{\omega^2 L^7}{112E^2I^2} > \frac{c\omega L^3}{12EI} \qquad (5.25)$$

For example, if $E = 10^{11}$ N/m^2, ω = 2500 N/m, c = 1m, then the beam is propped if L < 75m, i.e. for all practical situations. Therefore, the design criteria derived in section 5.4 are on the conservative side because the cantilever beam will be propped for all practical situations.

5.6 A beam with fixed ends

The configuration of the structure to be considered in this section is shown in figure 5.9, together with the notation. Also in the figure is the bending moment and shear force diagrams. As for the cantilever, two modes of failure will be analysed; the beam can detach from the main roof, or it can crack perpendicular to the beam axis.

The deflection of a beam with fixed ends is given by:-

$$y = \frac{\omega}{12EI}\left(Lx^3 - \frac{L^2x^2}{2} - \frac{x^4}{2}\right) + \frac{\omega x}{2Gbc}(x-L) \qquad (5.26)$$

Using expression (5.5), the strain energy is readily computed as:-

$$W = \frac{\omega L^5}{120Ebc^3} + \frac{\omega L^3(1+\nu)}{12Ebc} \qquad (5.27)$$

The incremental crack area $dA = bdL$, using the failure condition (5.3), and noting that $\mathcal{G}_{1c} = dU_s/dA$:-

$$\mathcal{G}_{1c} = \frac{\omega^2 L^2}{4b^2cE}\left(\frac{L^2}{6c^2} + 1 + \nu\right) \qquad (5.28)$$

Making the assumption that $K_{1c}^2 = E\mathcal{G}_{1c}$, the failure condition for a beam detaching from the main roof is:-

$$K_{1c}^2 = \frac{\omega^2 L^2}{4b^2c}\left(\frac{L^2}{6c^2} + 1 + \nu\right) \qquad (5.29)$$

The beam will only detach from the main roof if it is deflected under its own weight, and then $\omega = dbc$. Figure 5.10 is a graph of K_{1c}/d as a function of L, for various beam thicknesses c, and $\nu = 0.25$.

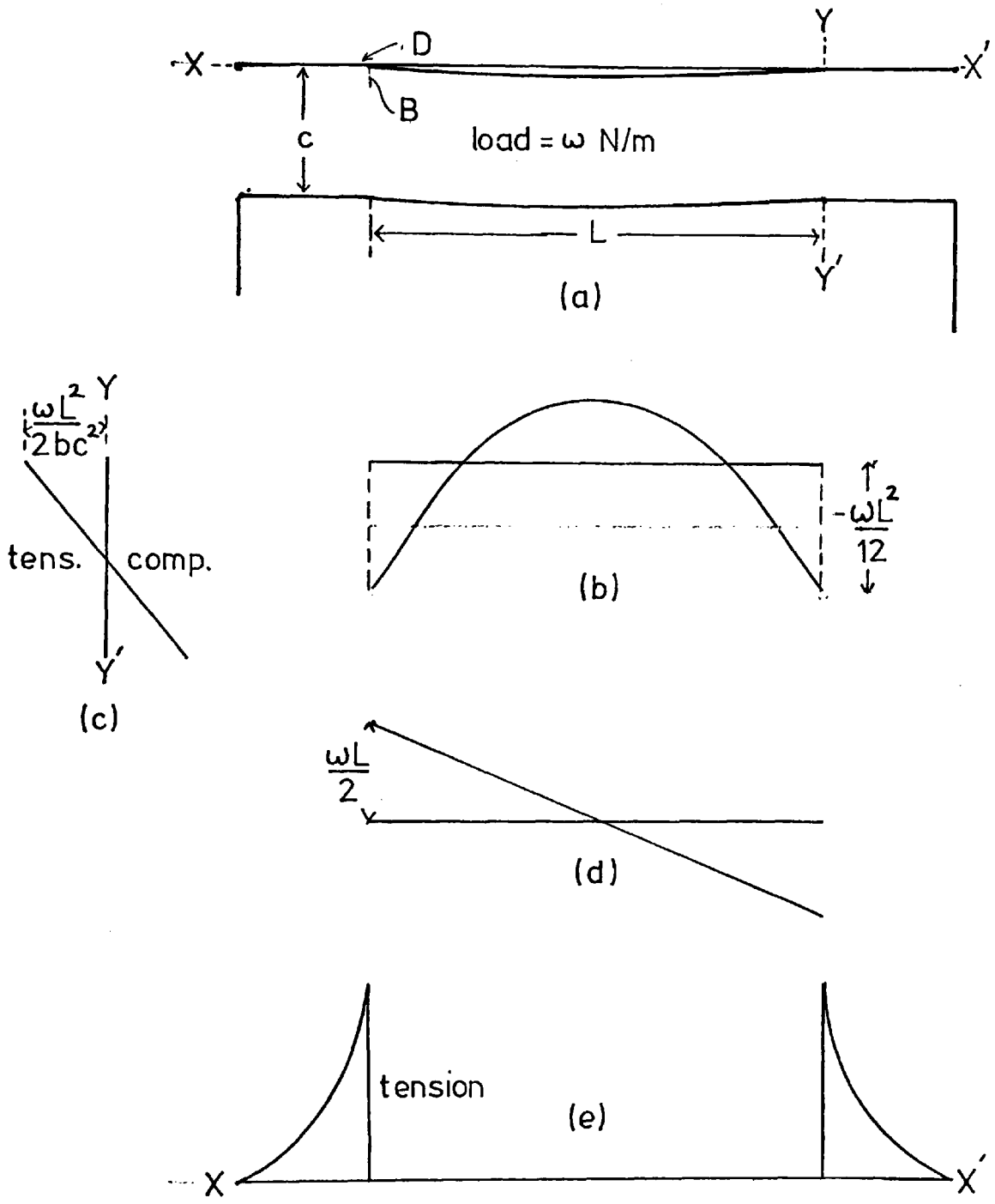

Fig 5.9 a) Rock beam detaching from main roof
b) Bending moment diagram.
c) Horizontal stress along the vertical section Y-Y'
d) Shear-force diagram.
e) Vertical stress along the section X-X'.

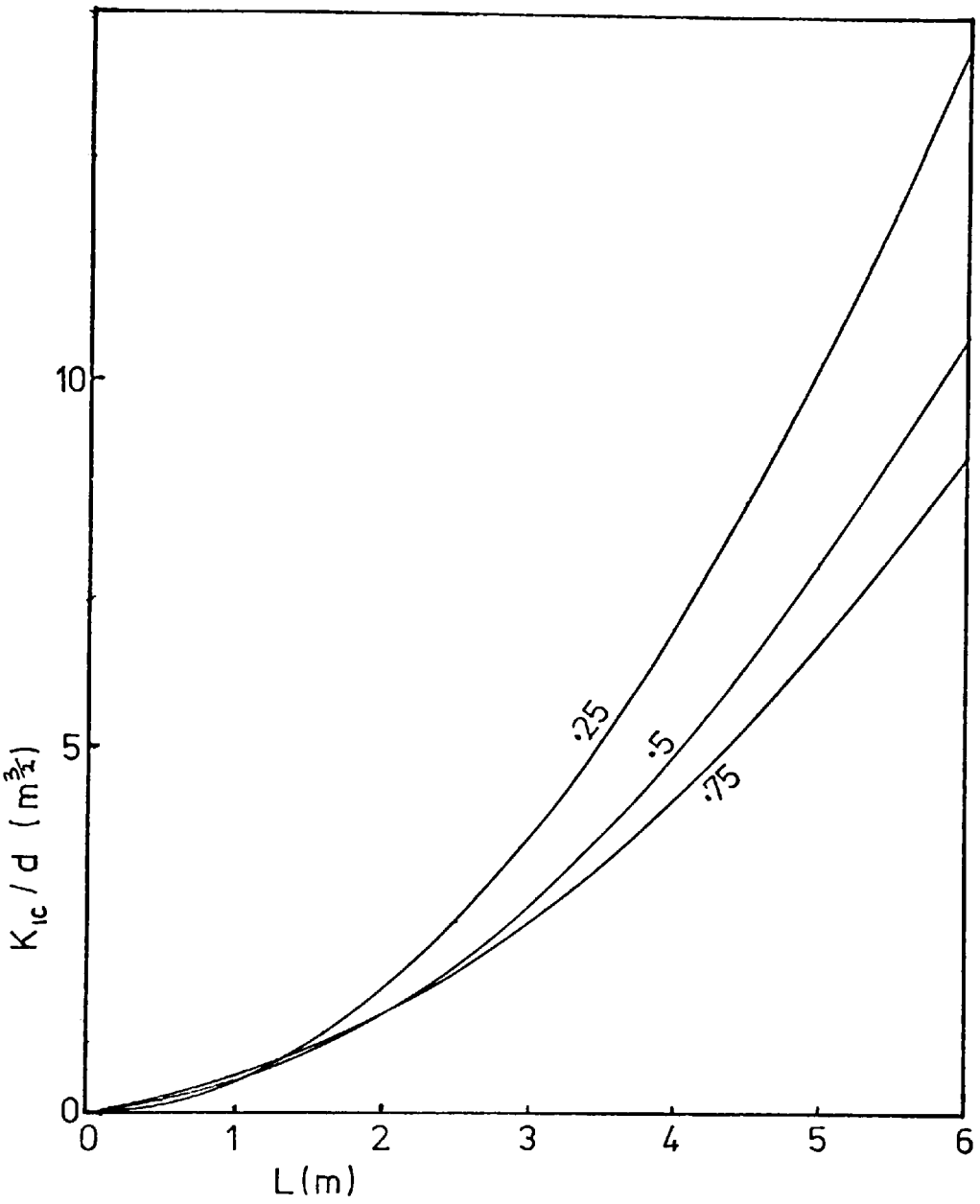

Fig 5·10 Graphical representation of equation (5·29) for $\nu = 0{\cdot}25$. The numbers on the curves indicate the beam thickness, c (in m).

From figure 5.9, it can be seen that the maximum bending moment and tensile stress occurs at the top ends of the beam. From this, it would be expected that cracking would start at these points, and Obert and Duvall (1967) give design criteria based on this assumption. However, Hobbs (1969) showed, using scale models, that failure occurred at the centre of the beam, as shown in figure 5.11. Practical experience also shows this to be a more common mode of failure (Thomas 1973).

It is possible that the assumption regarding the ends of the beam being fixed, is incorrect. If the ends of the beam rotated then the bending moment at the centre of the beam would be increased. The amount of rotation necessary to increase the bending moment at the centre of the beam, such that it is the maximum, can readily be calculated.

The bending moment at any point on the beam, as in figure 5.9, is given by:-

$$M = \frac{1}{EI}\left(\frac{-\omega x^2}{2} + C_1 x + C_2\right) \qquad (5.30)$$

where C_1 and C_2 are constants. At the centre of the beam, $dM/dx = 0$, therefore $C_1 = \omega L/2$. The condition that the bending moment at the centre of the beam equals that at the end is:-

$$\frac{1}{EI}\left(\frac{\omega L^2}{4} - \frac{\omega L^2}{8} + C_2\right) = \frac{-C_2}{EI} \qquad (5.31)$$

or

$$C_2 = \frac{-\omega L^2}{16} \qquad (5.32)$$

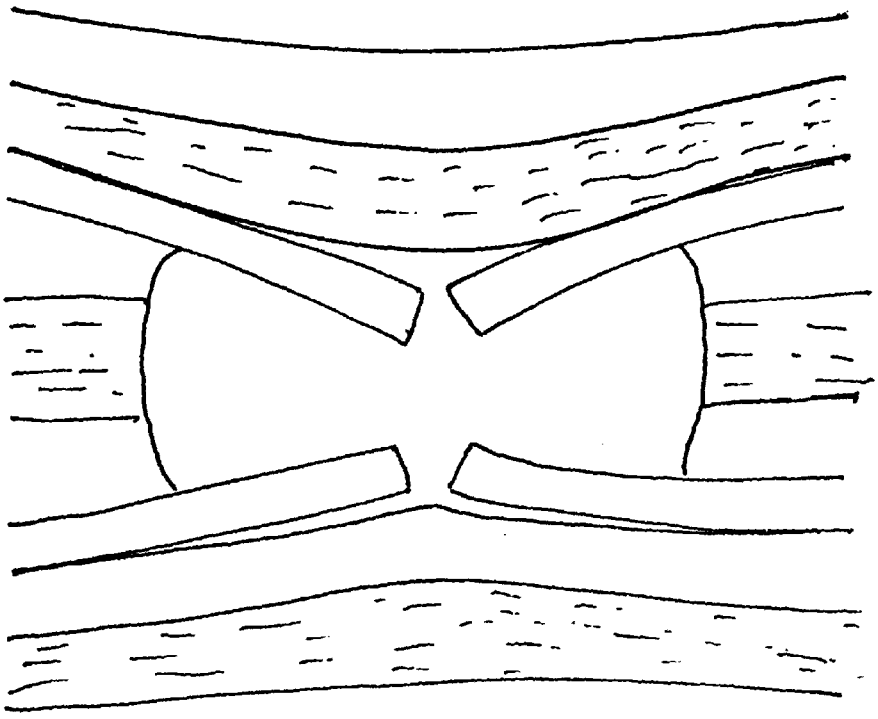

Fig 5.11 A common mode of failure of rock beams [after Thomas (1973)].

Substitution of C_1 and C_2 into (5.30) and integrating gives:-

$$\frac{dy}{dx} = \frac{1}{EI}\left(\frac{\omega L x^2}{4} - \frac{\omega x^3}{6} - \frac{\omega L^2 x}{16} - \frac{\omega L^3}{96}\right) \qquad (5.33)$$

At $x = 0$, $dy/dx = -\omega L^3/96EI$, which is the angle of rotation of the end of the beam necessary to cause the bending moment at the centre of the beam to exceed that at the ends.

The maximum bending moment for a beam with the bending moment at the centre to be equal to that at the ends is $\omega L^2/16$ which is less than that for a beam with fixed ends. Therefore, if a failure criterion is derived for a beam with fixed ends, it will be valid for a beam with end rotation, but with an additional factor of safety.

The derivation of the failure condition for a beam with a crack at each end is similar to that for a cantilever. Referring to figure 5.9, consider cracks starting simultaneously at the ends of the beam. In practice this is unlikely to happen, but the assumption takes the worst possible case. Again, the shear strain energy is unimportant in this case because the length of the beam does not change.

The deflection of the beam is given by:-

$$y = \frac{\omega}{EI}\left(\frac{Lx^3}{12} - \frac{L^2x^2}{24} - \frac{x^4}{24}\right) \qquad (5.34)$$

Substituting $I = b(c-t)^3/12$, and integrating to give the strain energy, as in equation (5.5) gives:-

$$W = \frac{\omega^2 L^5}{120Eb(c-t)^3} \qquad (5.35)$$

The incremental crack area, dA, is assumed to be 2bdt, so that from equation (5.3), at failure:-

$$\mathcal{G}_{1c} = \frac{\omega^2 L^5}{80Eb^2(c-t)^4} \qquad (5.36)$$

Substitution of $K_{1c}^2 = \mathcal{G}_{1c}E$ and letting $t \to 0$, leads to the result that, at failure:-

$$K_{1c} \doteq \frac{\omega L^{5/2}}{9bc^2} \qquad (5.37)$$

As a comparison, the conventional tensile strength failure condition is:-

$$T_0 = \frac{\omega L^2}{2bc^2} \qquad (5.38)$$

The similarity and simplicity of the two results (5.35) and (5.36) means that the fracture failure condition is as simple to apply as the tensile strength one. Figure 5.12 is a plot of the function K_{1c}/ω for various beam thicknesses.

It is interesting to compare the failure condition (5.35) with one derived from the tensile strength, as from equation (5.1). The tensile stress at the top ends of the beam is given by:-

$$\sigma = \frac{\omega L^2}{2bt^2} \qquad (5.39)$$

For a body containing a penny-shaped crack of diameter 2t, the stress intensity factor is given by Paris and Sih (1965) as:-

$$K_1 = 2\sigma\sqrt{\frac{t}{\pi}} \qquad (5.40)$$

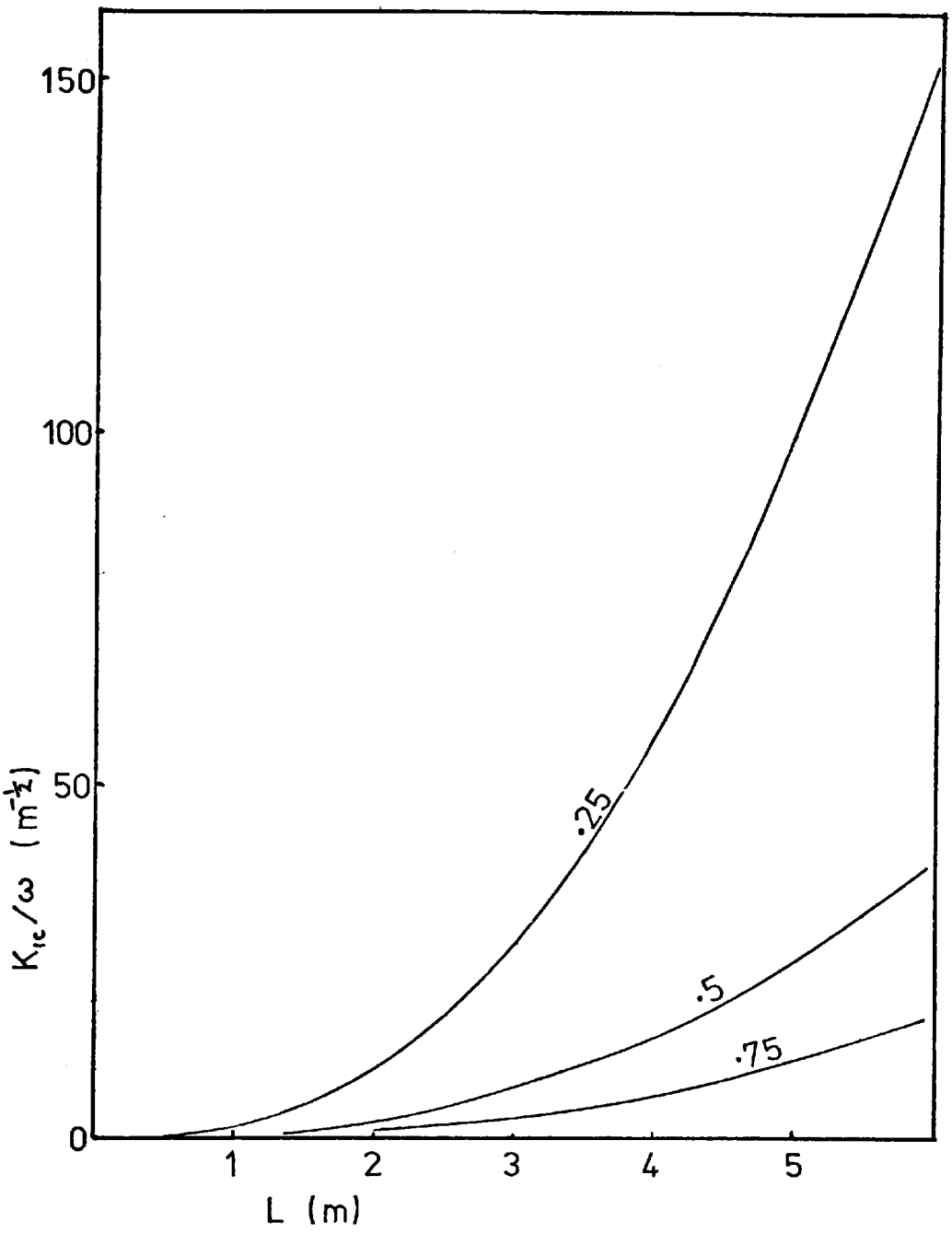

Fig 5.12 Graphical representation of equation (5.37). The numbers on the curves indicate the beam thickness, c (in m).

By equating (5.36) with (5.38) after substitution of the effective grain size, 2t can be determined.

The calculation shows that the two failure conditions are equivalent if:-

$$t = \frac{\pi L}{80} \qquad (5.41)$$

For any value of L, t is very large (e.g. t = 7.8 cm when L = 2m). This is an unrealistically large grain size for any rock type, and shows that equation (5.36) is very much an underestimate of the true failure condition for a granular material.

The failure condition (5.36) can also be compared with (5.19), and it can be shown that the two expressions are equivalent if t = 0.1c when c = 0.5m and L = 2m. Thus the failure condition (5.36) gives a realistic estimate of the safety of a beam with a small, but finite crack.

An alternative failure condition can be derived from a consideration of gross energy changes in a beam which is collapsing. If cracks were to appear in a beam, at the top ends, the end result might be a simply supported beam. In practice, such a situation would not occur, but by making this assumption, the magnitude of energy changes involved can be estimated. From equation (5.34) the energy of the beam W_1 is known before the cracking starts. After failure, a similar analysis shows that the energy in the beam W_2 is given by:-

$$W_2 = \frac{\omega^2 L^5}{20Ebc^3} \qquad (5.42)$$

The energy absorbed by the cracking process is simply $2\mathcal{G}_{1c}bc$. Therefore the condition that the beam will fail is:-

$$2\mathcal{G}_{1c}bc = \frac{\omega^2 L^5}{Ebc^3}\left(\frac{1}{20} - \frac{1}{120}\right) \qquad (5.43)$$

and by substitution,

$$K_{1c} \simeq \frac{1}{7}\,\frac{\omega L^{5/2}}{bc^2} \qquad (5.44)$$

This estimate of the failure condition is, as might be expected, more conservative than (5.36). The method by which the result was derived is very simple, and can be extended to most structures where the unfailed and failed conditions are in themselves stable. For example, this method would not be suitable for the cantilever beam, as described in section 5.5, because after failure the strain energy is not calculable (the beam falls to the tunnel floor).

As for the cantilever beam, the above failure conditions are conservative ones because the beam will be propped as its deflection increases.

It was mentioned above that, if there were a rotation at the ends of a beam, the bending moment might occur at the centre of the beam. The effect of a crack initiating at the centre of the beam will now be considered.

In figure 5.13, a hypothetical mode of failure is shown. A beam is assumed to break in two halves, and each half can be modelled by a cantilever. The deflection of the beam before failure is given by:-

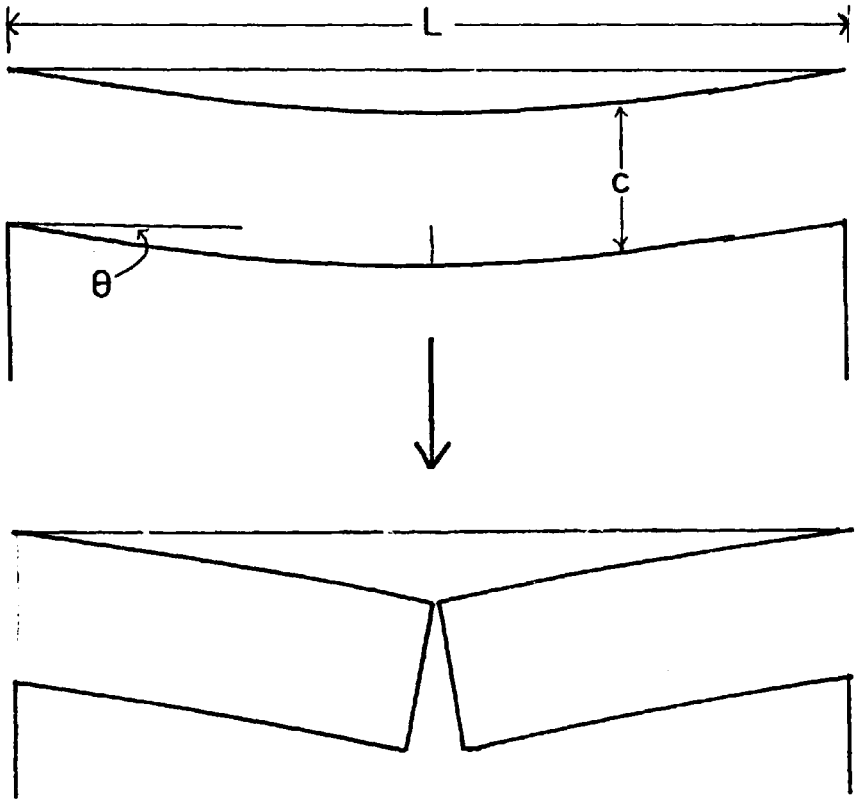

Fig 5 13 Failure model of a rock beam where the tensile stress is greatest at the centre of the beam.

$$y = \frac{\omega}{EI}\left(\frac{Lx^3}{12} - \frac{L^2x^2}{24} - \frac{x^4}{24} + \frac{\theta EI}{\omega}\left(x - \frac{x^2}{L}\right)\right) \qquad (5.45)$$

where θ is the angle of rotation of the beam ends. The strain energy is calculated as:-

$$W_1 = \frac{\omega^2 L^2}{12Ebc^3}\left(\frac{L^3}{10} - \frac{\theta Ebc^3}{\omega}\right) \qquad (5.46)$$

For a cantilever (i.e. half the beam after it has failed):-

$$y = \frac{1}{EI}\left(\frac{\omega \ell x^3}{6} - \frac{\omega x^4}{24} - \frac{\omega \ell^2 x^2}{4} + EI\theta x\right) \qquad (5.47)$$

where $\ell = L/2$, and:-

$$W_2 = \frac{\omega^2 L^2}{8Ebc^3}\left(\frac{3L^3}{20} - \frac{Ebc^3\theta}{\omega}\right) \qquad (5.48)$$

Therefore, the change in strain energy, caused by the beam failing, is:-

$$W_2 - W_1 = \frac{\omega^2 L^2}{Ebc^3}\left(\frac{L^3}{96} - \frac{\theta Ebc^3}{24\omega}\right) \qquad (5.49)$$

The energy absorbed by the crack, as the beam fails, is simply $\mathcal{G}_{1c}bc$. Substituting $K_{1c}^2 = \mathcal{G}_{1c}E$, the failure condition is:1

$$K_{1c}^2 = \frac{\omega^2 L^2}{bc^3}\left(\frac{L^3}{96} - \frac{\theta Ebc^3}{24\omega}\right) \qquad (5.50)$$

From equation (5.31), the slope, θ, at the ends of a beam, for which the bending moment at the centre equals that at the ends, is given as $-\omega L^3/8Ebc^3$. Substitution of this value in equation (5.49)

gives the failure condition:-

$$K_{1c} = \frac{\omega L^{5/2}}{7.9bc^2} \qquad (5.51)$$

Comparison of this result with (5.43) shows that the failure condition for a beam failing in the centre is not greatly different from that for end failure. However, if θ is of greater magnitude than $-\omega L^3/8Ebc^3$, then K_{1c} will also have to be greater for failure not to occur.

Figure 5.14 is a comparison of the four failure conditions, (5.29), (5.37), (5.44) and (5.51). The equations have been calculated for a beam 1m broad, 0.5m thick, and with $\nu = 0.25$.

5.7 Failure by Spalling

A stress analysis of cracks shows that tensile stresses develop at crack tips, even under compressive loading. Under such conditions, the cracks propagate in the direction of maximum compressive stress (Bieniawski 1967a). Fairhurst & Cook (1966) have suggested that this mechanism might be responsible for the failure of rock faces by slabbing or spalling (figure 5.15). As cracks propagate along the direction of maximum compressive stress, the tensile stress perpendicular to the cracks becomes zero. This allows the rock to fail by buckling, and such a mode of behaviour has been observed in the laboratory by Hobbs (1969), and in mines. The theory can also explain the failure of rock specimens in the laboratory where tensile cracks develop along the direction of maximum compressive stress.

The mode of failure, as proposed by Fairhurst and Cook, can be analysed to give a failure condition in terms of fracture toughness.

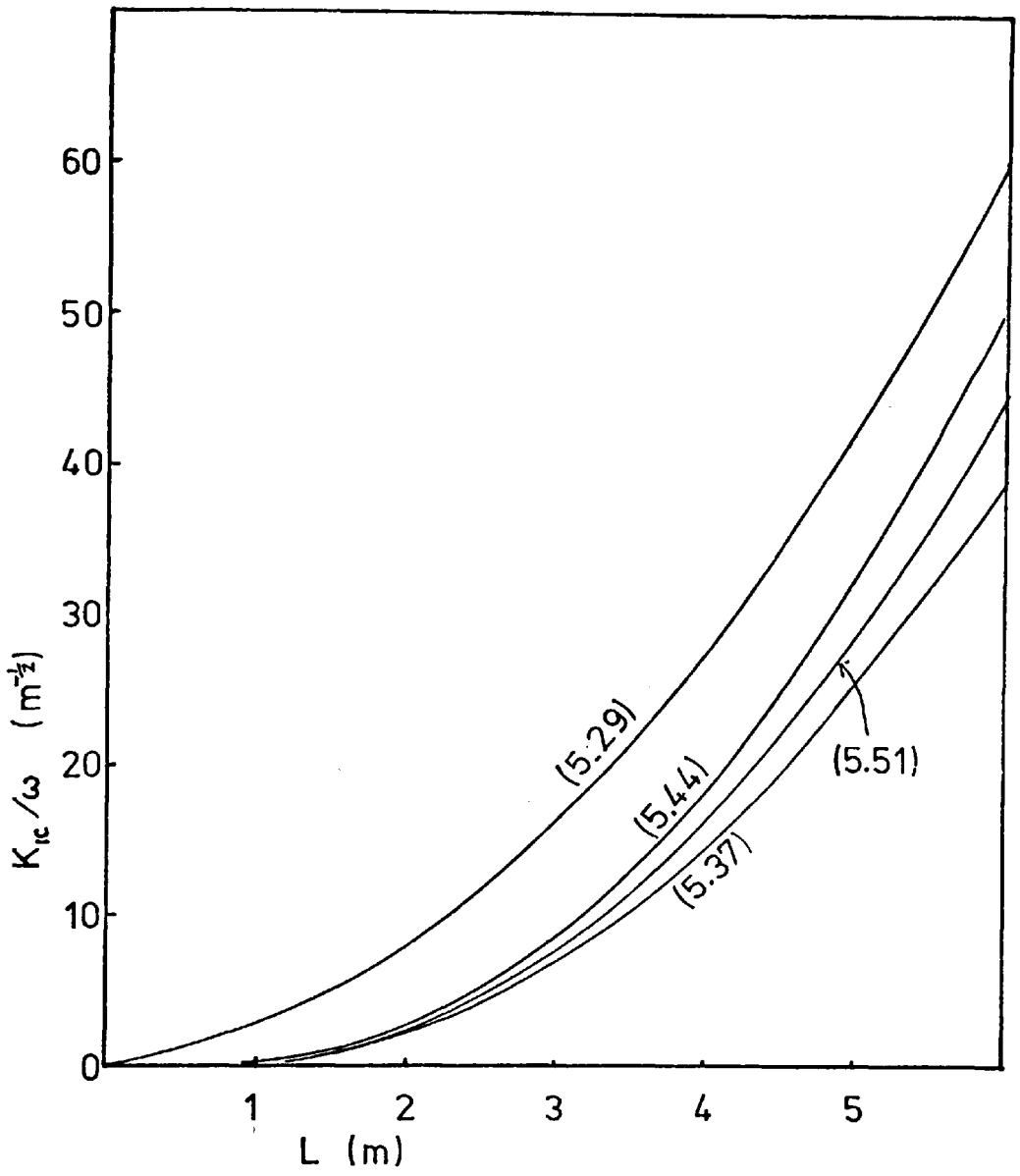

Fig 5.14 A comparison of the four failure conditions, (5.29), (5.37), (5.44), (5.51).

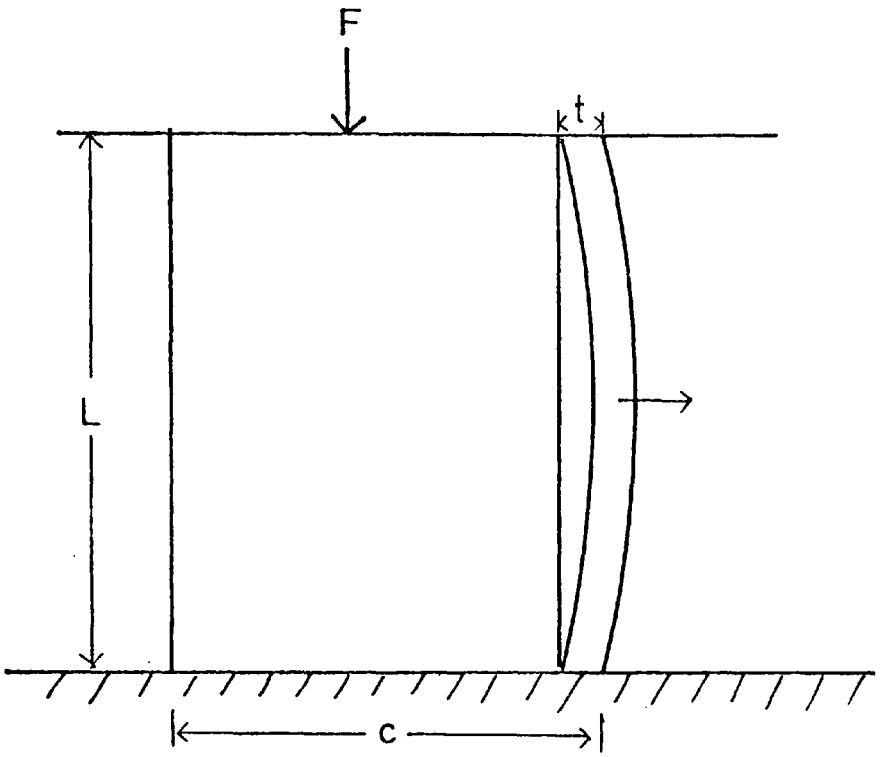

Fig 5.15 A model of rock failure by spalling from a pillar.

In figure 5.15 it is assumed that failure has occurred by the spalling of a slab, of thickness t, from a pillar of height L and width c, breadth b. The pillar is under a constant load which does not change as failure occurs. There is a strain energy W, stored in the pillar due to the load and is given by:-

$$W = \frac{1}{2}\frac{F^2 L}{Ebc} \tag{5.52}$$

Assume that the slab breaks off, and the strain energy in the pillar increases due to there being the same load over a smaller cross-sectional area. Furthermore, it is assumed that there are only energy changes in the pillar, but not in the surrounding opening. The difference in strain energy due to the spalling, dW, is:-

$$dW = \frac{1}{2}\frac{F^2 L}{Eb}\left(\frac{1}{c-t} - \frac{1}{c}\right) \tag{5.53}$$

and if t is small compared to c,

$$dW = \frac{1}{2}\frac{F^2 Lt}{Ebc^2} \tag{5.54}$$

An amount of energy is absorbed by the creation of a new crack surface, and is given by:-

$$U = \mathcal{G}_{1c} bL \tag{5.55}$$

(neglecting the areas at the ends of the slab). For failure to occur, the change in strain energy must be equal to the energy absorbed by the cracking process, i.e.

$$\mathcal{G}_{1c} bL = \frac{1}{2} \frac{F^2 Lt}{Ebc^2} \qquad (5.56)$$

Now, $K_{1c}^2 = E\mathcal{G}_{1c}$, and the stress on the pillar, σ, = F/bc. Therefore, at failure:-

$$t = \frac{2K_{1c}^2}{\sigma^2} \qquad (5.57)$$

Until now, no assumption has been made as to the mechanism of failure. Experimental evidence suggests that failure occurs by the buckling of near-surface slabs of rock. By Euler's analysis, buckling will occur when:-

$$F = \frac{\pi^2 EI}{L^2} \qquad (5.58)$$

where $I = bt^3/12$. Substituting the stress $\sigma = F/bt$, buckling will occur when:-

$$t < \sqrt{\frac{12\sigma L^2}{\pi^2 E}} \qquad (5.59)$$

By comparing equations (5.56) and (5.58), the overall condition for failure is:-

$$\sqrt{\frac{12\sigma L^2}{\pi^2 E}} > \frac{2K_{1c}^2}{\sigma^2} \qquad (5.60)$$

or,

$$K_{1c} < \sqrt[4]{\frac{3\sigma^5 L^2}{\pi^2 E}} \qquad (5.61)$$

and, at failure

$$t = \frac{2K_{1c}^2}{\sigma^2} \qquad (5.62)$$

Therefore, if the measured K_{1c} value for a rock is less than that given by equation (5.60), then failure will occur by spalling. As an example, let $\sigma = 2.5 \times 10^6$ N/m^2, L = 3m, E = 10^{11} N/m^2, and for failure to occur:-

$$K_{1c} < 3 \times 10^5 \text{ N/m}^{3/2}, \text{ and } t = 7.2 \text{ cm.}$$

This is comparable to the measured value of K_{1c}, for slate of 5×10^5 N/m$^{3/2}$.

So far, this analysis has used the assumption that failure has occurred at a rock pillar, and so implies that the shape and extent of the opening has no effect. The failure condition for spalling in a long, rectangularly profiled opening will now be derived.

For a rectangular opening, the strain energy change, caused by spalling can be derived from the model of a crack in an infinite plate, of unit thickness (figure 5.16). This arrangement is similar to a fracture toughness test used in metallurgy but the remote tensile stress, σ, is usually tensile. The strain energy of an infinite plate, containing a slit is given by:-

$$W = \frac{\sigma^2}{2} \frac{\pi a^2}{E} \qquad (5.63)$$

for plane stress. Now assume that the slit extends, due to spalling, by an amount t. The difference in strain energy is:-

$$dW = \frac{\sigma^2}{2} \frac{\pi}{E} \left(a^2 - (a-t)^2 \right)$$

$$= \sigma^2 \frac{\pi a t}{E} \quad \text{for small t.} \qquad (5.64)$$

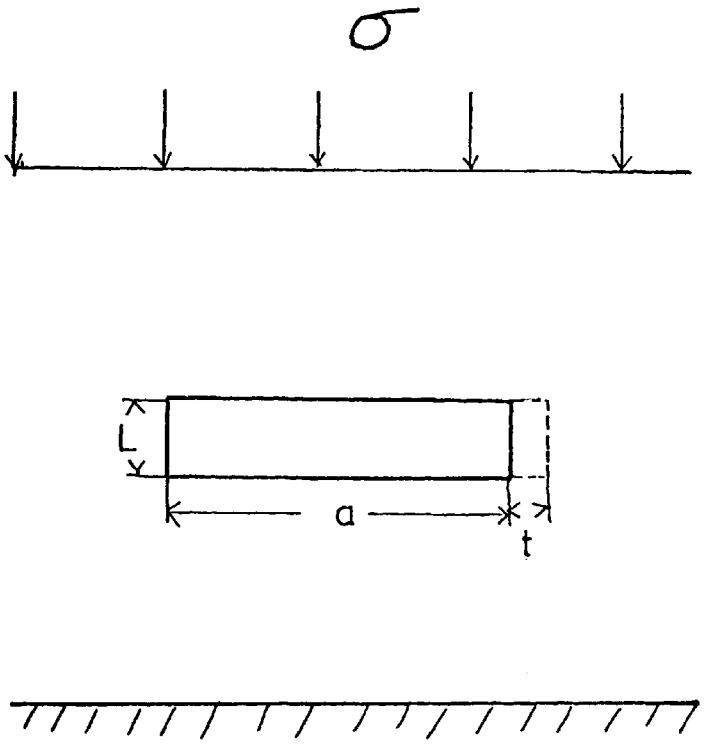

Fig 5.16 Model of failure at a rectangularly profiled underground opening

As before, the energy absorbed by the cracking process is simply $\mathcal{G}_{1c}L$ for a slab of unit breadth, and failure will occur when:-

$$\mathcal{G}_{1c}L < \sigma^2 \frac{\pi a t}{E}$$

or,

$$t > \frac{K_{1c}^2 L}{\sigma^2 \pi a} \qquad (5.65)$$

The condition for buckling is as before in (5.58), and the overall condition for failure is:-

$$\sqrt{\frac{12\sigma L^2}{\pi^2 E}} > \frac{K_{1c}^2 L}{\sigma^2 \pi a}$$

or,

$$K_{1c} < \sqrt[4]{\frac{12\sigma^5 a^2}{E}} \qquad (5.66)$$

In this result, the failure is dependent upon the length a, of the opening, instead of its height, as in (5.60). As an example, let $a = 10m$, $E = 10^{11}$ N/m^2, $\sigma = 2.5 \times 10^6$, and failure will occur when $K_{1c} < 1.04 \times 10^6$ N/m$^{3/2}$. This compares with K_{1c} for slate of 5×10^5 N/m$^{3/2}$. If the height of the opening is 3m then the thickness of rock slabs which break off is 1.5 cm.

The criterion (5.65) is the more critical for determining the safe limit for K_{1c}, and it is probably advisable to use it for predicting safe conditions.

5.8 Discussion of Fracture Failure Criteria

The results derived in this chapter have been summarised in table 5.1. The approximate failure conditions, derived by consideration of gross energy changes, have not been included in the table. It can be seen that the conditions for failure for the cantilever are more critical than for a beam with supported ends.

The failure conditions have all been derived using the assumption that $K_{1c}^2 = EG_{1c}$. However, in section 4.7 it was shown that, for concrete CNRBB specimens, this relation is not true, and $G_{1c} \simeq 9K_{1c}^2/E$. If there were a similar discrepancy between experiment and theory for rock specimens, then it would appear that the failure conditions, derived above, are 9 times too conservative. This factor will change for different rocks, and would have to be determined experimentally. Note however, that G_{1c} could not be determined from CNRBB specimens, as described in section 4.7.

Experiments should therefore be conducted to investigate how conservative are the failure conditions described above. It is possible that it is uneconomic to work to the margin of safety implied in the failure criteria, and the formulae might have to be adjusted accordingly.

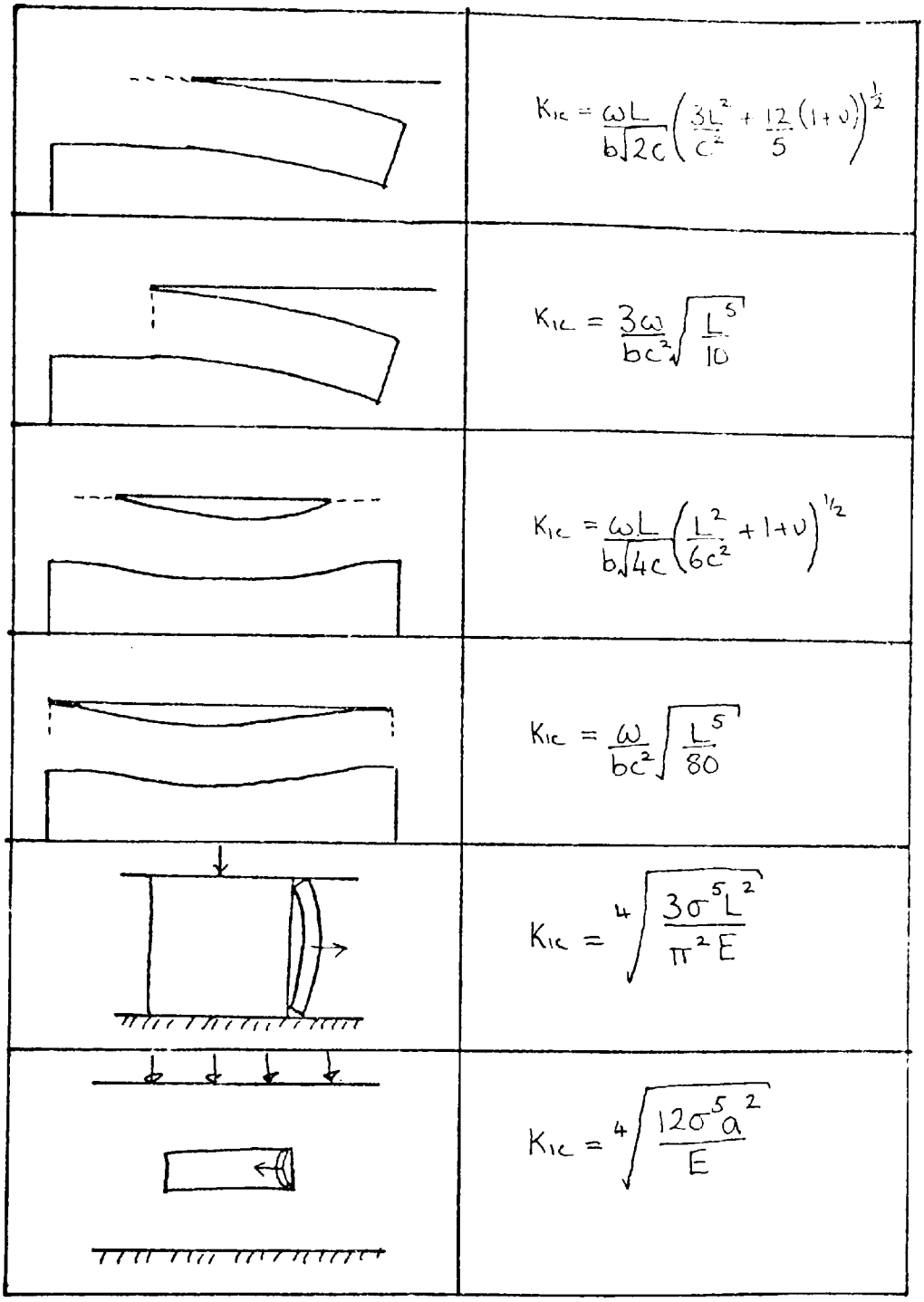

Table 5.1 Summary of conditions of failure for some simple rock structures. --- denotes the direction of crack propagation.

CHAPTER 6

The results from previous chapters are summarised and concluded, and suggestions are made for a future program of work.

6.1 The Application of Fracture Mechanics to Rock and Concrete

The conventional strength failure criteria are only suitable for elastic, isotropic rock, and can take little account of any discontinuities which inevitably occur in any rock mass. Stress analysis shows that infinite tensile stresses occur at the tip of a crack in a body, and theoretically, an infinite tensile strength would be necessary to ensure that failure does not occur. This paradox can be resolved by the use of Fracture Mechanics.

Many authors have shown that the tensile strength of rock is particularly difficult to measure, and each method of measurement often gives a large scatter of results. This thesis shows that, in many circumstances, the tensile strength tests can be replaced by fracture toughness tests, and the results used directly in fracture failure criteria.

The review of literature, in chapter 2, has shown that Fracture Mechanics is applicable to ceramic materials, such as rock and concrete. For example, the emission of microseisms from rock specimens under pressure indicates that failure occurs by the initiation and propagation of cracks in the material.

Most researchers have used the Notched Beam under Bending method of fracture toughness testing of ceramics, but Kaplan (1961) has shown that there are several difficulties associated with this method. The measured value of the fracture toughness, K_{1c}, is a function of the specimen size and loading arrangement. For example, the measured K_{1c} decreases K_{1c} decreases by 30% when the loading span is doubled. Furthermore, the specimen shape makes it unsuitable as a test for in situ rock or concrete.

Kaplan found that the measured K_{1c} and critical strain energy release rate, $\mathcal{G}_{1c}$ were not related by the equation $K_{1c}^2 = E\mathcal{G}_{1c}$. Moavenzadeh and Kuguel (1969) explained this discrepancy as being due to an error in the measurement of the actual crack area. The true crack area can be up to 20 times that of the nominal beam cross-sectional area, the multiplication factor being a function of the aggregate size in the concrete.

In real situations, the measured fracture energy, α_{eff}, taking the nominal crack area, is more useful in the analysis of structures. If a structure were to fail, the crack path would be similar to that for a laboratory specimen, and the energy absorbed would be more accurately represented by α_{eff}. For this reason, this thesis has concentrated on the measurement of $\mathcal{G}_{1c}$ ($= 2\alpha_{eff}$), using the nominal crack area.

To measure $\mathcal{G}_{1c}$ it is necessary to propagate a crack slowly, so that excess energy is not absorbed as noise, kinetic energy, etc. Nakayama (1965) showed that this could be achieved for a notched beam if the notch were cut part-way through the beam. Another method is to use a servo-controlled testing machine under strain control, where the strain is measured across the opening crack.

Because of the difficulties of the Notched Beam under Bending test, three new fracture toughness tests have been developed which reduce some of the difficulties. The easiest shape to cut from in situ rock, or concrete, is a cylinder, and the new tests are based on cylindrical specimens.

The three new testing methods are:-

1. The Circumferentially Notched Round Bar under Bending (CNRBB).
2. The Circumferentially Notched Round Bar under Eccentric Loading (CNRBEL).
3. The Slotted Disc under Diametral Loading (SDDL).

The stress intensity factors for these testing configurations have been derived from stress concentration factors for thin notches. The stress intensity factors are:-

1. For CNRBB,

$$K_1 = \frac{3M}{2}\sqrt{\frac{1}{\pi a^5(1+.112\frac{a}{t})}} \qquad (6.1)$$

2. For CNRBEL,

$$K_1 = \frac{p}{2}\left\{3e\sqrt{\frac{1}{\pi a^5(1+.112\frac{a}{t})}} - \sqrt{\frac{1}{\pi a^3(1+.2\frac{a}{t})}}\right\} \qquad (6.2)$$

3. For SDDL, a) with one slot,

$$K_1 = \frac{F}{\sqrt{\pi r b}}\, g\left(\frac{t}{b}\right) \qquad (6.3)$$

b) with two slots,

$$K_1 = \frac{F}{\pi r}\left(\frac{1}{b}\tan\frac{\pi t}{b}\right)^{\frac{1}{2}} h\left(t/b\right) \qquad (6.4)$$

where g(t/b) and h(t/b) are polynomial functions of t/b.

6.2 Results from CNRBB, CNRBEL, and SDDL Fracture Toughness Tests on Concrete

The new tests, CNRBB and CNRBEL, have several advantages over the Notched Beam under Bending:-

1. The specimens are quickly and easily prepared from in situ rocks or concrete, and is economic of material.
2. The loading of the specimens is easy and the point of initiation of the crack can be predetermined.
3. The path of propagation of the crack is fixed by the circumferential notch, and the nominal crack area should be constant for geometrically similar specimens.

CNRBB tests were conducted, using a servo-controlled testing machine, in both strain and displacement control. Results show that the measured K_{1c} and area under the load-displacement graph are independent of the mode of testing.

Fracture toughness tests on fine-grained concrete can be carried out with small deviations in the results. A sample of 5 specimens is usually sufficient to achieve a standard deviation of less than 10%.

The CNRBB test gives K_{1c} values for 4.1 cm diameter specimens which are independent of notch depth, if the notch is deeper than about 5 mm. Results are also independent of the testing speed if the vertical displacement rate is less than 2×10^{-3} mm/sec.

If metal collars are used to extend the length of CNRBB specimens, the measured K_{1c} values are reduced by 20% due to strain energy effects.

Consequently the use of metal collars is not recommended.

For CNRBEL tests, the K_{1c} measurements are relatively independent of notch depth, but a deep notch increases the scatter in the results. The CNRBB and CNRBEL tests give comparable results for the same material.

The measurement of $\mathcal{G}_{1c}$ is not independent of specimen notch depth for the CNRBB test, and when compared with K_{1c} does not satisfy the equation $K_{1c}^2 = E\mathcal{G}_{1c}$. It is possible that the nominal crack area is only one tenth of the true crack area, and the ratio between the two areas is not independent of the notch depth. Very much more investigation has to be carried out on $\mathcal{G}_{1c}$ measurements from CNRBB tests before the values can be considered to be useful.

The SDDL test does not give valid K_{1c} results when only one slot is cut. Using two slots, the SDDL test gives K_{1c} measurements about 20% higher than from CNRBEL tests. Very few experiments have been carried out using this method, and a different conclusion might appear from a more detailed investigation. For example, the effect of slot depth on K_{1c} values has not been established.

The CNRBEL test requires the least amount of material and is easier to load and would seem to be the most convenient test.

The SDDL specimens are more difficult to prepare than either the CNRBB or CNRBEL specimens. However, the test requires the least thickness of material, and is most suitable for rocks which break off in thin slabs, e.g. slate.

6.3 Fracture Toughness Tests on Rocks

Fracture toughness tests were conducted on dolomite and slate rocks, using the CNRBB and CNRBEL methods respectively. The rocks were tested using the same techniques established for concrete.

From 40 specimens of dolomite, it was possible to draw a histogram of K_{1c} results and identify three populations. An average K_{1c} value was calculated for each population, and the standard deviation of each was comparable to that which might be expected from concrete specimens. The three values were attributed to different mineral components within the rock, and observations of the crack surfaces support this interpretation.

Two samples of 12 specimens of slate were tested parallel (PAB) and perpendicular (PEB) to the bedding plane. In six tests the slate broke at a place other than at the notch root, and no result was obtained. It is important, when testing weak rock such as slate, to use as deep a notch as possible to ensure that failure does occur at the notch root.

The fracture toughness of the slate tested PEB was found to be more than twice that for the slate tested PAB. There was a large scatter in the results for the latter tests, and the highly irregular crack surfaces resulting from these tests suggest that the stress at the notch root is more complicated than that characterised by K_1.

It has been shown that the CNRBB and CNRBEL tests can provide a quick and simple method for measuring the fracture toughness of rocks. Furthermore, the tests are sensitive enough to be able to identify the fracture toughness of various mineral components within a rock.

6.4 Fracture Failure Criteria

This thesis has concentrated on deriving failure conditions for situations in which failure occurs under tensile stress. In this case, fracture initiation and strength failure are usually coincidental.

Fracture failure conditions have been derived for three simple structures. These are, a rock cantilever, a rock beam with various end conditions, and spalling. However, the analysis is equally applicable to concrete structures. In each case, a failure condition has been derived from a consideration of the energy changes involved in propagating a crack through a structure.

The stability conditions have been shown to be conservative ones and are equivalent to there being a small, but finite crack, in the structure. In each case, a crack length in the structure does not have to be assumed, and the criteria are in terms of readily measurable parameters.

The failure conditions use the measured K_{1c} values derived from the previously described new fracture toughness tests. As the results from these tests are more accurate than tensile strength results, the fracture failure criteria can be applied with some confidence. Furthermore, the criteria are very simple and as easy to apply as conventional tensile strength ones.

6.5 Proposals for Future Work

The stress intensity factors have been derived in chapter 3 by assuming that the test material behaves isotropically. For most rocks, this assumption would be incorrect, and the stress intensity factor should be amended to allow for anisotropy. Corten (1969) has

suggested how this might be carried out.

The effect of anisotropy on the stress intensity factor is particularly important for the SDDL test. It is envisaged that this test will be used for assessing the effect of K_{1c} anisotropy of slate-like materials. The slots in SDDL specimens can be readily cut at any angle, relative to the bedding plane, and so K_{1c} can be measured at any angle.

The measurement of K_{1c}, in CNRBB and CNRBEL tests, assumes that a crack has propagated from the base of the circumferential notch. However, it is necessary for micro-cracking to occur, prior to failure, so that a crack is propagating from a 'zero radius' notch. Therefore, the specimen fails as a crack propagates from a straight crack front, and an analysis is needed to determine the error by assuming that failure occurs at the sawn notch.

The error can readily be estimated if the total load-deflection curve is known as a crack propagates through a specimen, and this curve can be derived from experiments or finite elements (Hardy et al 1973).

The fracture tests described in this thesis have not been compared with the commonly used Notched Beam under Bending. It is important that this comparison should be made before the new tests can become widely accepted.

Only a limited number of test variables have been investigated, such as testing speed and notch depth for the CNRBB test. There are many more variables which might have an effect on the measured K_{1c} values, and these have to be investigated before a standard testing technique can be established for each test. Some of these variables are:-

1. The loading span for the CNRBB test. Previous researchers have shown that an increase in the loading span of the Notched Beam under Bending test decreases the measured K_{1c} value.
2. The testing speed for CNRBEL tests.
3. The length of CNRBEL specimens.
4. The diameter of SDDL specimens.
5. The breadth and slot depth for SDDL specimens.
6. The testing speed for SDDL tests.

The limitations of the tests have also to be determined. For example, the experiments described in this thesis used a very fine-grained concrete. For most industrial uses, a much larger aggregate size is preferred. Consequently, the diameter of the CNRBB and CNRBEL specimens would have to be increased. For any aggregate size, there is probably an optimum specimen size such that a reasonable scatter in results is commensurate with the minimum use of material.

Once a testing technique has been established, the tests have considerable application in the investigation of the fracture properties of other granular, brittle materials. For example, soil-cement and bitumin mixes might be suitable for fracture toughness testing. Furthermore, these materials are often used in road construction and fail under tensile stresses, and the failure criteria, developed in chapter 5, might be extended to cover such situations.

The main advantage of the tests described in this thesis, over pre-existing methods, is that the tests can be conducted on samples from in situ concrete. Sometimes it is convenient to test moulded specimens which are cast at the same time as the concrete is mixed.

For example, it is common practice to make cubes for compressive testing and quality control. If a fracture toughness test were devised which could use these cubes, then the measured K_{1c} might also be used for quality control.

A fracture toughness specimen, based on a cube, is shown in figure 6.1. Deep, parallel-sided notches are cut into two opposite faces of a cube, and the specimen is loaded eccentrically as shown. Thus, the test is similar to the CNRBEL. A similar arrangement has been used by Liebowitz (1969) to investigate the fracture of metal bars.

The stress intensity factor for deep notches is given by:-

$$K_1 = \frac{F}{b(\pi a)^{\frac{1}{2}}} \left[\frac{2e}{a} - 1\right] \qquad (6.1)$$

where b is the cube width, and the other parameters are defined in figure 6.1. A rigorous analysis, similar to that described in chapter 3, would give an expression for K_1 for notches of arbitrary depth. Note that because of the wide crack front, the measured K_{1c} is for conditions of plane strain.

Because of the large size of the industrial concrete cubes (15 cm) it is unlikely that the width of the cut notches would be very critical. The notches could be cut with widely available equipment, and the test could readily be carried out in many laboratories.

It has been shown in chapter 4 that the measured K_{1c} value is independent of whether a CNRBB specimen is loaded in strain or displacement control. Most laboratories use testing machines which

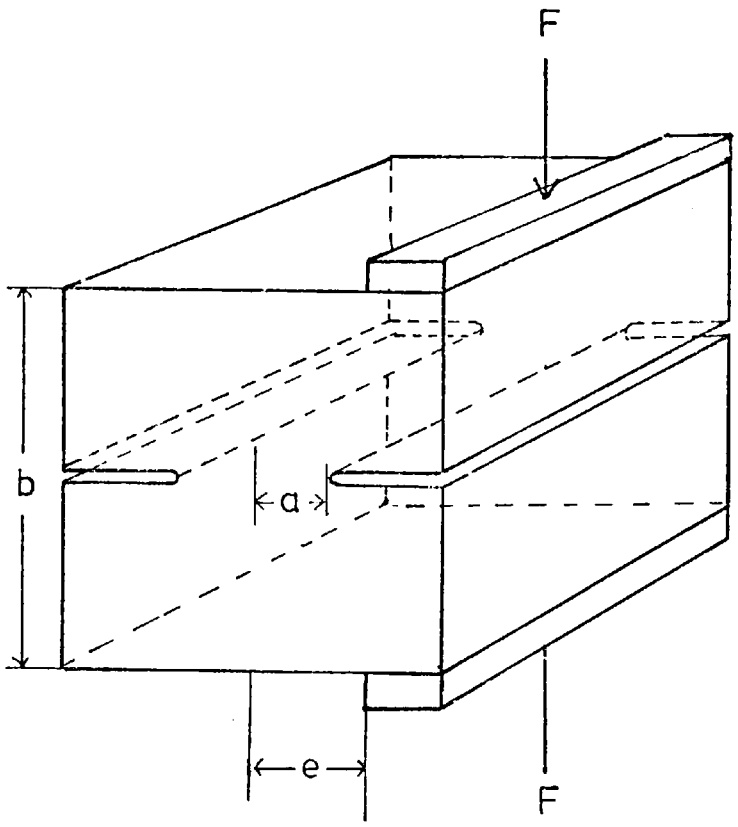

Fig 6.1 Proposed new testing arrangement to measure the fracture toughness of concrete cubes.

have no facility for servo-control. If the new fracture toughness tests could be shown to give the same results, regardless of the type of testing machine, then they could find a wider use than the Notched Beam under Bending. Therefore, a testing program is proposed to investigate the effect of testing machine stiffness on K_{1c} measurements.

There are two limiting factors to the choice of testing machine for use with the CNRBB and CNRBEL tests. Both tests give a low failure load - below the range of most testing machines. Also, a very low rate of loading is required, to allow time for micro-cracks to develop. The first limitation could be overcome by incorporating a load transducer into the loading arrangement for the CNRBB and CNRBEL tests. The second limitation might present a more difficult problem in some laboratories.

It has been postulated that the SDDL gives higher K_{1c} results than the CNRBEL test because of strain energy effects. The two tests might give the same result if either strain or load control is used.

In the first mode of control, the strain is measured across an opening crack, and the only reservoir of strain energy is between the extremeties of the strain measuring device. If the strain extensometer were made small, the strain energy effect would be reduced, and all tests might give the same result.

In load control, the amount of energy stored in the testing machine is very much greater than that in the specimen. In this case, the stiffness of the specimen should have little effect, and the tests might give the same result. If this were true, then the majority of testing machines, which are in effect under load control, would give

the same result for all tests.

The failure conditions, derived in chapter 5, have had no experimental verification at all. It is difficult to provide a uniform loading of beams, and can only be achieved using centrifugal loading. However, the failure conditions could be modified for single-point loading, which could be readily verified experimentally.

The failure conditions for spalling might be valid for laboratory-sized specimens which fail by spalling. For example, the theory predicts that, at failure, $K_{1c} \alpha \sigma^{5/4}$. By measuring K_{1c} and σ, this could readily be verified.

The failure conditions have all assumed that cracks have opened under pure tension. In most situations, there are shear stress as well, and the analysis should take this into account. The resistance of a material to cracking under shear forces is characterised by the material constant K_{11c}. K_{11c} is more difficult to measure than K_{1c} but unless its magnitude is known, it is not possible to assess the relative effects of shear or tensile failure.

A suggested experimental method for measuring K_{11c} is shown in figure 6.2. The two cracks are under conditions of almost pure shear if the loading arrangement is very stiff to prevent bending moments. The stress intensity factor K_{11} can be derived from Neuber's work on stress concentration factors, in a similar manner as for K_1. With modification, the experiment could be conducted with cylindrical specimens.

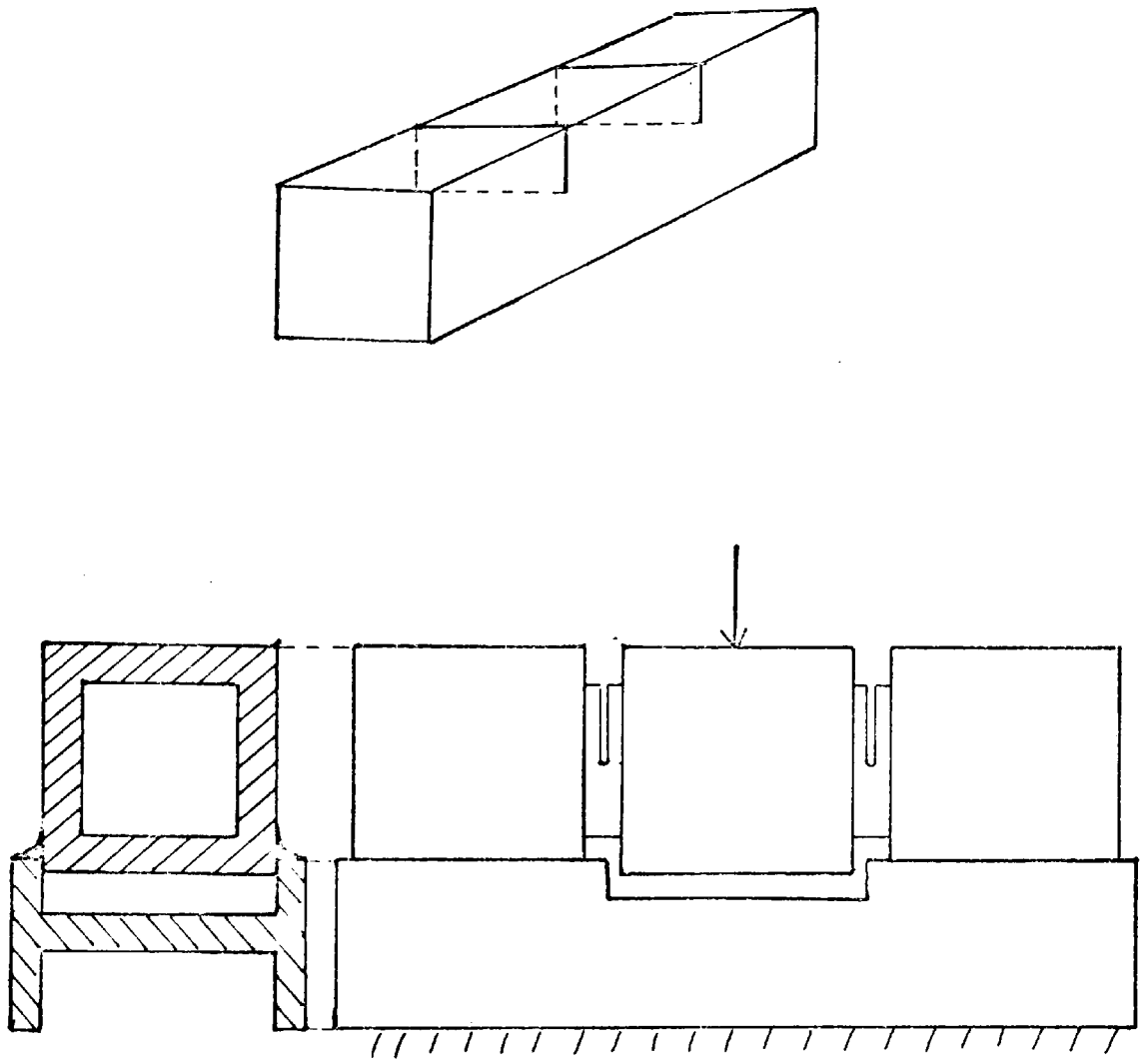

Fig 6.2 Proposed specimen shape and loading arrangement to measure K_{IIc} for concrete.

References

Bieniawski, Z.T. (1967a). 'Mechanism of Brittle Fracture of Rocks, parts I, II, III', Int. Journ. Rock Mech. Min. Sci. Vol. 4, pp 395 - 430.

Bieniawski, Z.T. (1967b). 'Stability Concept of Brittle Fracture Propagation in Rock', Engineering Geology. Vol. 2 (3), pp 149 - 162.

Bowie, O.L. (1964). 'Rectangular Tensile Sheet with Symmetric Edge Cracks', Trans. A.S.M.E. Journ. of Applied Mechanics. Vol 31, Ser. E, (2), June, pp 208 - 212.

Brace, W.F. (1961). 'Dependence of Fracture Strength of Rock on Grain Size', Penn. State Univ. Mineral Expt. Sta. Bull. Vol 76, pp 99 - 103.

Brace, W.F. and Walsh, J.B. (1962). 'Some Direct Measurements of the Surface Energies of Quartz and Orthoclase', The American Mineralogist'. Vol. 47, Sept - Oct, pp 1111 - 1122.

Brown, J.H. (1972). 'Measuring the Fracture Toughness of Cement Paste and Mortar', Magazine of Concrete Research. Vol. 24 (81), pp 185 - 196.

Brown, J.W. and Singh, M.M. (1966). 'An Investigation of Microseismic Activity in Rock under Tension', Trans. Soc. Mining Engrs. Vol. 235, Sept. pp 255 - 265.

Brown, W.F. and Srawley, J.E. (1969). 'Plane Strain Crack Toughness Testing of High Strength Metallic Materials'. A.S.T.M. special technical publication 410.

Cook, N.G.W. (1965). 'The Failure of Rock', Int. Journ. Rock Mech. Min. Sci. Vol. 2, pp 389 - 403.

Corten, H.T. (1969). 'Fracture Mechanics of Composites', (in) Fracture - an advanced treatise, Vol. 7. Fracture of non-metals and composites. (ed. H. Liebowitz). Pub. Academic Press.

Evans, R.H. (1946). 'Extensibility and Modulus of Rupture of Concrete', Structural Engineer (London). Vol. 24, Dec. pp 639 - 659.

Fairhurst, C. and Cook, N.G.W. (1966). 'The Penomenon of Rock Splitting Parallel to the Direction of Maximum Compression in the Neighbourhood of a Surface', Proc. 1st. Congr. Int. Soc. Rock Mech. (Lisbon). Vol. 1, pp 687 - 692.

Friedman, M., Handin, J. and Alani, G. (1972). 'Fracture Surface Energy of Rocks', Int. Journ. Rock Mech. Min. Sci. Vol. 9, pp 757 - 766.

Gilman, J.J. (1960). 'Direct Measurements of the Surface Energies of Crystals', Journ. of Applied Physics. Vol. 31 (12), pp 2208 - 2218.

Glucklich, J. (1963). 'Fracture of Plain Concrete', Journal of the Engineering Mech. Div. (Proc. A.S.C.E.). Vol. 89 (E.M.6), pp 127 - 138).

Glucklich, J. and Cohen, L.J. (1968). 'Strain Energy and Size Effect in Brittle Materials', Materials Research and Standards. Vol. 8 (10), pp 17 - 22.

Griffith, A.A. (1921). 'The Phenomena of Rupture and Flow of Solids', Phil. Trans. Roy. Soc. London. Vol A221, pp 163 - 198.

Gurney, C. and Hunt, J. (1967). 'Quasi-static Crack Propagation', Proc. Roy. Soc. Vol A229, pp 508 - 524.

Hardy, M.P., Hudson, J.A. and Fairhurst, C. (1973). 'The Failure of Rock Beams, Parts I and II', Int. Journ. Rock Mech. Min. Sci. Vol. 10, pp 53 - 82.

Hardy, H.R. and Jayaraman, N.I. (1970). 'An investigation of Methods for the Determination of the Tensile Strength of Rocks', Proc. of the 2nd Congr. Int. Soc. for Rock Mech. (Beograd).

Harris, D.O. (1967). 'Stress Intensity Factors for Hollow Circumferentially Notched Round Bars', Journal of Basic Engineering, (Trans. A.S.M.E.), March, pp 49 - 54.

Hobbs, D.W. (1969). 'Scale Model Studies of Strata Movement Around Mine Roadways. IV, Roadway Shape and Size', Int. Journ. Rock Mech. Min. Sci. Vol. 6, pp 365 -

Hudson, J.A., Crouch, S.L. and Fairhurst, C. (1972). 'Soft, Stiff and Servo-controlled Testing Machines: A review with reference to rock failure', Engineering Geology, Vol. 6 (3), pp 155 - 189.

Irwin, G.R. (1948). 'Fracture Dynamics', (in) Fracture of Metals, Am. Soc. Metals, Cleveland, pp 147 - 166.

Irwin, G.R. (1957). 'Analysis of Stresses and Strains Near the Tip of a Crack Traversing a Plate', Journ. Applied Mech. Vol. 24, pp 361 - 364.

Irwin, G.R. (1960). 'Fracture Mechanics in Structural Mechanics', (in) Proc. 1st. Symp. on Naval Structural Mechanics. Pub. Pergamon Press.

Irwin, G.R. and Kies, J.A. (1954). 'Critical Energy Rate Analysis of Fracture Strength', Welding Journal. Vol. 33 (4), pp 193 - 198.

Jaeger, J.C. and Cook, N.G.W. (1969). 'Fundamentals of Rock Mechanics. Pub. Chapman and Hall.

Kaplan, M.F. (1961). 'Crack Propagation and the Fracture of Concrete', Journ. Am. Concrete Inst. Proc. Vol. 58 (28), pp 591 - 610.

Krech, W.W. (1974). 'The Energy Balance Theory and Rock Fracture Energy Measurements for Uniaxial Tension', Proc. 3rd. Congr. Int. Soc. Rock Mech. Denver. Vol. 2, part A, pp 167 - 173.

Krech, W.W. and Chamberlain, P.G. (1974). 'New Techniques for Measuring Rock Fracture Energy', Soc. Petroleum Engrs. Vol. 14 (3), pp 237 - 242.

Liebowitz, H. (1969). 'Fracture and Carrying Capacity of Notched Columns', (in) Fracture: An advanced Treatise, Vol. IV. Engineering Fracture Design. Pub. Academic Press.

Lott, J. and Kesler, C.E. (1966). 'Crack Propagation in Plain Concrete', Symp. on Structure of Portland Cement Paste and Concrete. Washington D.C. Highway Research Board Special Report no. 90, pp 204 - 213.

Moavenzadeh, F. and Kuguel, R. (1969). 'Fracture of Concrete', Journal of Materials. Vol. 4 (3), Sept. pp 497 - 519.

Nakayama, J. (1965). 'Direct Measurement of Fracture Energies of Brittle, Heterogeneous Materials', Journ. Am. Cer. Soc. Vol. 48, pp 583 - 587.

Naus, S.J. and Lott, J.L. (1969). 'Fracture Toughness of Portland Cement Concretes', Journ. Am. Concrete Inst. Proc. Vol. 66 (6), June, pp 481 - 489.

Neuber, H. (1937, 1958 translation). Theory of Notch Stresses: Principles for exact calculation of strength with reference to structural form and material. Pub. U.S. Atomic Energy Commission Office of Technical Information.

Obert, L. and Duvall, W.I. (1967). Rock Mechanics and the Design of Structures in Rock. Pub. J. Wiley and Sons.

Obreimoff, J.W. (1930). 'The Splitting Strength of Mica', Proc. Roy. Soc. London. Vol. A127, pp 290 - 297.

Orowan, E. (1950). 'Fundamentals of Brittle Behaviour in Metals', Symp. on Fatigue and Fracture of Metals. M.I.T. June, 1950.

Paris, P.C. and Sih, G.C. (1964). 'Stress analysis of Cracks' (in) A.S.T.M. Special Technical Publication 381.

Peng, S.D. (1970). 'Fracture and Failure of Chelmsford Granite', Ph.D. thesis, Stanford Univ. Calif.

Perkins, T.K. and Krech, W.W. (1966). 'Effect of Cleavage Rate and Stress Level on Apparent Surface Energies of Rocks', Soc. Petrol. Engrs. Journ. Vol. 6 (4). pp 308 - 315.

Shoemaker, A.K. (1965). Discussion (in) 'Critical Appraisal of Fracture Mechanics' A.S.T.M. Special Technical Publication 381. pp 23 - 29.

Thomas, L.J. (1973). An Introduction to Mining. Pub. Hicks Smith & Sons, Sydney.

Westergaard, H.M. (1939). 'Bearing Pressures and Cracks', Journ. App. Mech. (Trans. A.S.M.E.) Ser. E, Vol. 61, June, pp A49 - A53.

Weiss, V. and Yukawa, S. (1964). 'Critical Appraisal of Fracture Mechanics', (in) A.S.T.M. Special Publication 381. pp 1 - 29.